Ian Veigl, BSc.

Numerical studies on slope stability analysis for drained and undrained material behavior

Masterarbeit

zur Erlangung des akademischen Grades

Diplom-Ingenieur

eingereicht an der

Technischen Universität Graz

Betreuer

Ass. Prof. Dipl.- Ing. Dr. techn. Franz Tschuchnigg

Dipl. – Ing. Simon Oberhollenzer, BSc.

Institut für Bodenmechanik, Grundbau und Numerische Geotechnik

Graz, April 2020

Eidesstattliche Erklärung

Ich erkläre an Eides statt, dass ich die vorliegende Arbeit selbstständig verfasst, andere als die angegebenen Quellen/Hilfsmittel nicht benutzt, und die den benutzten Quellen wörtlich und inhaltlich entnommenen Stellen als solche kenntlich gemacht habe. Das in TUGRAZonline hochgeladene Textdokument ist mit der vorliegenden Arbeit identisch.

…… Datum

……. Unterschrift

Affidavit

I declare that I have authored this thesis independently, that I have not used other than the declared sources/resources, and that I have explicitly indicated all material which has been quoted either literally or by content from the sources used. The text document uploaded to TUGRAZonline is identical to the present thesis.

……. Datum

……. Unterschrift

Acknowledgment

It is a great pleasure to express my deep gratitude towards my supervisors Ass. Prof. Dipl.-Ing. Dr. techn. Franz Tschuchnigg and Dipl.-Ing. BSc. Simon Oberhollenzer for their support, motivation, patience and discussions throughout writing this thesis.

I also want to thank all the employees of the faculty of civil engineering for providing with such a great education over the past six years.

I would like to thank my peers and friends Alexander, Linda, Tina and Tino for the great time we had. Without you, my university life wouldn´t have been that much fun.

Further, I would like to thank my parents Kornelia and Andreas as well as my sister Alena and my niece Amilia for all their support.

Finally, I would like to thank all my friends and for the travels all over the world we did in recent years.

Kurzfassung

Die am häufigsten verwendeten Methoden zur Berechnung von Sicherheitsfaktoren von Böschungen in der numerischen Geotechnik sind verschiebungsbasierende Finite-Elemente Analysen unter Verwendung von SRFEA (strength reduction finite element analysis) sowie Finite-Elemente Limit Analysis (FELA). Rigorose Lösungen mit FELA sind auf eine assoziierte Fließregel begrenzt, weshalb Davis (1968) reduzierte Festigkeitsparameter in Kombination mit einer assoziierten Fließregel empfiehl um ein nicht-assoziiertes Verhalten zu modellieren. Da dieser Ansatz zu sehr konservativen Ergebnissen führte, optimierte Tschuchnigg et al. (2015) diese Methode. Die Anwendung der optimierten Methode zeigt eine gute Übereinstimmung mit den Resultaten der verschiebungsbasierten Finite-Element Analyse (SRFEA). Die am häufigsten verwendete Methode zur Durchführung von SRFEA erfolgt über eine schrittweise Verminderung des effektiven Reibungswinkels φ‘, sowie der effektiven Kohäsion c‘. Die modifizierte Methode (DLL) für $0°<\psi'<\varphi'$ führt zu geringeren Sicherheitsfaktoren, da diese Methode zusätzlich die Reduktion des effektiven Dilatanzwinkels ψ‘ (auch für $\psi' < \varphi'$) berücksichtigt. In diversen Studien konnte gezeigt werden, dass die automatische wie auch die manuelle Festigkeitsreduktion gute Übereinstimmungen aufweisen. Des Weiteren konnte eine gute Übereinstimmung der 2D und 3D Finite-Elemente Berechnungen, unter Berücksichtigung nicht assoziierter Plastizität ($\psi'<\varphi'$) gezeigt werden. Für die Berechnung mit assoziierter Plastizität ($\psi'=\varphi'$) wurde eine Optimierung des Berechnungsablaufes in 3D vorgenommen, um passable Ergebnisse zu erzielen. Der letzte Teil der Arbeit beschäftigt sich mit dem Vergleich von drainierten und undrainierten Materialverhalten. Die Resultate dieser Arbeit zeigen den wesentlichen Einfluss der Drainagebedingungen, Kavitation sowie der Saugeffekte auf den Sicherheitsfaktor auf.

Stichwörter: Böschungsstabilität, Festigkeitsreduktion mit finiten Elementen, Finite-Elemente Limit Analysis, drainertes und undrainiertes Materialverhalten, Davis Ansatz

Abstract

In numerical geotechnical engineering displacement-based strength reduction finite element analysis (SRFEA), and finite element limit analysis (FELA) are the primary methods to compute the safety factors of slopes. Since rigorous solutions of FELA are limited to associated plasticity, Davis (1968) suggested to use reduced strength parameters in combination with an associated flow rule to model non-associated plasticity. The original approach leads to very conservative results. Therefore, a modified approach was developed by Tschuchnigg et al (2015). The enhanced approach leads to a good agreement with SRFEA. FELA is still slightly conservative. On the one hand, it is very common to perform SRFEA with a step-by-step reduction of the effective friction angle φ' and the effective cohesion c'. On the other hand, when performing SRFEA using the modified (DLL) technique, lower safety factors for $0°<\psi'<\varphi'$ are obtained due to a step-wise reduction of the effective dilatancy angle ψ' from the beginning. It has been shown in different studies that automatic and manual strength reduction are in very good compatibility. Furthermore, the influence of 3D effects on the safety factor showed that the results from 2D and 3D are in good agreement when performing SRFEA with non-associated plasticity ($\psi'<\varphi'$). For associated plasticity ($\psi'=\varphi'$), optimized settings for the calculation procedure must be used in 3D SRFEA to obtain satisfactory results. The final part of the thesis deals with the comparison of drained and undrained material behavior for a slope. It could be shown that the drainage conditions as well the influence of cavitation and suction highly influence the safety factor.

Keywords: slope stability, strength reduction finite element analysis, finite element limit analysis, drained and undrained material behavior, Davis approach

Table of contents

List of symbols and abbreviations

Capital letters

D^e	Elastic stiffness matrix
E’	Young`s modulus
E_{50}^{ref}	Reference secant stiffness in standard drained triaxial test
E_{Oed}^{ref}	Reference tangent stiffness for primary oedometer loading
E_{ur}^{ref}	Reference unloading/reloading stiffness from drained test
FEA	Finite element analysis
FELA	Finite element limit analysis
FoS	Factor of safety
G_0^{Ref}	Reference shear modulus at very small strains
HS	Hardening soil
HSS	Hardening soil with small strain stiffness
K_0^{NC}	K_0-value for normal consolidation
LB	Lower boundary
MC	Mohr Coulomb
M_{SF}	Incremental multiplier
SRFEA	Strength reduction with finite element analysis
UB	Upper boundary

Small letters

c’	Effective cohesion
c'_{mob}	Mobilized effective cohesion
c*	Reduced effective cohesion according to Davis (1968)
$c'_{failure}$	Effective cohesion at failure
c_u	Undrained shear strength
f	Yield function
g	Potential function
m	Power of stress-level dependency of stiffness
p^{ref}	Reference stress for stiffness
p’	Effective mean stress
q	Deviatoric stress
q_a	Asymptotic value of the shear stress
q_f	Deviatoric stress at failure
u	Pore water pressure
|u|	Total displacements

Greek letters

α	Slope angle
β	Strength factor according to Davis (1968)
β_0	Strength factor according to Davis (1968) at initial conditions
$\beta_{failure}$	Strength factor according to Davis (1968) at failure
ε	Strain
ε^e	Elastic strain
ε^p	Plastic strains
$\dot{\varepsilon}$	Strain rate
$\dot{\varepsilon^e}$	Elastic strain rate
$\dot{\varepsilon^p}$	Plastic strain rate
ε_1	Total principal strain
ε_{vol}	Total volumetric strain
$\gamma_{0.7}$	Threshold shear strain at which $G_S=0.722G_0$
γ^p	Plastic shear strain
$\dot{\gamma^p}$	Plastic shear strain rate
γ	Unit weight
γ_{sat}	Saturated unit weight
γ_{unsat}	Unsaturated unit weight
λ	Plastic multiplier
ν	Poisson´s ratio
ν_{UR}	Poisson´s ratio for unloading/reloading
σ'	Effective stress
σ'_1	Principle effective stress
σ'_3	Principle effective stress
σ	Total stress
σ_1	Principle total stress
σ_3	Principle total stress
σ'_{xx}	Cartesian effective stress
σ'_{yy}	Cartesian effective stress
φ’	Effective friction angle
φ*	Reduced effective friction angle according to Davis (1968)
φ'_{mob}	Mobilized effective friction angle
$\varphi'_{failure}$	Effective friction angle at failure
ψ’	Effective dilatancy angle
ψ_{mob}’	Mobilized effective friction angle
$\psi'_{failure}$	Effective dilatancy angle at failure

1 Introduction

In numerical geotechnical engineering displacement based finite element analysis with a strength reduction finite element technique (SRFEA) and finite element limit analysis (FELA) are mainly used to compute the factors of safety (FoS). In this thesis, several numerical studies on slope stability have been conducted. When performing SRFEA, the effective strength parameters of the soil are reduced simultaneously until no equilibrium in the system can be reached. The safety factor is defined as the ratio of the available strength divided by the mobilized strength. In the present thesis, two different strength reduction techniques, namely implemented and modified (DLL), are performed and compared. The standard (implemented) SRFEA deals with an incrementally reduction of the effective friction angle φ' and the effective cohesion c'. The effective dilatancy ψ' angle is kept constant for $\psi' < \varphi'_{red.}$. The modified (DLL) technique considers additionally a reduction of this soil parameter. For associated plasticity (ψ'=φ') as well as for an effective dilatancy angle ψ'=0° both techniques are expected to obtain the same results, but for 0°<ψ'<φ' differences between the implemented and modified (DLL) SRFEA are expected. Both strength reduction techniques are performed automatically and manual. Additionally, upper and lower bounds of the failure load (and consequently the safety factor) are computed. Since FELA is limited to associated plasticity (ψ'=φ'), Davis (1968) suggested using reduced effective strength parameters of the soil. The original approach of Davis leads to very conservative results, hence an alternative procedure, was developed by Tschuchnigg et al (2015). All analyzes are performed using a linear elastic-perfectly plastic soil constitutive model in combination with a Mohr Coulomb (MC) failure criterion. Additionally, especially when performing undrained analyzes, the Hardening soil small (HSS) model (Benz, 2006) is used. In the first section of this thesis, safety factors by means of drained 2D and 3D SRFEA as well for 2D FELA are determined. The influence of the strength reduction techniques (implemented and modified (DLL)), mesh discretization, shape functions, constitutive models, and the flow rule on the obtained factor of safety are part of the study. For 3D SRFEA, the influence of the model depth on the obtained FoS is included in the present thesis. For selected studies, considering drained material behavior, parameter studies of numerical control parameters are performed with 2D and 3D SRFEA (e.g. tolerated error, arc length control…). To study the influence of the impact of the drainage conditions on the FoS, 2D SRFEA are performed with undrained material behavior by means of effective strength and stiffness parameters (denoted as Undrained (A)). Drained and undrained FEA and undrained FEA with ignored undrained behavior during the strength reduction phase are performed and compared for a slope excavation. In a further step, the impact of cavity and the effect of suction on the obtained FoS are part of the research. Furthermore, stress paths, the development of excess pore pressures and volumetric strains are evaluated for the interpretation of the obtained results, performing SRFEA with different drainage conditions.

2 Theoretical part

2.1 Constitutive models

Constitutive models describe the mechanical behavior of soils under loading. Especially for soils, different loading conditions (primary loading, unloading and reloading) must be considered. With mathematical (differential-) equations, depending on the constitutive model, stresses, strains and displacements can be computed. Since soil is a very inhomogeneous, naturally grown material, a lot of assumptions must be made to describe its behavior. Many constitutive models are based on lab-tests, whereas each of them deals with uncertainties. Over the last decade, finite element analysis in geotechnical engineering has become very important, and the complexity of the soil models have increased significantly. However, in this thesis, two constitutive soil models, namely Mohr Coulomb (MC) and Hardening soil small model (HSS) (Benz, 2006), are used and compared.

2.1.1 Mohr Coulomb model (MC)

The Mohr Coulomb (MC) model describes the soil with a linear elastic-perfectly plastic material behavior in combination with a Mohr Coulomb failure criterion. The linear part of the MC model is based on the Hook´s law considering isotropic elasticity. The strains in the linear part are reversible, as for the plastic part, the strains are irreversible. To evaluate if the soil is in the plastic part or not, a yield function f, depending on stresses and strains, is introduced. Plastic yielding is given for f=0. An ideal plastic constitutive model is a model with a fixed yield surface, which is only defined by the model parameters, and it is not affected by plastic strains. All points with a stress state within the yield surface behave only in elastic reversible strains. The final strains shown in Eq. (1), and strain rates shown in Eq. (2), are split up into an elastic and a plastic part.

$$\varepsilon = \varepsilon^e + \varepsilon^p \tag{1}$$

$$\dot{\varepsilon} = \dot{\varepsilon^e} + \dot{\varepsilon^p} \tag{2}$$

With the Hook´s law, shown in Eq. (3), the relationship between the stress rates and the elastic strains rates can be described.

$$\sigma'^{\cdot} = D^e \dot{\varepsilon^e} = D^e \cdot (\dot{\varepsilon} - \dot{\varepsilon^p}) \tag{3}$$

Plastic strains are proportional to the derivative of the yield function with respect to the stress rates (Hill, 1950), which means that the plastic strain rates are a normal vector of the yield surface. This classical form of the theory corresponds to associated plasticity (φ'=ψ'). However, for a Mohr Coulomb yield function associated plasticity overestimates the effective dilatancy. Hence, a plastic potential function g is introduced in addition to the yield function f. In case that

f≠g, non-associated plasticity (ψ'<φ') is considered. Plastic strains can be estimated after Eq. (4) with a plastic multiplier λ.

$$\dot{\varepsilon^p} = \lambda \frac{\partial g}{\partial \sigma'} \tag{4}$$

As shown in Eq. (5) λ is zero for linear elastic behavior, as for perfectly plastic behavior, λ is positive, as shown in Eq. (6).

$$\lambda = 0 \quad \text{for:} \quad f < 0 \quad \text{or:} \quad \frac{\partial f^T}{\partial \sigma'} \; D^e \dot{\varepsilon} < 0 \qquad \text{(Elasticity)} \tag{5}$$

$$\lambda > 0 \quad \text{for:} \quad f = 0 \quad \text{or:} \quad \frac{\partial f^T}{\partial \sigma'} \; D^e \dot{\varepsilon} > 0 \qquad \text{(Plasticity)} \tag{6}$$

Fig. 1 shows the reversible elastic and irreversible plastic strains in a stress-strain diagram.

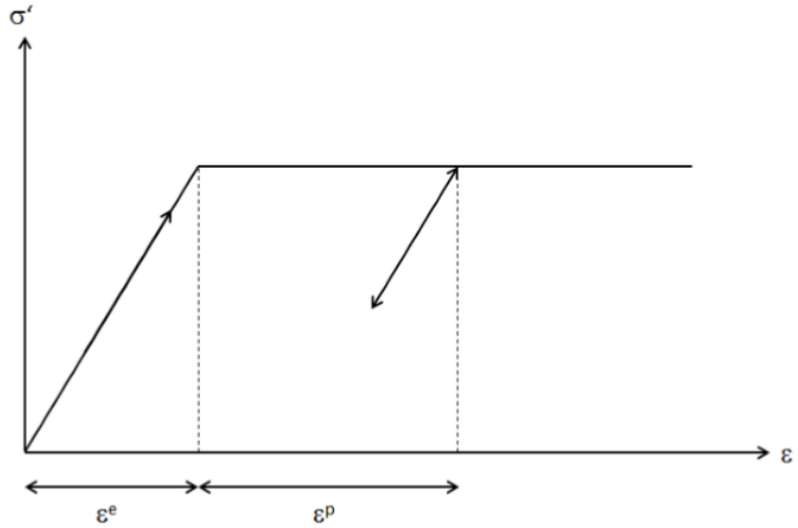

Fig. 1 Linear elastic-perfectly plastic model (Brinkgreve, 2018)

The Mohr Coulomb yield condition is an extension of the MC failure criterion for the general stress state. For the major σ'_1 and the minor σ'_3 effective principal stress, the flow condition is defined as shown in Eq. (7), where full Mohr Coulomb yield condition consists of six yield functions. In addition to the six yield functions f, the Mohr Coulomb model includes six potential functions g. One of these is shown in Eq. (8). Fig. 2 illustrates these six yield functions together which represent a fixed hexagonal cone in principal stress space.

$$f_{(\{\sigma\})} = (\sigma_1 - \sigma_3) - (\sigma_1 + \sigma_3) \cdot \sin\varphi - 2c \cdot \cos\varphi \quad (7)$$

$$g_{(\{\sigma\})} = \frac{1}{2}(\sigma_1 - \sigma_3) + \frac{1}{2}(\sigma_1 + \sigma_3) \cdot sin\,\psi \quad (8)$$

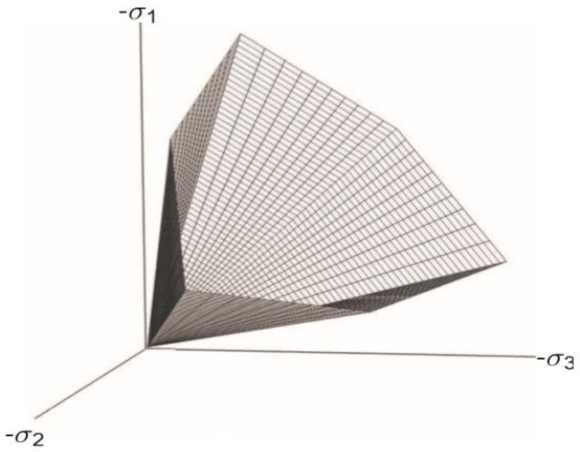

Fig. 2 Yield surface of the MC model on principal stress state (Brinkgreve, 2018)

As shown in Table 1, five soil parameters are required to describe the mechanical behavior of the linear elastic-perfectly plastic Mohr Coulomb model. It should be mentioned that only one stress independent stiffness E' can be taken into account. Hence, the history of the soil formation (over- or normal consolidated) as well as the loading type (normal, un- and reloading) cannot be considered within this model (Brinkgreve, 2018).

Table 1 Required parameters for MC model

Young´s modulus	E'	[kPa]
Poisson´s ratio	ν'	[-]
Effective cohesion	c'	[kPa]
Effective friction angle	φ'	[°]
Effective dilatancy angle	ψ'	[°]

2.1.2 Hardening soil small model (HSS)

The yield surface of the Hardening soil model (HS) model (Schanz, 1999) is not fixed on a principal stress state. The yield surface expands (or shrinks) when plastic strains occur, which is called hardening. It is distinguished between shear and compression hardening. The model considers a stress dependent soil stiffness as well as a mobilized dilatancy angle and introduce a yield cap (for volumetric hardening). The failure criterion is defined according to Mohr Coulomb. As shown in Fig. 3, the relationship between the strains in direction of the major principal stresses and the deviatoric stress for the HS model is given by a hyperbola.

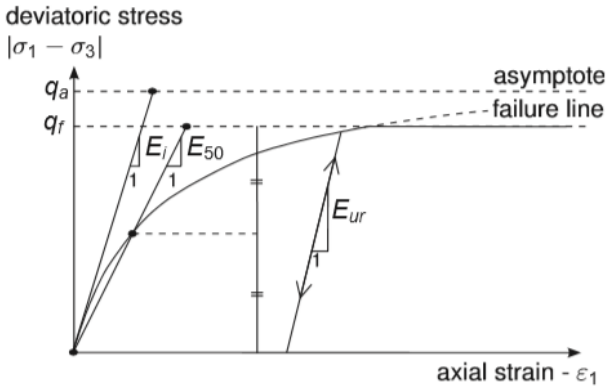

Fig. 3 Hyperbolic relationship between ε_1 and q (Brinkgreve, 2018)

The asymptotic value of the shear strength is called q_a and the initial stiffness E_i. The parameters of the stiffness values are all related to a reference stress p_{Ref} (usually 100 kPa) and a power m which depends on the type of soil. Using Eq. (9) and Eq. (10), the soil stiffness parameters E_{50} and E_{UR} can be determined.

$$E_{50} = E_{50}^{ref} \cdot \left(\frac{c \cdot cos\varphi - \sigma_3{}' \cdot sin\varphi}{c \cdot cos\varphi + p^{ref} sin\varphi} \right)^m \tag{9}$$

$$E_{UR} = E_{UR}^{ref} \cdot \left(\frac{c \cdot cos\varphi - \sigma_3{}' \cdot sin\varphi}{c \cdot cos\varphi + p^{ref} sin\varphi} \right)^m \tag{10}$$

As for all plasticity models, there is a relation between the plastic shear strains γ^p and the plastic volumetric strains $\varepsilon_V{}^p$. The relationship for the HS model, shown in Eq. (11), is linear and considers a mobilized dilatancy angle ψ_m. Furthermore, this mobilized dilatancy angle ψ_m depends on the effective mobilized friction angle φ'_m.

$$\dot{\varepsilon_v^p} = sin\,\psi_m \dot{\gamma}^p \tag{11}$$

The yield surface of the HS model is not fixed on a principal stress state, and it has to be distinguished between shear and compression hardening. Shear hardening does not consider plastic volume strains. Therefore, a second type of yield surface, shown in Fig. 4, is introduced to enable closing the elastic region for compressive stress paths. This cap type yield surface is essential to describe the model with an independent input of E_{50}^{Ref} and E_{Oed}^{Ref} because E_{50}^{Ref} controls the plastic strains according to the shear yield surface. E_{Oed}^{Ref} controls the plastic strains that are connected to the yield cap.

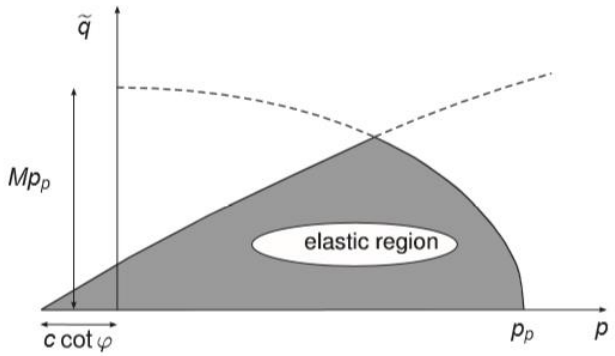

Fig. 4 Two yield surfaces of the HS model (Brinkgreve, 2018)

Fig. 5 shows the hexagonal shape of the yield surface of the classical MC failure criterion in combination with the cap yield surface.

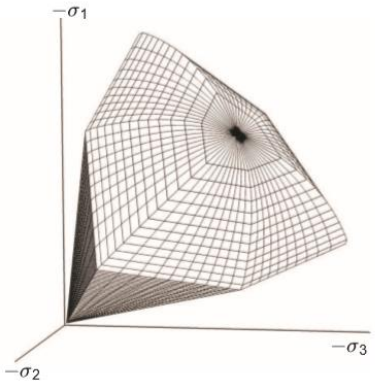

Fig. 5 Total yield contour of HS model (Brinkgreve, 2018)

The Hardening soil small (HSS) model (Benz, 2006) is an advanced model based on the Hardening soil (HS) model. It requires two more soil parameter to describe the mechanical behavior (G_0 and $\gamma_{0.7}$). In geotechnical engineering, the stiffness parameters for various problems should be related to strain rates (see Fig. 6). With the HSS model an increased soil stiffness for very small strains and its non-linear dependency on strain amplitude is taken into account.

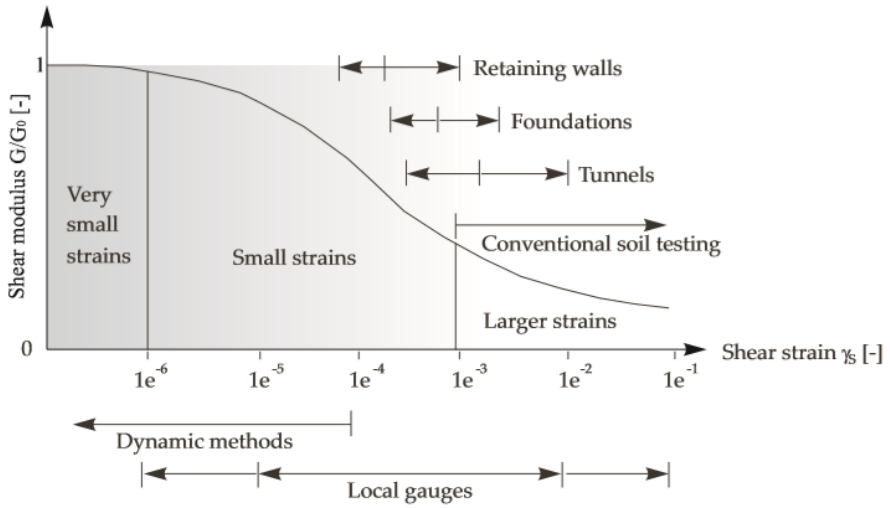

Fig. 6 Strain ranges for different applications in geotechnics (Brinkgreve, 2018)

Table 2 summarizes the required parameters for the Hardening soil small (HSS) model. As mentioned above, compared to the HS model, two more parameters (namely G_0 and $\gamma_{0.7}$) are necessary for the HSS model (Brinkgreve, 2018).

Table 2 Required parameters for HSS model

Power of stress-level dependency of stiffness	m	[-]
Secant stiffness in standard drained triaxial test	E_{50}^{Ref}	[-]
Tangent stiffness for primary oedometer loading	E_{Oed}^{Ref}	[kPa]
Unloading/Reloading stiffness from drained test	E_{Ur}^{Ref}	[kPa]
Effective cohesion	c’	[kPa]
Effective friction angle	φ’	[°]
Effective dilatancy angle	ψ’	[°]
Poisson´s ratio for unloading-reloading	ν_{Ur}	[-]
K_0-value for normal consolidation	K_0^{NC}	[-]
Reference shear modulus at very small strains	G_0^{Ref}	[kPa]
Threshold shear strain at which $G_S=0.722G_0$	$\gamma_{0.7}$	[-]

2.1.3 Flow rule

In finite element analysis the choice of the flow rule is crucial of the development of the plastic strains. If the stress state lies in the linear elastic part of the model, only elastic reversible strains occur. The elastic strains can be calculated with the Hook´s law. But if the stress state reaches the failure limit, irreversible plastic strains occur. The choice of the flow rule decides about the further development of the plastic strains consequently. Between two flow rules, associated ($\psi'=\varphi'$) and non-associated ($\psi'<\varphi'$), is distinguished. Performing FEA considering an associated flow rule, the derivatives of the plastic strains are proportional and consequently, the plastic strains are perpendicular to the yield surface (see Fig. 7). In case of a Mohr Coulomb failure criterion, the effective friction angle φ' is equal to the effective dilatancy angle ψ' of the material. Since for soils the effective dilatancy angle ψ' is smaller than the effective friction angle φ', the volumetric plastic strains are overestimated when performing an analysis based on associated plasticity. However, when performing FEA considering a non-associated flow rule the plastic strains act perpendicular to the plastic potential, but not to the yield surface anymore. Consequently, the volumetric plastic strains decrease by reducing the effective dilatancy angle ψ'. Due to the approximate infinite bulk modulus of the soil only deviatoric and no volumetric strains can occur when performing an analysis with undrained material behavior. Hence, such an analysis can only be carried out with an effective dilatancy angle $\psi'=0°$. Fig. 7 shows the definition of the different flow rules in a σ'-τ diagram (Egger, 2012).

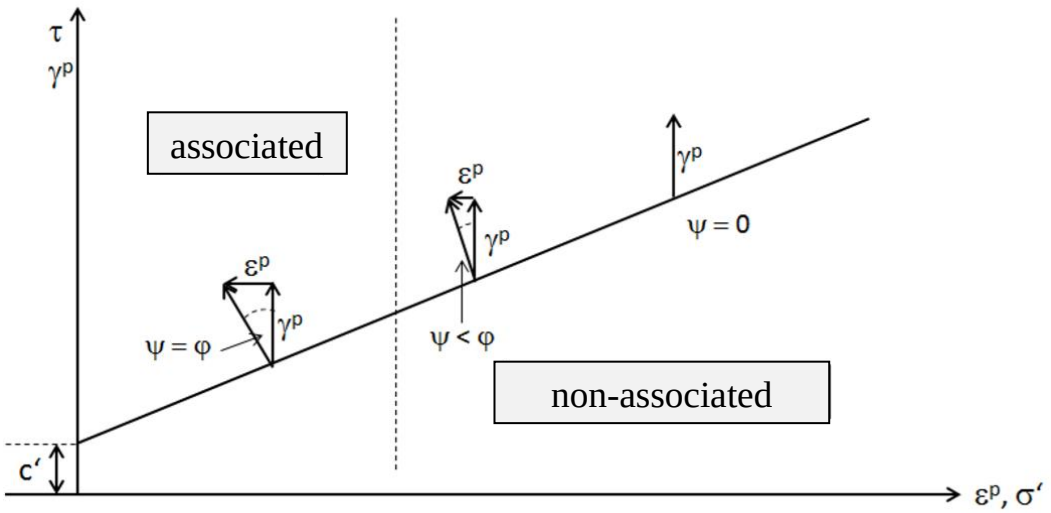

Fig. 7 Associated and non-associated flow rule (Egger, 2012)

2.2 Numerical methods

2.2.1 Strength reduction finite element analysis (SRFEA)

In practical engineering SRFEA is mostly used to compute the factor of safety (FoS) of various geotechnical problems. The strength parameters of the soil are reduced incrementally until no equilibrium can be reached, assuming the Mohr Coulomb failure criterion. The factor of safety is defined as the ratio of the available and the mobilized strength of the material. This thesis aims to distinguish between two different strength reduction techniques, namely implemented (standard) and modified (DLL). All SRFEA are performed using the finite element code Plaxis (Brinkgreve, 2018). During an implemented strength reduction technique (see Eq. (12)), the tangent of the effective friction angle φ' and the effective cohesion c' are reduced simultaneously until no equilibrium can be established. The effective dilatancy angle ψ', for this technique is kept constant as long as $\varphi'_{red}>\psi'$. At the point where $\varphi'_{red}=\psi'$, φ' and ψ' are reduced simultaneously. Fig. 8 (a) represents the implemented strength reduction technique in a σ'-τ' diagram.

$$FOS = \frac{tan\varphi'}{tan\varphi'_{mob}} = \frac{c'}{c'_{mob}} \tag{12}$$

On the other hand, tan ψ' is reduced simultaneously from the beginning (also for (φ'>ψ') in the modified (DLL) SRFEA (see Eq. (13)). Fig. 8 (b) shows the method in a σ'-τ' diagram.

$$FOS = \frac{tan\varphi'}{tan\varphi'_{mob}} = \frac{c'}{c'_{mob}} = \frac{tan\psi'}{tan\psi'_{mob}} \tag{13}$$

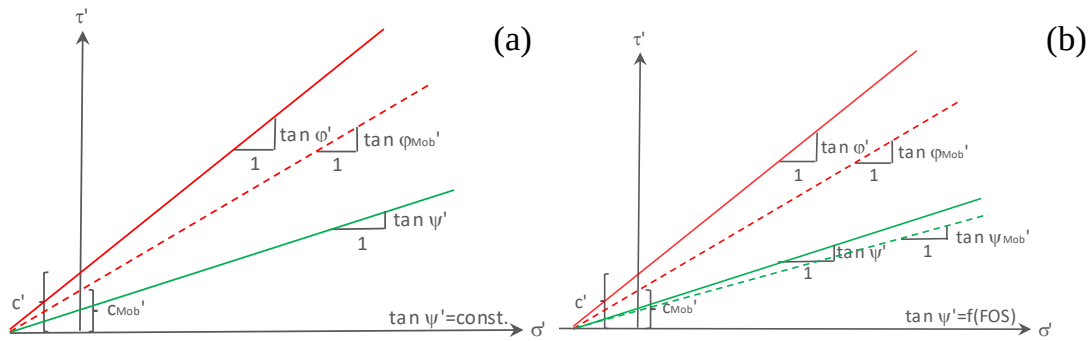

Fig. 8 SRFEA: (a) Implemented, (b) Modified (DLL) (according to Oberhollenzer, 2017)

For associated plasticity (φ'=ψ') as well as ψ'=0°, both techniques are expected to deliver the same results (Oberhollenzer, 2017). In the following, both reduction techniques are performed "automatically" and "manually". During a φ'-c'-(ψ') reduction (safety analysis) the strength parameters are reduced automatically. On the other hand, the user can reduce the strength parameters of the soil manually during a plastic phase "by hand". For the manual strength reduction, the safety analysis is omitted, and the strength parameters of the soil are reduced until failure occurs. The incremental reduction of the effective friction angle φ' is 0.25° per step. c_{mob}' and ψ_{mob}' are estimated, with Eq. (12) and Eq. (13), based on the current effective mobilized friction angle φ_{mob}'.

2.2.2 Finite element limit analysis (FELA)

2.2.2.1 Introduction

Finite element limit analysis (FELA) is based on the lower and upper bound theorems of plasticity. Thus, it is possible to bracket the factor of safety from below and above. The difference between these two boundaries is an indicator of the resulting deviation of the true collapse load and consequently of the true factor of safety. Therefore, this deviation is used to refine the meshes until a suitably accuracy of the true factor of safety is found. The lower bound theorem represents a stress field where equilibrium equations, the stress boundary conditions, and the yield criterion are satisfied, and no failure of the material occurs. Kinematics is not considered for the lower bound theorem. Consequently, the failure load is smaller than the true collapse load. The upper bound theorem on the other hand considers displacements but the stress equations are not in equilibrium anymore. The theorem sets the external work equal to the internal rate by satisfying the mechanical boundary conditions. The upper bound satisfies the velocity boundary conditions as well as the strain and velocity compatibility condition. The failure load performing FELA with the upper bound theorem of plasticity is higher than the true collapse load (Oberhollenzer, 2017).

2.2.2.2 Davis approach

For a plastic field, stress and velocity characteristic are only equal when considering associated plasticity (ψ'=φ'). Hence, as shown in Eq. (14), Davis (1968), suggested to use reduced strength parameters c* and tanφ* of the soil to model non-associated plasticity (ψ'<φ'). The parameter $\beta_{failure}$, shown in Eq. (15) is a function of the effective friction angle φ' and the effective dilatancy angle ψ'.

$$\begin{aligned} c^* &= \beta_{failure} \cdot c' \\ tan\,\varphi^* &= \beta_{failure} \cdot tan\varphi' \end{aligned} \tag{14}$$

$$\beta_{failure} = \beta_0 = \frac{cos\,\varphi' \cdot cos\,\psi'}{1 - sin\varphi' \cdot sin\psi'} \tag{15}$$

Since the original approach after Davis (denoted as Davis A) leads to very conservative results, two modifications were developed by Tschuchnigg et al (2015) to determine the FoS more precisely (subsequently denoted as Davis B and Davis C). Based on the reduced strength parameters according to Davis A, the parameter β is determined within an iterative procedure based on current effective strength parameters. Performing FELA in combination with Davis B, the parameter $\beta_{failure}$, as shown in Eq. (16), changes during the iterations, because the non-associativity (φ'-ψ') changes. The effective dilatancy angle ψ' is reduced in the same way as the effective friction angle φ'. Due to the fact that the effective dilatancy angle ψ' is reduced when using the Davis B approach, the results are therefore best comparable with the modified (DLL) strength reduction technique.

$$\beta_{failure} = \frac{cos\,\varphi'_{failure}\,cos\,\psi'_{failure}}{1 - sin\,\varphi'_{failure}\,sin\psi'_{failure}} = \frac{cos\left(arctan\left(\frac{tan\varphi'}{FoS}\right)\right) \cdot cos\left(arctan\left(\frac{tan\psi'}{FoS}\right)\right)}{1 - sin\left(arctan\left(\frac{tan\varphi'}{FoS}\right)\right) \cdot sin\left(arctan\left(\frac{tan\psi'}{FoS}\right)\right)} \tag{16}$$

Davis C approach is very similar to Davis B with the only difference that the effective dilatancy angle ψ' is kept constant for this procedure. The estimation of the parameter $\beta_{failure}$ is given in Eq. (17). Due to the fact that the effective dilatancy angle ψ' is kept constant the results are best comparable with the implemented strength reduction technique. Furthermore, it should be noted that for ψ'=0°, Davis B and Davis C lead to the same FoS.

$$\beta_{failure} = \frac{cos\,\varphi'_{failure}\,cos\,\psi'}{1 - sin\,\varphi'_{failure}\,sin\psi'} = \frac{cos\left(arctan\left(\frac{tan\varphi'}{FoS}\right)\right) \cdot cos\psi'}{1 - sin\left(arctan\left(\frac{tan\varphi'}{FoS}\right)\right) \cdot sin\psi'} \tag{17}$$

2.3 Drainage conditions

In geotechnics the drainage conditions of the soil influence the results strongly. Between two drainage conditions, namely drained and undrained is distinguished. A drained analysis is usually performed when the permeability of the soil is high (e.g. gravel or sand), the loading rate is low or short time behavior is not of interest. An undrained analysis on the other hand, is usually performed when the permeability of the soil is very low (e.g. clay) as well as when the loading rate is very high or short-term behavior has to be assessed. Consequently, excess pore pressures are generated. According to the definition of the flow rule (Fig. 7), the effective dilatancy angle ψ' has to be zero for undrained analysis, so that no volumetric strains can occur. Otherwise, unrealistic large "tensile" pore water pressures, and further resulting unrealistic large deviatoric stresses would be calculated.

2.3.1 Undrained analysis in terms of effective stresses (UD A)

The drainage type Undrained (A) in Plaxis enables performing an undrained analysis using the same effective strength and stiffness properties of the soil as for drained material behavior. Consequently, the determination of the undrained shear strength is based on the effective friction angle φ' as well as on the effective cohesion c'. Thus, the undrained shear strength c_u is a result of the FEA. The accuracy of the generated excess pore pressures during the calculation depends on the chosen constitutive soil model and the parameters. As shown in Fig. 9, the development of the pore pressure plays an essential role for the development of the effective stress path. Hence, the computed factor of safety may be influenced by the constitutive soil model. For undrained analysis in terms of effective stresses the constitutive Eq. (18) and the total stiffness matrix, shown in Eq. (19), are taken into account (Brinkgreve, 2018).

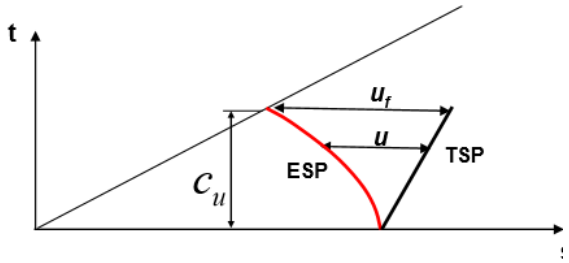

Fig. 9 Undrained analysis in terms of effective stresses (Schweiger, 2018)

$$\Delta\sigma = D'\Delta\varepsilon \tag{18}$$

$$D = D' + D_f \tag{19}$$

2.3.2 Cavitation cut off

As already mentioned, a computation with undrained material behavior is strongly influenced by excess pore pressures. Undrained material in combination with primary loading (e.g. embankment) leads to positive excess pore pressures, but in case of unloading (e.g. excavation), excess tensile pore pressures may occur. Consequently, the total stresses and the resulting safety factor are influenced by the loading type. Plaxis enables limiting excess tensile pore pressures by applying the control parameter *Cavitation Cut Off*. If it is activated, the tensile stresses of the water never get larger than the cavitation stress. But if it is not activated, endless tensile stresses are allowed. Section 6.5 explicitly demonstrates the influence of cavity, when performing undrained FEA (Brinkgreve, 2018).

2.3.3 Ignore Suction

Plaxis enables the performance of undrained analyzes with a control parameter, called *Ignore Suction*. If not activated, the effect of suction will be considered during the calculation, and excess pore pressures are controlled by an unsaturated bulk modulus of pore fluids. This bulk modulus is usually smaller than the bulk modulus of the water. It takes the compressibility of water and the soil-water retention curve into account. However, the default setting in Plaxis is *Ignore Suction*, where the effect of suction is neglected, and the soil behaves saturated. The computation of excess pore pressures is then only governed by the compressibility of water, which is much higher as for the case that suction is considered. An example in section 6.6 illustrates the influence of suction, when performing an undrained analysis (Brinkgreve, 2018).

3 Used software

3.1 Plaxis

Plaxis is a numerical software which uses a displacement based finite element code. The program includes a lot of different constitutive soil models; from simple soil models like the ideal-elastic plastic Mohr Coulomb (MC) to more complex soil models like the Hardening soil (HS) (Schanz, 1999) and the Hardening soil model with small strain stiffness (HSS) (Benz, 2006). Additionally, hydrologic conditions as well as structural elements (anchors, retaining walls, etc.…) can be modelled. Plaxis 2D Version 2016 and 2018 as well as Plaxis 3D Version 2018 are used in this thesis.

3.2 Optum

Optum is a geotechnical analysis software using the finite element method. For this thesis it is used to perform limit analysis to compute upper and lower bounds of the failure load. Optum performs with an adaptive mesh refinement during the calculation. Based on the development of the current shear strains the mesh is refined in three iteration steps in all analyzes discussed in the following. Optum G2 Version 2018 is used in this thesis.

4 2D Slope stability for drained material behavior

4.1 Introduction and overview

4.1.1 Problem definition and tasks

In this section, SRFEA (namely standard (implemented) and modified (DLL), discussed in 2.2.1) and FELA (discussed in 2.2.2) are compared for a homogeneous slope, presented in Fig. 10 performed as drained analysis using two different constitutive soil models, namely a linear elastic-perfectly plastic model including a Mohr Coulomb failure criterion (MC) and, for selected studies, a Hardening soil small (HSS) model (Benz, 2006). The calculations are performed with different definitions of the flow rule ($\psi'=\varphi'$, $\psi'=10°$ and $\psi'=0°$). In the first part of each subchapter, SRFEA are performed, using different meshes and shape functions (6n and 15n elements) with the implemented and modified (DLL) strength reduction technique. Additionally, SRFEA are performed manually, where the effective strength properties of the soil are reduced "by hand". The influence of numerical control parameters on the obtained safety factors is investigated on selected studies. FELA investigates the influence of the mesh discretization on the bounds (and the mean value). Since FELA is limited to associated plasticity ($\varphi'=\psi'$), the Davis approach is needed to model non-associated plasticity ($\varphi'>\psi'$). In the final step, the results from SRFEA and FELA are compared and critically evaluated. Furthermore, studies with a variation of the slope inclination and with different materials are carried out.

4.1.2 Model and geometry

The simple homogeneous slope analyzed, presented in Fig. 10, has a height of 10m and a constant inclination of 45°. A non-deformable bedrock is considered 20m below the surface and the width of the firm base is modelled with 40m. All further required dimensions for the model are shown in the following figure.

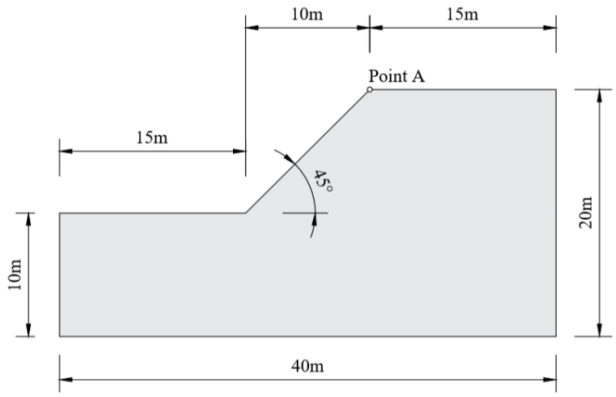

Fig. 10 Model and geometry

4.1.3 Constitutive model and material set

The material set for the analysis includes a cohesive high frictional material with a very high stiffness and a unit weight γ of 19kN/m³. Table 3 summarizes the required soil parameters for the ideal-plastic Mohr Coulomb soil model with a Mohr Coulomb failure criterion. Three strength parameters φ', ψ' and c' and two stiffness parameters E' and ν' are required to describe the mechanical material behavior. When performing FEA with non-associated flow rule, the effective dilatancy angles are ψ'=10° and ψ'=0°. For some further selected studies in a subsequent part of this chapter, it was necessary to imply a second MC (2) and a HSS (1) model. Unless otherwise stated MC (1) is always used.

Table 3 Material parameters of MC (1) model

MC (1)		
φ ‘	45	[°]
c'	6	[kPa]
ψ'	0°, 10°, 45°	[°]
E	40,000	[kPa]
ν	0.3	[-]

4.1.4 Meshes and shape functions

It is already known, that the mesh discretization and the element type for a displacement finite element method, under drained conditions, influences the safety factor strongly (Tschuchnigg, 2015). The study of the influence of the mesh on the lower and upper boundaries when performing FELA is also considered in this thesis. Three different meshes, namely coarse (144 elements), medium (467 elements) and fine mesh (1124 elements) for SRFEA, shown in Fig. 11, and FELA, shown in Fig. 12 are used for the analysis. When performing SRFEA, two different elements types (6-noded and 15n-elements) were used. Performing FELA, the mesh is refined in three iteration steps in the area where the failure occurs.

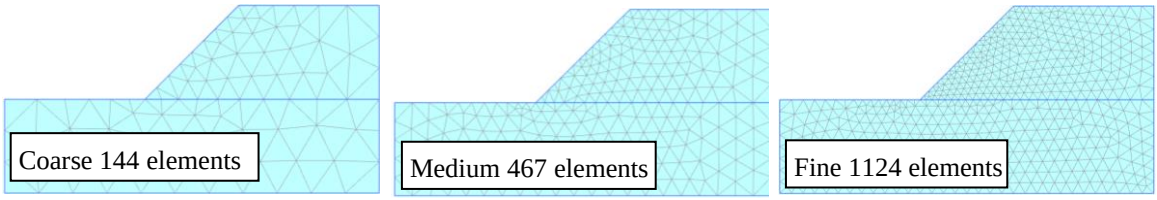

Fig. 11 Meshes for SRFEA

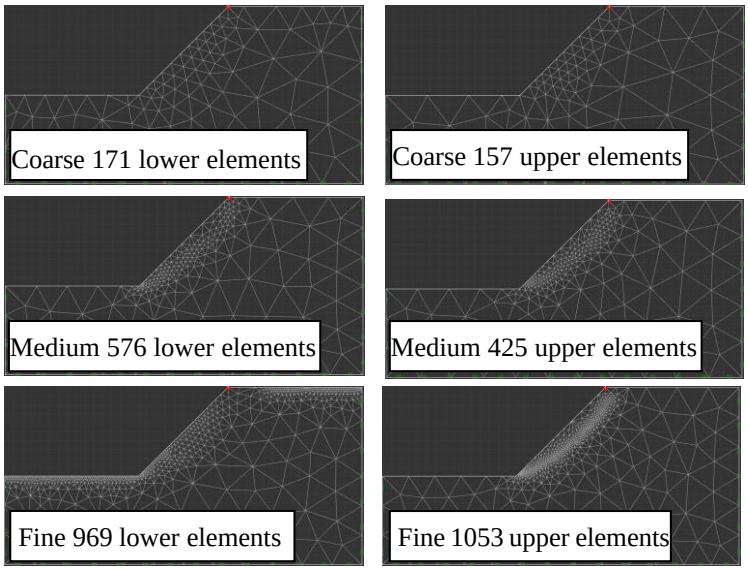

Fig. 12 Meshes for FELA

4.1.5 Calculation phases SRFEA

4.1.5.1 Initial phase (K_0 procedure)

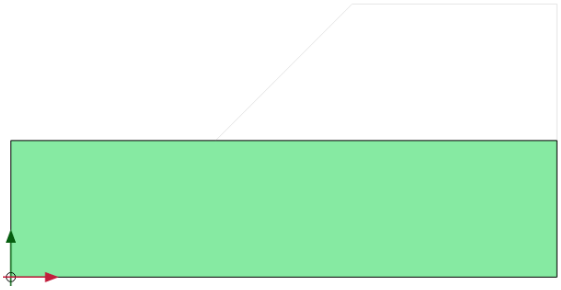

Fig. 13 Initial phase

To compute the initial effective stresses of the subsoil before construction, K_0 procedure is performed in a first calculation phase. The model of the subsoil is a rectangle with dimensions of 40x20m. The initial horizontal and vertical stresses are primarily influenced by the unit weight of the material and the history of its formation. The lateral earth pressure K_0 considers the loading history of the ground from the past, whether it is normal- or over consolidated (e.g. due to ice load in the past). However, it was previously shown by Oberhollenzer (2017) that the lateral earth pressure coefficient K_0 does not influence the FoS when performing with drained material behavior. With the empirical equation after Jaky (Eq. (20)), the lateral earth pressure coefficient K_0 is computed, where the value only depends on the effective friction angle φ' of the subsoil.

$$K_0 = 1 - sin\varphi' \tag{20}$$

As shown in Eq. (21), the effective vertical stresses are linear increasing with the depth, depending on the unit weight of the material.

$$\sigma'_{yy} = \gamma \cdot z \tag{21}$$

As shown in Eq. (22) the relationship between the vertical and horizontal effective initial stresses in the ground, is affected by the lateral earth pressure coefficient K_0.

$$\sigma'_{xx} = K_0 \cdot \sigma'_{yy} \tag{22}$$

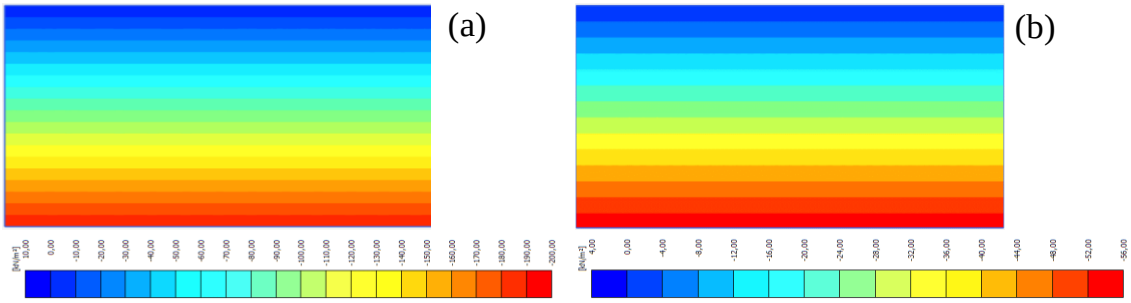

Fig. 14 (a) Initial horizontal effective stresses, (b) Initial vertical effective stresses

4.1.5.2 Plastic phase

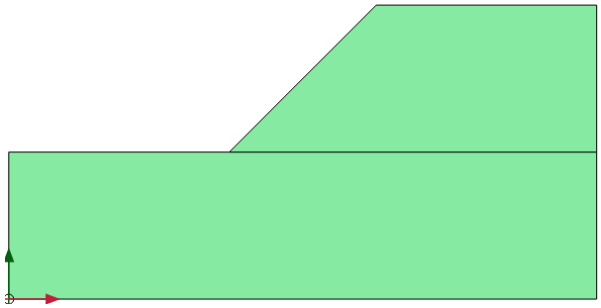

Fig. 15 Plastic phase

The second calculation phase is a plastic step which is required to compute the elastic-plastic deformations of the soil body after construction due to self-weight. The deformed soil body for different definitions of the flow rule is shown in Fig. 16.

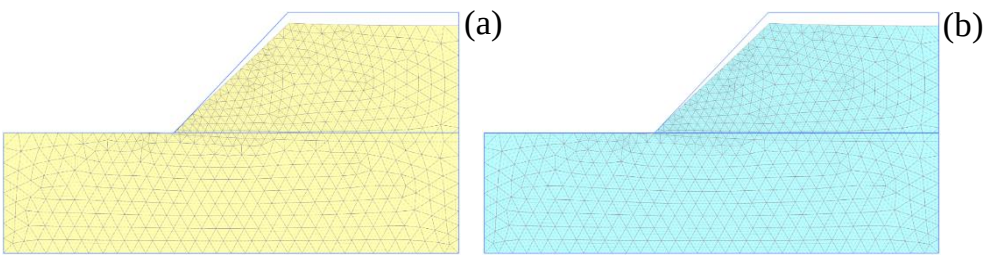

Fig. 16 Deformed soil body for different flow rules (a) ψ'=φ', (b) ψ'=0°

4.1.5.3 Safety analysis

A safety analysis in Plaxis, as a third calculation phase, is added to compute the safety factor when performing automatic SRFEA. To calculate the FoS when performing manual strength reduction, the strength parameters of the soil are reduced “by hand” until failure occurs (no safety analysis is required). Both strength reduction techniques, implemented and modified (DLL) are performed automatically and manual.

4.1.6 Calculation phases FELA

When performing finite element limit analysis (FELA) under drained conditions, the solution is independent on the initial stresses (Optum, 2018). Hence, only two calculation phases are required. The first calculation phase uses lower bound elements, the second calculation phase with upper bound elements. Both calculation phases are independent of each other.

4.2 Associated flow rule (ψ'=φ')

The aim of this chapter is to evaluate the influence of the mesh discretization and the shape function, on the obtained safety factor for ψ'=φ'. The first part deals with automatic and manual strength reduction with the displacement based finite element method (SRFEA) considering the implemented and modified (DLL) strength reduction technique. With finite element limit analysis (FELA), lower and upper bounds for three different meshes are computed. Subchapter 4.2.3 provides a comparison of the results from SRFEA and FELA.

4.2.1 SRFEA

4.2.1.1 Influence mesh discretization and shape function

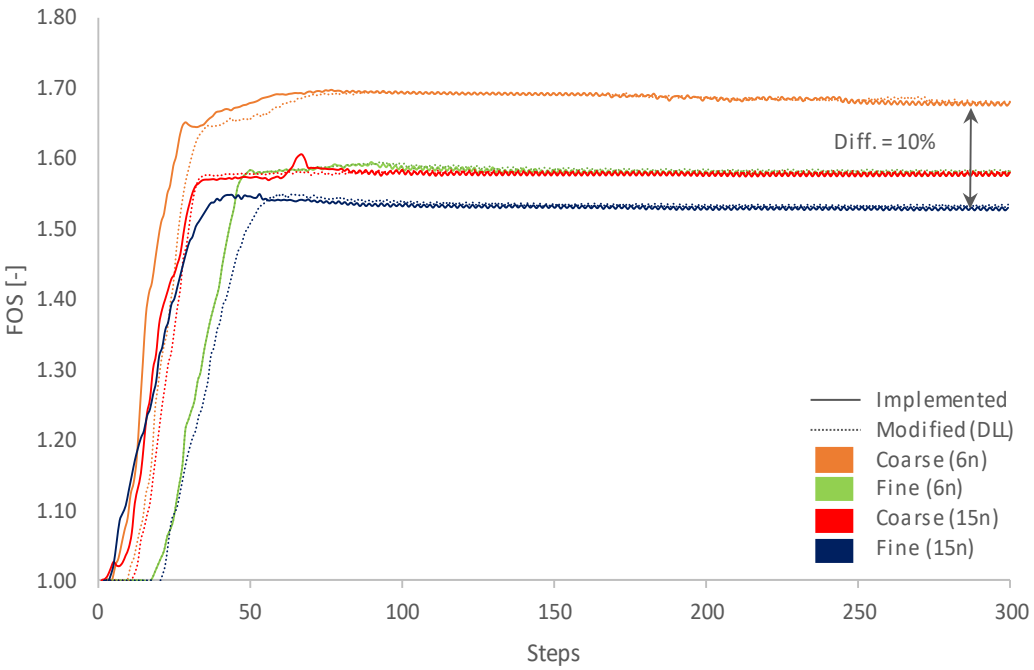

Fig. 17 Computed FoS for MC model: Comparison of implemented and modified (DLL) SRFEA for ψ'=φ'

Fig. 17 shows the factor of safety, calculated by means of the automatic strength reduction in combination with a Mohr Coulomb model for two different meshes and shape functions. The results of the implemented strength reduction technique are illustrated with full lines, whereas dotted lines demonstrate the results for the modified (DLL) technique. The evaluation of the factor of safety over calculation steps clearly indicates, that the number of finite elements and the shape function have a substantially influence on the result. Finer meshes, as well the use of higher ordered shape functions leads to a decrease of the obtained factor of safety. A factor of safety of 1.68 when performing SRFEA with a 6n-coarse mesh and 1.53 with a 15n-fine mesh is achieved. Furthermore, it should be noted that the

implemented and modified (DLL) strength reduction leads, as expected, to the same FoS.

4.2.1.2 SRFEA automatic vs. SRFEA manual

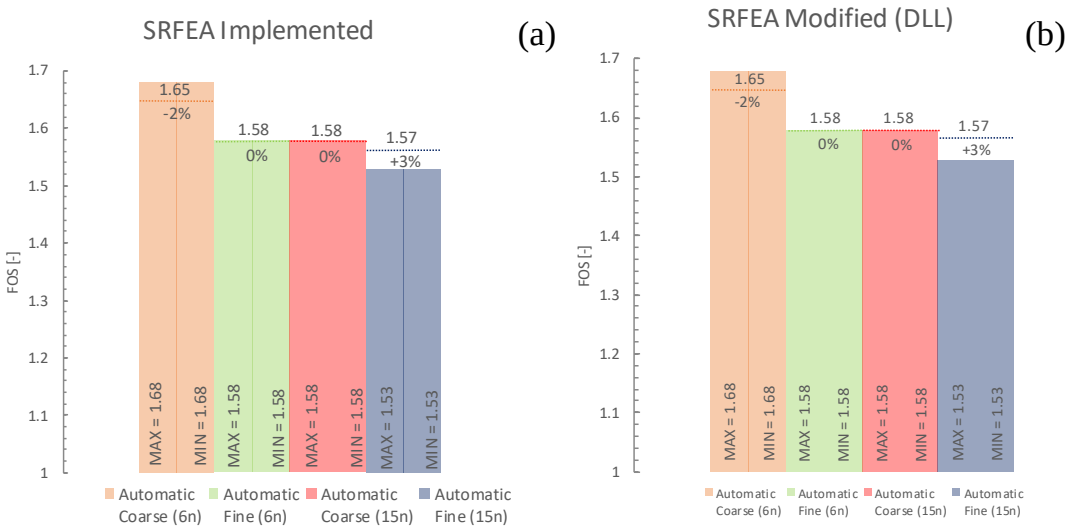

Fig. 18 Comparison of automatic and manual SRFEA for ψ'=φ': (a) SRFEA implemented, (b) SRFEA modified (DLL)

In Fig. 18 automatic and manual SRFEA are compared performing with the implemented and modified (DLL) strength reduction technique in combination with a Mohr Coulomb model. The vertical beams represent the maximum and minimum factor of safety computed during the automatic strength reduction. The horizontal dotted lines represent the manual factor of safety. As shown in Fig. 18 (a), both strength reduction techniques are in good agreement for all meshes and shape functions and differ with less than 3%. Fig. 18 (b) represents the comparison of the automatic and manual SRFEA performing the modified (DLL) strength reduction technique. Since, associated plasticity is considered the implemented and modified (DLL) strength reduction technique lead to the same results. The manual safety factor as well as the automatic FoS are strongly influenced by the mesh discretization and the shape function. However, no clear trend of the development of the manual factor of safety is visible.

4.2.1.3 Failure mechanism

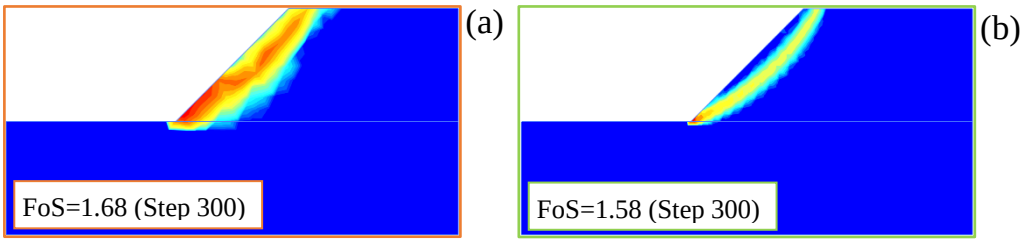

Fig. 19 Overview failure mechanism SRFEA implemented: (a) Coarse (6n), (b) Fine (6n)

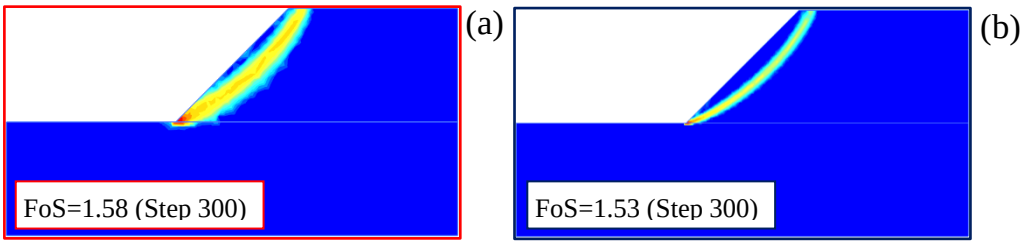

Fig. 20 Overview failure mechanism SRFEA implemented: (a) Coarse (15n), (b) Fine (15n)

Fig. 19 and Fig. 20 demonstrate the incremental deviatoric strains for different meshes and shape functions performing SRFEA with the implemented technique. The figures representing the failure mechanism performing SRFEA with the modified (DLL) technique are shown in Fig. 87 and Fig. 88 (appendix). Since the factor of safety is the same for the implemented and modified (DLL) SRFEA, the failure mechanism also looks very similar. Fig. 19 illustrates the failure mechanisms based on 6n-coarse and 6n-fine meshes. Fig. 20 shows the failure mechanism considering a 15n-coarse and 15n-fine mesh. The failure mechanism is influenced by the number of finite elements and the shape function.

4.2.1.4 Numerical settings

To study the influence of numerical control parameters on the manual safety factor, SRFEA is performed with altered values of *arc length control* (On/Off) and the *tolerated error* (0.1%, 1% and 3%). The difference between automatic and manual SRFEA is calculated with Eq. (23).

$$Error = 100 \times \left(\frac{|SRFEA_{Automatic} - SRFEA_{Manual}|}{SRFEA_{Manual}} \right) \tag{23}$$

- Arc length control (ALC)

Table 4 represents the influence of the numerical control parameter *arc length control* on the obtained manual FoS performing SRFEA (ψ'=φ'). A deactivation (ALC Off) of the setting (default setting in Plaxis ALC On) leads to higher manual factors of safety when performing SRFEA with coarse and medium meshes. For a fine mesh, the setting does not influence the obtained FoS.

Table 4 Influence arc length control on the obtained FoS (SRFEA implemented) - ψ'=φ'

	SRFEA automatic	SRFEA manual		Difference Eq. (23) [%]	
		ALC Off	ALC On	ALC Off	ALC On
Coarse (15n)	1.58	1.60	1.58	1.3 %	0.0 %
Medium (15n)	1.55	1.58	1.57	1.9 %	1.3 %
Fine (15n)	1.53	1.57	1.57	2.5 %	2.5 %

- Tolerated error

Table 5 and Table 6 represent the influence of the numerical control parameter *tolerated error* on the manual safety factor (ψ'=φ'). Three different tolerated errors (0.1%, 1% and 3%) are used for the investigation. Performing manual SRFEA, differences up to 6% compared to the automatic SRFEA are evaluated. However, as performing manual SRFEA with a tolerated error of 0.1%, the result fits very well with the automatic SRFEA with a maximum difference of 0.7%. Furthermore, it should also be noted that for a tolerated error of 3%, the mesh discretization has less influence on the manual FoS.

Table 5 Influence tolerated error on obtained FoS (SRFEA implemented) - ψ'=φ'

	SRFEA automatic	SRFEA manual		
Tolerated error		0.1 %	1 %	3 %
Coarse (15n)	1.58	1.57	1.58	1.63
Medium (15n)	1.55	1.55	1.57	1.62
Fine (15n)	1.53	1.54	1.57	1.62

Table 6 Difference SRFEA automatic and manual for different tolerated errors (SRFEA Implemented**)** - ψ'=φ'

	Difference$^{Eq. (23)}$ [%]		
Tolerated error	0.1 %	1%	3%
Coarse (15n)	0.6 %	0.0 %	3.2 %
Medium (15n)	0.0 %	1.3 %	4.5 %
Fine (15n)	0.7 %	2.6 %	5.9 %

4.2.2 FELA

4.2.2.1 Influence mesh discretization

Fig. 21 shows the results performing finite element limit analysis (FELA) for three different meshes, considering associated plasticity (ψ'=φ'). The full lines represent the lower and upper bounds, whereas dotted lines the mean value of the bounds. The computation of the mean value is carried out in Eq. (24). Since, FELA is limited to associated plasticity (ψ'=φ'), the Davis approach is not necessary for this calculation. The use of finer meshes leads to different boundaries, but it seems that the mean value is independently on the number of finite elements. A mean value of about 1.54 is obtained as performing FELA for all meshes. Using a coarse mesh, a difference of 7% between the bounds and the mean value is evaluated. However, this difference becomes smaller than 1% when performing with a fine mesh.

$$FELA_{Mean} = \frac{|FELA_{LB} + FELA_{UB}|}{2} \tag{24}$$

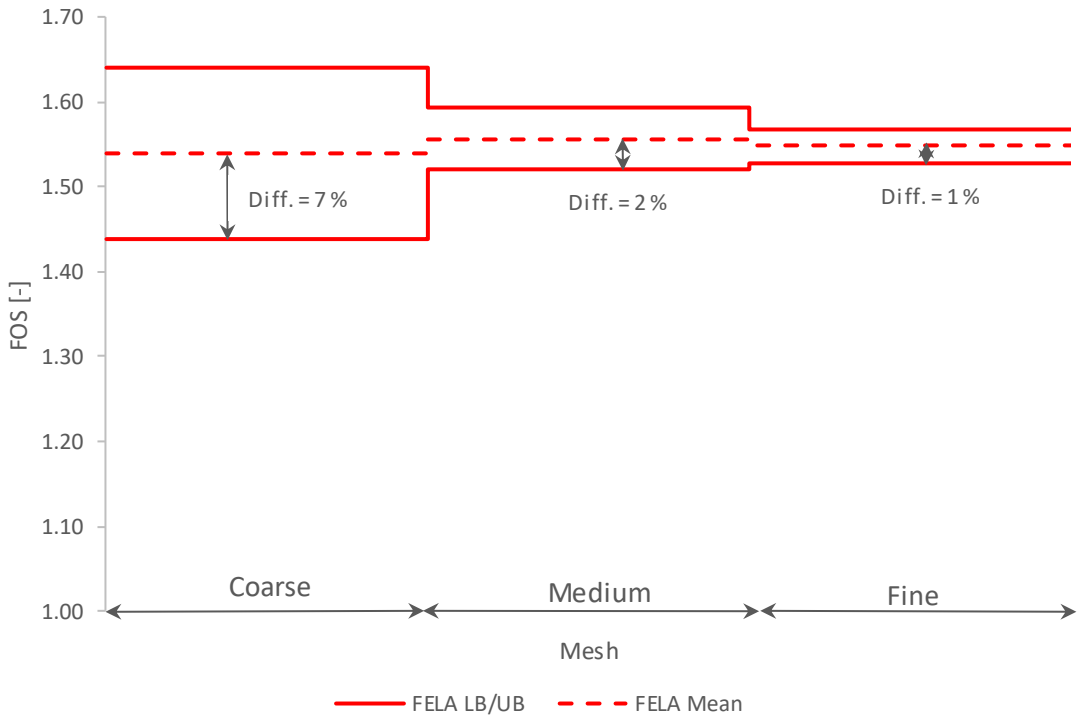

Fig. 21 Performing FELA with different meshes - ψ'=φ'

4.2.2.2 Failure mechanism

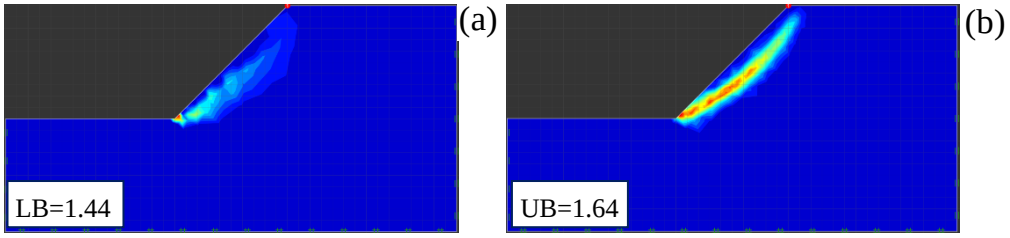

Fig. 22 Overview shear strains FELA for a coarse mesh: (a) Lower elements, (b) Upper elements

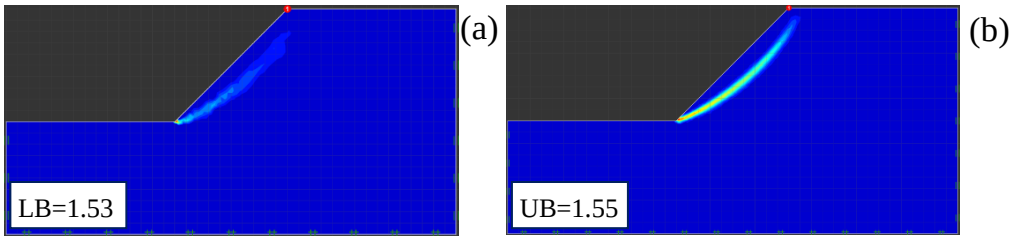

Fig. 23 Overview shear strains FELA for a fine mesh: (a) Lower elements, (b) Upper elements

Fig. 22 represents the shear strains, performing FELA with a coarse mesh for lower and upper elements. Fig. 23 demonstrates the shear strains using a fine mesh. The extent of the slip surface is strongly influenced by the number of finite elements.

4.2.3 Comparison SRFEA and FELA

Table 7 compares the results from SRFEA with FELA for two different mesh discretization and two different element types (only for SRFEA). For SRFEA the factor of safety is strongly influenced by the number of elements and the shape function. When performing FELA, the mean value is independent on the number of finite elements. It becomes evident, that the results, when performing SRFEA with a 15n-fine mesh, fits very well with the results from FELA with only a difference of 0.6%. Compared to FELA, differences up to 9.1% are evaluated when performing SRFEA with a 6n-coarse mesh.

Table 7 Comparison SRFEA and FELA - ψ'=φ'

	SRFEA implemented		FELA			Difference [%]
	Element type	FoS	LB	UB	Mean	
Coarse	6n	1.68	1.44	1.64	1.54	9.1%
	15n	1.58				2.6%
Fine	6n	1.58	1.53	1.55	1.54	2.6%
	15n	1.53				0.6 %

4.3 Non-associated flow rule (ψ'=10°)

The aim of this chapter is to evaluate the influence of the mesh discretization and the shape function on the obtained safety for ψ'=10°. As already elaborated in chapter 4.2, the first part works with automatic and manual strength reduction with the displacement based finite element method (SRFEA), considering the implemented and modified (DLL) strength reduction technique. Lower and upper bounds for three different meshes are computed with finite element analysis (FELA). Since FELA is limited to associated plasticity (ψ'=φ'), the computation is performed with the Davis approach to model non-associated plasticity. A comparison of SRFEA and FELA is given in subchapter 4.3.3.

4.3.1 SRFEA

4.3.1.1 Influence mesh discretization and shape function

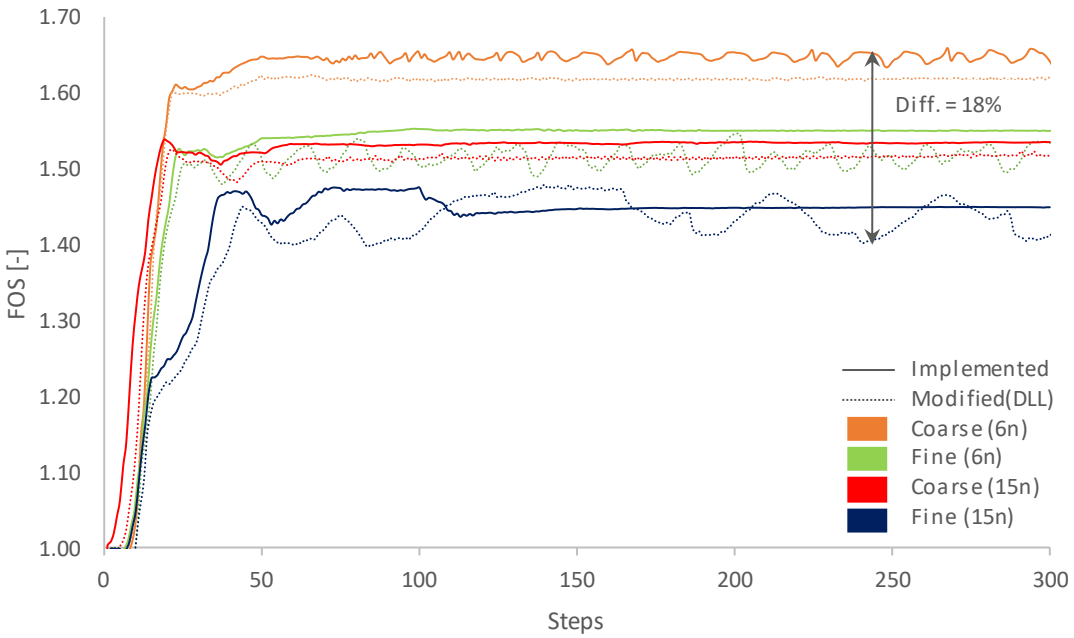

Fig. 24 Computed FoS for MC model: Comparison of implemented and modified (DLL) SRFEA for ψ'=10°

Fig. 24 shows the factor of safety, calculated by means of the automatic strength reduction in combination with a Mohr Coulomb model for two different meshes and two shape functions. The results of the implemented strength reduction technique are illustrated as full lines, whereas dotted lines demonstrate the results of the modified (DLL) strength reduction technique. The evaluation of the factor of safety over calculation steps clearly indicates that the number of finite elements and the shape function have a substantial influence on the results. Finer meshes as well as the use of higher ordered shape functions lead to lower safety factors. Since, the implemented technique does not consider a reduction of the effective

strength parameter ψ', slightly higher FoS are obtained compared to the modified (DLL) technique for all meshes and shape functions. Furthermore, for fine meshes (6n and 15n), a slightly oscillation of the FoS occurs when performing the modified (DLL) strength reduction. A maximum factor of safety of 1.66 is obtained performing implemented SRFEA with a 6n-coarse mesh. The minimum factor of safety of 1.40 is obtained when performing the modified (DLL) SRFEA with a 15n-fine mesh.

4.3.1.2 SRFEA automatic vs. SRFEA manual

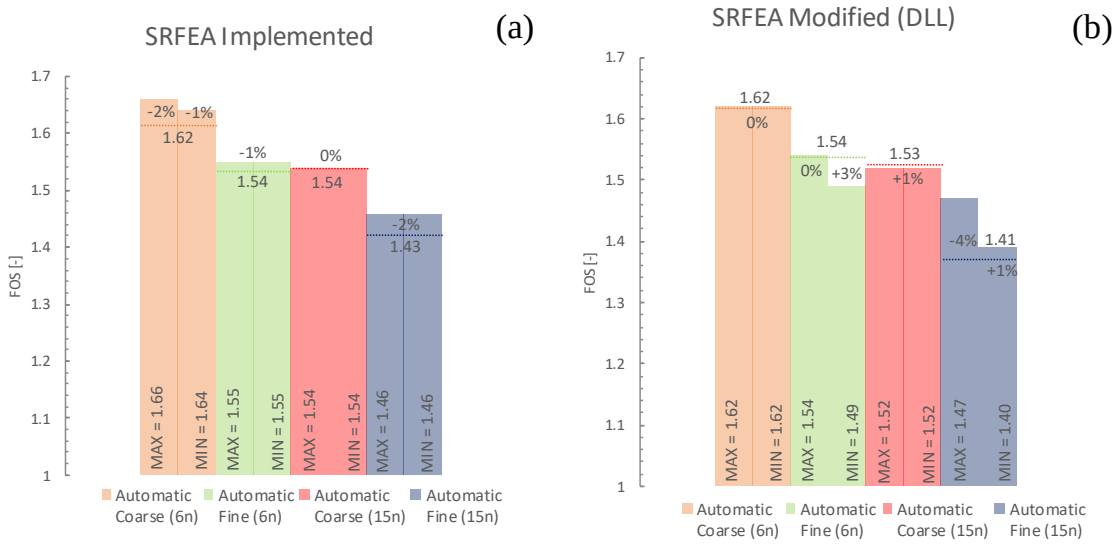

Fig. 25 Comparison of automatic and manual SRFEA for ψ'=10°: (a) SRFEA implemented, (b) SRFEA Modified (DLL)

In Fig. 25 automatic and manual SRFEA are compared using the implemented and modified (DLL) strength reduction technique in combination with a Mohr Coulomb model. Vertical beams represent the maximum and minimum safety factor, computed with the automatic strength reduction. The horizontal dotted lines demonstrate the factor of safety, performing the manual SRFEA. As shown in Fig. 25 (a) the automatic and manual SRFEA (implemented) are in good agreement for all meshes and shape functions and differ from each other with less than 2%. Fig. 25 (b) represents the comparison of the automatic and manual SRFEA performing the modified (DLL) strength reduction technique. Automatic and manual strength reduction are in good agreement for all meshes and shape functions and differ from each other with less than 4%. The manual factor of safety is, as already shown with the automatic FoS, strongly influenced by the mesh discretization and shape function for implemented and modified (DLL) SRFEA. Furthermore, the same manual safety factors for a 6n-coarse and a 6n-fine mesh are obtained for the implemented and modified (DLL) strength reduction technique.

4.3.1.3 Failure mechanism

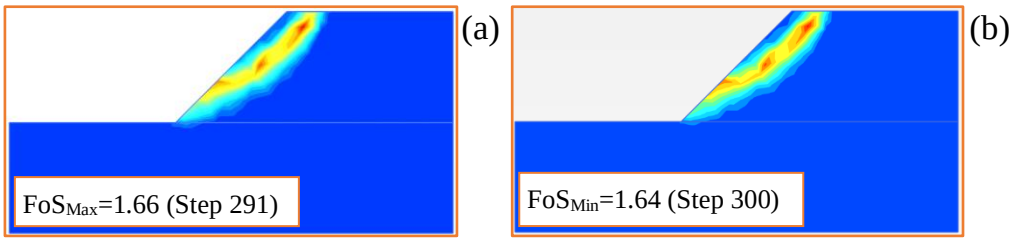

Fig. 26 Overview failure mechanism SRFEA implemented: (a) Coarse (6n) (FoS$_{Max}$), (b) Coarse (6n) (FoS$_{Min}$)

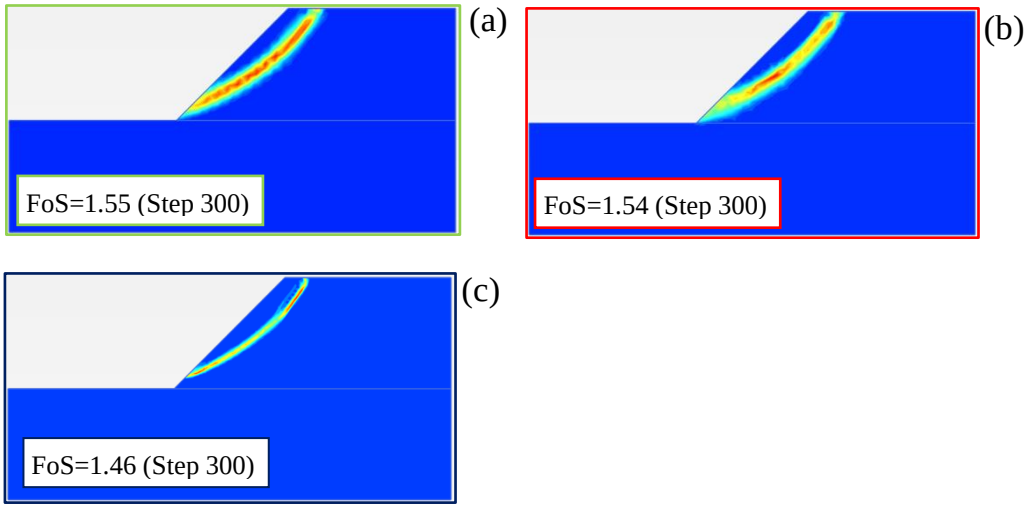

Fig. 27 Overview failure mechanism SRFEA implemented: (a) Fine (6n), (b) Coarse (15n), (c) Fine (15n)

Fig. 26 and Fig. 27 represent the incremental deviatoric strains for different meshes and shape function, when performing implemented SRFEA. The failure mechanisms as carrying out the modified (DLL) strength reduction technique are shown in Fig. 89 and Fig. 90 (appendix). Fig. 26 shows the failure mechanism for the maximum and minimum obtained safety factor, performing SRFEA with a 6n-coarse mesh, due to the small oscillation of the factor of safety (1.64-1.66), no difference of shape of failure mechanism is noticed. Fig. 27 shows the failure mechanism performing SRFEA with different meshes and shape functions. Overall, the failure mechanism is the same for all meshes, but its extent is influenced by the number of finite elements and the shape function.

4.3.1.4 Numerical settings

To study the influence of numerical control parameters on the manual safety factor, SRFEA is performed with altered values of *arc length control* (On/Off) and the *tolerated error* (0.1%, 1% and 3%). Furthermore, the influence of the *incremental multiplier* (0.002, 0.01, 0.1), when performing automatic SRFEA is part of the study. The difference between automatic and manual SRFEA is computed with Eq. (23).

$$Error\ [\%] = 100 \times \left(\frac{|SRFEA_{Automatic} - SRFEA_{Manual}|}{SRFEA_{Manual}} \right) \tag{23}$$

- Arc length control

Table 8 represents the influence of the numerical control parameter *arc length control* on the obtained manual safety factor, performing implemented SRFEA (ψ'=10°). A deactivation (ALC Off) of the setting (default in Plaxis ALC On) leads to higher FoS when performing SRFEA with 15n-fine and 15n-medium meshes, but for 15n-coarse mesh, no difference is noticeable. Differences up to 3.4% (for a fine mesh) between the automatic and manual SRFEA have to be noted, when arc length control is not activated.

Table 8 Influence arc length control on obtained FoS (SRFEA implemented) - ψ'=10°

	SRFEA automatic	SRFEA manual		Difference Eq. (23) [%]	
		ALC Off	ALC On	ALC Off	ALC On
Coarse (15n)	1.54	1.54	1.54	0.0%	0.0%
Medium (15n)	1.50	1.53	1.51	2.0%	0.7%
Fine (15n)	1.46	1.50	1.43	3.4%	1.4%

Table 9 demonstrates the influence of the numerical control parameter *arc length control* on the obtained manual FoS, as performing modified (DLL) SRFEA (ψ'=10°). Similar to performing implemented SRFEA, a deactivation (ALC Off) of the setting (default in Plaxis ALC On) leads to higher FoS for 15n-fine and 15n-medium meshes. For a 15n-coarse mesh no difference is noticeable. Differences up to 7.4% between automatic and manual SRFEA have to be noticed when arc length control is not activated.

Table 9 Influence arc length control on obtained FoS (SRFEA modified (DLL)) - ψ'=10°

	SRFEA automatic	SRFEA manual		Difference Eq. (23) [%]	
		ALC Off	ALC On	ALC Off	ALC On
Coarse (15n)	1.52	1.53	1.53	0.7 %	0.7 %
Medium (15n)	1.44-1.50	1.53	1.46	2.0 - 6.3%	1.4 - 2.7%
Fine (15n)	1.40-1.47	1.50	1.41	2.0 - 7.1 %	0.7 - 4.1%

- Tolerated error

Table 10 and Table 11 show the influence and difference of the numerical control parameter *tolerated error* on the obtained manual FoS performing SRFEA implemented (ψ'=10°). Three different tolerated errors (0.1%, 1% and 3%) are part of the investigation. Compared to the automatic SRFEA, differences up to 9.6% have to be noted when performing manual SRFEA with a tolerated error of 3%. However, performing manual SRFEA with tolerated errors of 0.1% and 1%, the results correspond very well with the automatic SRFEA (with maximum differences up to 4.7%). When performing SRFEA manually with a tolerated error of 3%, the mesh discretization has no influence on the FoS.

Table 10 Influence tolerated on obtained FoS (SRFEA implemented) – ψ'=10°

	SRFEA automatic	SRFEA manual		
Tolerated error		0.1%	1%	3%
Coarse (15n)	1.54	1.53	1.54	1.60
Medium (15n)	1.50	1.43	1.51	1.60
Fine (15n)	1.46	1.40	1.43	1.60

Table 11 Difference SRFEA automatic and manual for different tolerated errors (SRFEA implemented) – ψ'=10°

	Difference Eq. (23) [%]		
Tolerated error	0.1%	1%	3%
Coarse (15n)	0.6 %	0.0 %	3.9 %
Medium (15n)	4.7 %	0.7 %	6.7 %
Fine (15n)	4.1 %	2.1 %	9.6 %

Table 12 and Table 13 show the influence and difference of the numerical control parameter *tolerated error* on the obtained manual FoS, performing SRFEA modified (DLL) (ψ'=10°). Three different tolerated errors (0.1%, 1% and 3%) are used in the investigation. Compared to the automatic SRFEA, differences up to 12.9% have to be noted when performing manual SRFEA with a tolerated error of 3%. However, when performing manual SRFEA with tolerated errors of 0.1% and 1%, the results fits very well with the automatic SRFEA (with maximum differences up to 7.5%). As for implemented SRFEA, performing SRFEA manually with a tolerated error of 3%, the mesh discretization has no influence on the results.

Table 12 Influence tolerated on obtained FoS (SRFEA modified (DLL)) – ψ'=10°

	SRFEA automatic	SRFEA manual		
Tolerated error		0.1%	1%	3%
Coarse (15n)	1.52	1.51	1.53	1.58
Medium (15n)	1.44 - 1.50	1.44	1.46	1.58
Fine (15n)	1.40 - 1.47	1.36	1.41	1.58

Table 13 Difference SRFEA automatic and manual for different tolerated errors (SRFEA modified (DLL)) – ψ'=10°

	Difference [%]		
Tolerated error	0.1%	1%	3%
Coarse (15n)	0.7 %	0.7 %	3.9 %
Medium (15n)	0.0 – 4.0 %	1.4 – 2.7 %	5.3 - 9.7 %
Fine (15n)	2.9 – 7.5 %	0.7 – 4.1 %	7.5 - 12.9 %

- Incremental multiplier M_{SF}

Table 14 and Table 15 show the influence of the numerical control parameter *incremental multiplier* on the obtained safety factor when performing automatic SRFEA. Three different incremental multipliers (0.002, 0.01 and 0.1) are part of the research. It is evident, that this numerical control parameter has no significant influence on the FoS when performing SRFEA implemented as well SRFEA modified (DLL). Fig. 95, Fig. 96, Fig. 97 and Fig. 98 (appendix) show the FoS vs. steps for each mesh and shape function, considering different values of the incremental multiplier.

Table 14 Influence of the incremental multiplier on the obtained FoS (SRFEA implemented) – ψ'=10°

	Incremental multiplier		
Mesh	0.002	0.01	0.1
Coarse (6n)	1.65	1.65	1.65
Fine (6n)	1.55	1.55	1.55
Coarse (15n)	1.53	1.53	1.53
Fine (15n)	1.46	1.46	1.45

Table 15 Influence of the incremental multiplier on the obtained FoS (SRFEA modified (DLL)) – ψ'=10°

	Incremental multiplier		
Mesh	0.002	0.01	0.1
Coarse (6n)	1.62	1.62	1.62
Fine (6n)	1.52	1.49 – 1.54	1.54
Coarse (15n)	1.52	1.52	1.52
Fine (15n)	1.39 – 1.47	1.40 – 1.47	1.40 – 1.48

4.3.2 FELA

4.3.2.1 Influence mesh discretization

Fig. 28 shows the results as performing finite element limit analysis (FELA) for three different meshes in combination with non-associated plasticity (ψ'=10°). The full lines represent the lower and upper bounds and the dotted lines illustrate the mean value of the bounds. The mean value is computed in Eq. (24). Since FELA is limited to associated plasticity (ψ'=φ'), the Davis approach is necessary for the present computation. Performing FELA in combination with Davis A leads to very conservative results ($FELA_{Mean}$= 1.23). When performing FELA in combination with Davis B, where the effective dilatancy angle ψ' is reduced in the same way as the effective friction angle φ', a mean value of 1.40 is reached for all meshes. Performing FELA in combination with Davis C, a slightly higher mean value of 1.43 is obtained. The effective dilatancy angle ψ' is kept constant for this procedure. Performing FELA with a coarse mesh the difference between the bounds and the mean value is about 10%, but when using a fine mesh, the difference is reduced.

$$FELA_{Mean} = \frac{|FELA_{LB} + FELA_{UB}|}{2} \tag{24}$$

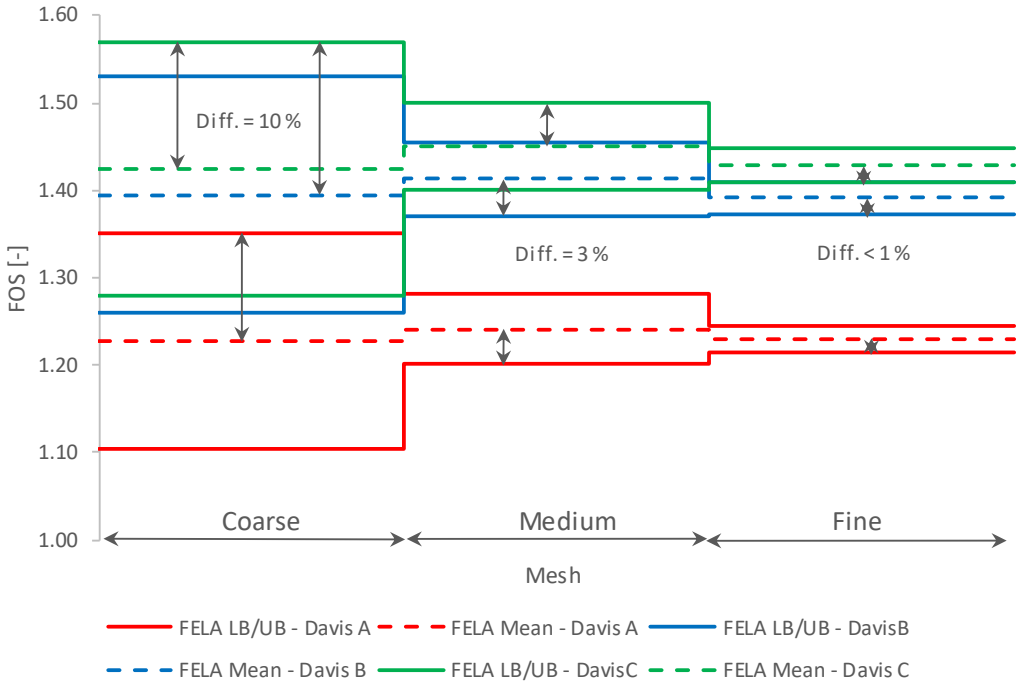

Fig. 28 Performing FELA in combination with different Davis approaches for different meshes – ψ'=10°

4.3.2.2 Failure mechanism

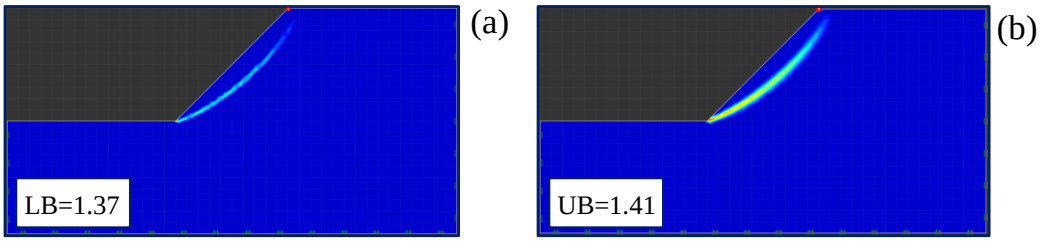

Fig. 29 Overview shear strains FELA (Davis B) for a fine mesh : (a) Lower elements, (b) Upper elements

Fig. 29 demonstrates the shear strains using a fine mesh. The failure mechanism considering the approach after Davis A, and Davis C are shown in Fig. 91, Fig. 92, Fig. 93 and Fig. 94 (appendix).

4.3.3 Comparison SRFEA and FELA

Table 16 summarizes the results from SRFEA and FELA in combination with different Davis approaches for two different meshes and shape functions (for SRFEA). Performing FELA in combination with Davis A, leads to very conservative results which are not in good agreement with the results from SRFEA. FELA in combination with Davis B is in good agreement with the results from modified (DLL) SRFEA. Performing FELA in combination with Davis C (it does not consider a reduction of the effective dilatancy angle ψ'), these results are best compatible with the implemented SRFEA. Table 16 confirms that the upper and lower bounds of FELA, considering Davis B and Davis C, are in good agreement with the obtained factor of safety from SRFEA for a 15n-fine mesh, but they are still slightly conservative.

Table 17 shows the difference between SRFEA and FELA. Analyzes based on 6n-elements and a coarse mesh lead to large differences between SRFEA and FELA (up to 18.5%). However, when using 15n-elements with a fine mesh the differences between SRFEA modified (DLL) and FELA (Davis B) is smaller than 6%, for SRFEA implemented and FELA (Davis C) even smaller 3%.

Table 16 Comparison SRFEA and FELA (Davis approach) – ψ'=10°

	SRFEA impl. (*modified)		FELA – Davis A			FELA – Davis B			FELA – Davis C		
		FoS	LB	UB	Mean	LB	UB	Mean	LB	UB	Mean
Coarse	6n	1.64 – 1.66 (*1.62)	1.10	1.35	1.23	1.26	1.53	1.40	1.28	1.57	1.43
	15n	1.54 (*1.52)									
Fine	6n	1.55 (*1.49 - 1.54)	1.21	1.25	1.23	1.37	1.41	1.39	1.41	1.45	1.43
	15n	1.46 (*1.40 - 1.47)									

Table 17 Difference SRFEA and FELA (Davis approach) – ψ'=10°

		Difference [%]		
		Davis A	Davis B	Davis C
Coarse	6n	33.3 – 35% (*31.7%)	17.1 – 18.5% (*15.7%)	14.7 – 16.1% (13.3%)
	15n	25.2 % (*19.1%)	9.1% (*8.6%)	7.7% (*6.3%)
Fine	6n	26.0% (*21.1-25.2%)	11.5% (*7.2-10-10.8%)	8.4% (*4.2-7.7%)
	15n	18.7 % (*13.8 -19.5%)	3.5 % (*0.7 - 5.7%)	2.1% (*2.1 - 2.8%)

4.4 Non-associated flow rule (ψ'=0°)

The aim of this section is to evaluate the influence of the mesh discretization and shape functions (for SRFEA) on the obtained factor of safety for ψ'=0°. As already shown in chapter 4.2 and 4.3, the first part works with the automatic and manual strength reduction with the displacement based finite element method (SRFEA), considering the implemented and modified (DLL) strength reduction technique. As for the finite element analysis technique, lower and upper bounds for three different meshes are computed. Since FELA is limited to associated plasticity (ψ'=φ'), the necessity of the Davis approach (A, B &C) is treated in this study to model non-associated plasticity. FELA in combination with Davis B and Davis C lead to the same results in terms of an effective dilatancy angle ψ'=0°.

4.4.1 SRFEA

4.4.1.1 Influence mesh discretization and shape function

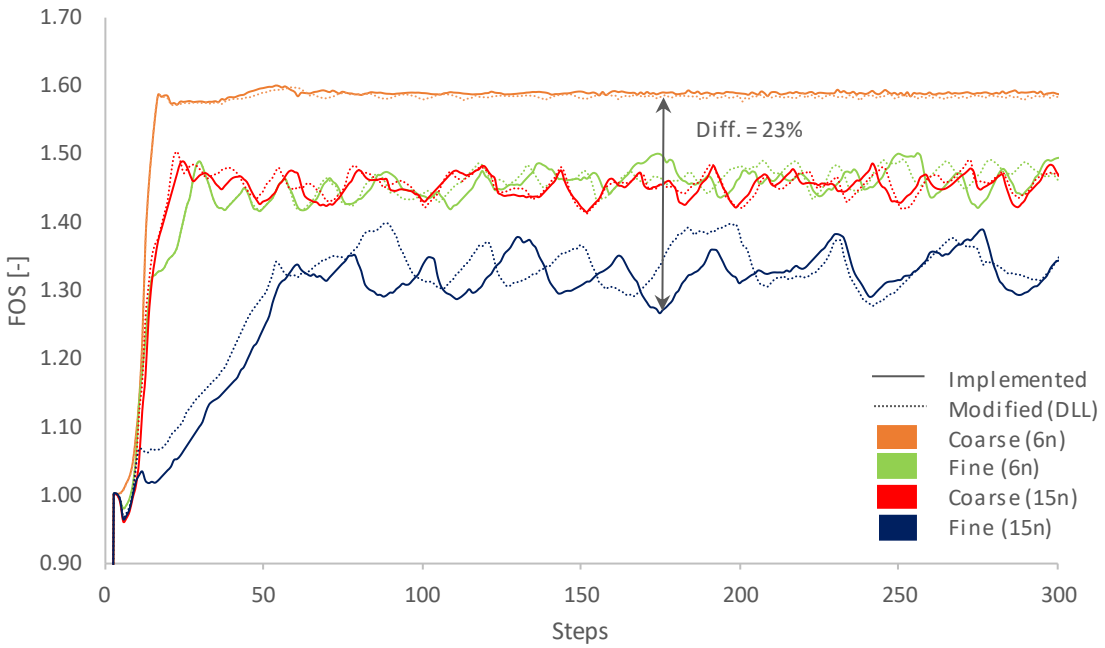

Fig. 30 Computed FoS for MC model: Comparison of implemented and modified (DLL) SRFEA for ψ'=0°

Fig. 30 shows the factor of safety, calculated by means of the automatic strength reduction in combination with a Mohr Coulomb model for two different meshes and two shape functions. The results of the implemented strength reduction technique are represented with full lines, whereas dotted lines demonstrate the results for the modified (DLL) strength reduction. The evaluation of the factor of safety over calculation steps clearly indicates that the number of finite elements and the shape function have a substantial influence on the obtained FoS. Finer

meshes as well as the use of higher ordered shape functions lead to lower safety factors. Due to the high degree of non-associativity (φ'-ψ') and the steep slope inclination, a scatter of the factor of the safety is observed. However, the range of this scatter remains the same when performing SRFEA with the implemented and the modified (DLL) technique. A maximum factor of safety of 1.59 is obtained when performing SRFEA with 6n-coarse mesh. The minimum factor of safety of 1.28 is achieved when using a 15n-fine mesh. Furthermore, it should be mentioned that, when performing SRFEA with a 6n-coarse mesh, no oscillations are observed.

4.4.1.2 SRFEA automatic vs. SRFEA manual

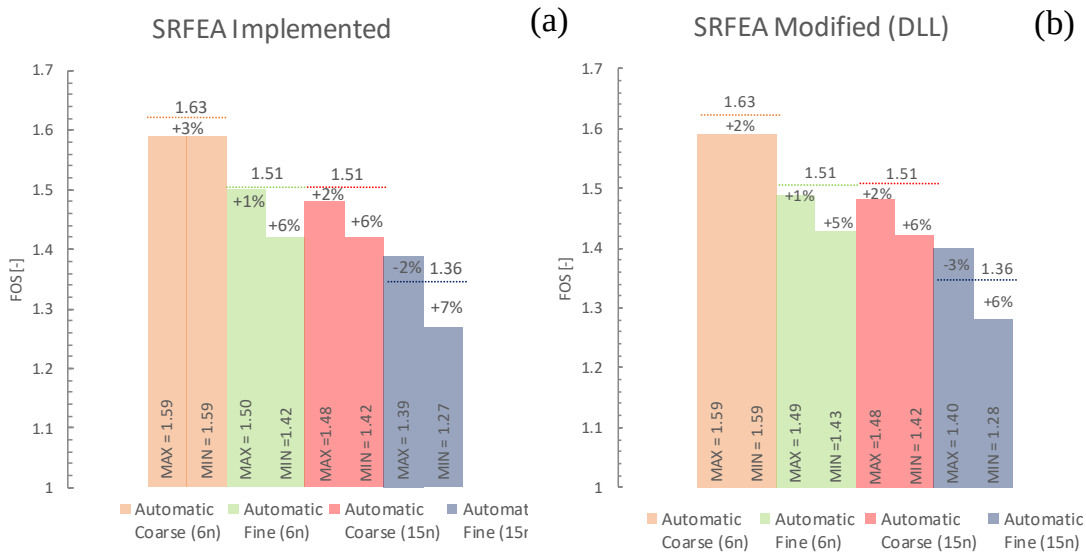

Fig. 31 Comparison of automatic and manual SRFEA for ψ'=0°: (a) SRFEA implemented, (b) SRFEA modified (DLL)

In Fig. 31 automatic and manual SRFEA are compared performing with the implemented and modified (DLL) strength reduction technique in combination with a Mohr Coulomb model. The vertical beams represent the maximum and minimum factors of safety computed during the automatic strength reduction. The horizontal dotted lines represent the manual factor of safety. As shown in Fig. 31 (a) both strength reduction techniques are in good agreement for all meshes and shape functions and differ from each other with less than 7%. Fig. 31 (b) represents the comparison of the automatic and manual SRFEA considering the modified (DLL) strength reduction technique. Since non-associated plasticity with an effective dilatancy angle ψ'=0° is considered for this analysis, the implemented and modified (DLL) strength reduction technique leads to the same results. The manual factor of safety is, as well as the automatic FoS, strongly influenced by the mesh discretization and shape function.

4.4.1.3 Failure mechanism

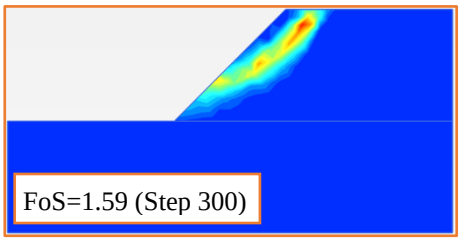

Fig. 32 Overview failure mechanism SRFEA implemented: Coarse (6n)

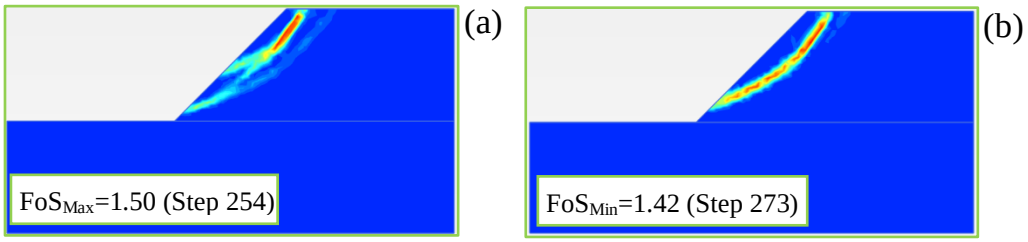

Fig. 33 Overview failure mechanism SRFEA implemented: (a) Fine (6n) - FoS_{Max}, (b) Fine (6n) - FoS_{Min}

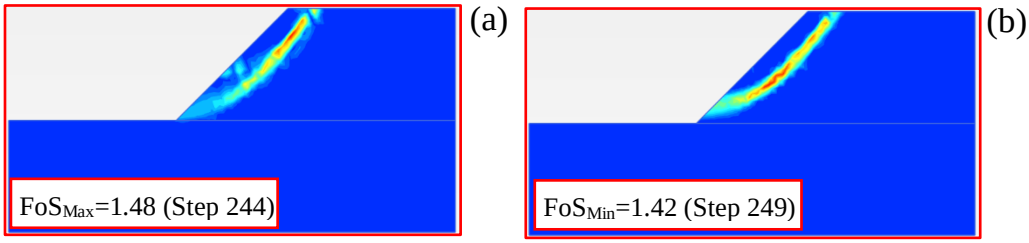

Fig. 34 Overview failure mechanism SRFEA implemented: (a) Coarse (15n) - FoS_{Max}, (b) Coarse (15n) - FoS_{Min}

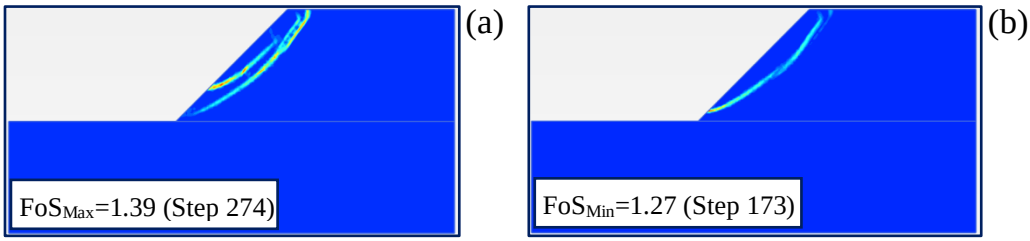

Fig. 35 Overview failure mechanism SRFEA implemented: (a) Fine (15n) - FoS_{Max}, (b) Fine (15n) - FoS_{Min}

Fig. 32, Fig. 33, Fig. 34 and Fig. 35 represent the incremental deviatoric strains performing SRFEA implemented with different meshes and shape functions. The figures representing the failure mechanism for the modified (DLL) strength reduction technique, are shown in Fig. 99 and Fig. 100 (appendix). Since, the factor of safety is the same for implemented and modified (DLL) SRFEA, also the failure mechanisms look similar. Due the high amount of non-associativity (φ'-ψ'), an oscillation of the obtained factor of safety, as already shown in Fig. 30, occurs. This scatter also leads to a change of the shape of the incremental deviatoric strains during the calculation. Only when performing SRFEA with a 6n-coarse mesh, no oscillations occur. The incremental deviatoric strains presented subsequently show

the failure mechanism for the maximum and minimum obtained safety factor for each mesh and node function. The failure mechanism is strongly influenced by the number of finite elements and the shape function.

4.4.1.4 Numerical settings

To study the influence of numerical control parameters on the manual safety factor, SRFEA is performed with altered values of *arc length control* (On/Off) and *tolerated error* (0.1%, 1% and 3%). Furthermore, the influence of the *incremental multiplier* (0.002, 0.01, 0.1), when performing automatic SRFEA, is included in the following study. The difference between automatic and manual SRFEA is computed according to Eq. (23).

$$Error\ [\%] = 100 \times \left(\frac{|SRFEA_{Automatic} - SRFEA_{Manual}|}{SRFEA_{Manual}} \right) \tag{23}$$

- Arc length control

Table 18 represents the influence of the numerical control parameter *arc length control* on the obtained manual FoS for non-associated plasticity (ψ'=0°). A deactivation (ALC Off) of the setting (default in Plaxis ALC On) leads to higher manual FoS when performing SRFEA with a medium mesh, but when using a coarse and fine meshes, the setting does not influence the results.

Table 18 Influence arc length control (SRFEA implemented) – ψ'=0°

	SRFEA automatic	SRFEA manual		Difference Eq. (23) [%]	
		ALC Off	ALC On	ALC Off	ALC On
Coarse (15n)	1.42 - 1.48	1.51	1.51	1.1 - 6.3 %	1.1 - 6.3 %
Medium (15n)	1.36 - 1.46	1.48	1.38	1.4 - 8.8 %	1.5 – 5.5 %
Fine (15n)	1.27 - 1.39	1.36	1.36	2.2 - 7.1 %	2.2 - 7.1 %

- Tolerated error

Table 19 and Table 20 demonstrate the influence of the numerical control parameter *tolerated error* on the obtained manual FoS, performing a standard SRFEA (ψ'=0°). Three different tolerated errors (0.1%, 1% and 3%) are used for this study. Performing manual SRFEA with a tolerated error of 3%, differences up to 21% compared to the automatic SRFEA were determined. However, when performing SRFEA with a tolerated error of 0.1% the results fit very well with the results from automatic SRFEA, with maximum differences up to 6.5%. Performing

manual SRFEA with a tolerated error of 3%, the mesh has no significant influence on the obtained safety factor.

Table 19 Influence tolerated error (SRFEA implemented) – ψ'=0°

	SRFEA automatic	SRFEA manual		
Tolerated error		0.1%	1%	3%
Coarse (15n)	1.42 - 1.48	1.50	1.51	1.54
Medium (15n)	1.36 – 1.46	1.33	1.38	1.54
Fine (15n)	1.27 - 1.39	1.30	1.36	1.54

Table 20 Difference SRFEA automatic and manual for different tolerated errors (SRFEA implemented) – ψ'=0°

	Difference [%]		
Tolerated error	0.1%	1%	3%
Coarse (15n)	1.4 - 5.6 %	2.0 - 6.3 %	4.1 - 8.5 %
Medium (15n)	2.2 – 8.9 %	1.5 – 5.5 %	5.5 - 13.2 %
Fine (15n)	2.4 – 6.5 %	2.2 - 7.1 %	9.7 - 21.3 %

- Incremental multiplier M_{SF}

Table 21 and Table 22 show the influence of the numerical control parameter *incremental multiplier* on the obtained safety factor when performing automatic SRFEA. Three different incremental multipliers (0.002, 0.01 and 0.1) are part of the study. It is evident, that the numerical control parameter does not influence the results strongly. Fig. 103, Fig. 104, Fig. 105 and Fig. 106 (appendix) represents the factor of safety, calculated by means of the automatic strength reduction for different meshes, node functions and incremental multiplier.

Table 21 Influence of the incremental multiplier on the obtained FoS (SRFEA implemented) – ψ'=0°

	Incremental multiplier		
Mesh	0.002	0.01	0.1
Coarse (6n)	1.59	1.59	1.59
Fine (6n)	1.41 – 1.50	1.42 – 1.50	1.42 – 1.50
Coarse (15n)	1.41 – 1.48	1.42 – 1.48	1.42 – 1.50
Fine (15n)	1.27 – 1.42	1.27 – 1.39	1.28 – 1.42

Table 22 Influence of the incremental multiplier on the obtained FoS (SRFEA modified (DLL)) – ψ'=0°

	Incremental multiplier		
Mesh	0.002	0.01	0.1
Coarse (6n)	1.59	1.59	1.59
Fine (6n)	1.41 – 1.50	1.43 – 1.49	1.43 – 1.50
Coarse (15n)	1.42 – 1.49	1.42 – 1.48	1.43 – 1.50
Fine (15n)	1.27 – 1.42	1.28 – 1.40	1.28 – 1.40

4.4.2 FELA

4.4.2.1 Influence mesh discretization

Fig. 36 represents the results performing finite element limit analysis (FELA) for three different meshes in combination with non-associated plasticity (ψ'=0°). The full lines represent the lower and upper bounds, the dotted lines illustrate the mean value of the boundaries. The mean value is computed according to Eq. (24). Since FELA is limited to associated plasticity (ψ'=φ'), the Davis approach is needed for the following computation. Performing FELA with Davis A leads, as already shown in the previous section, to very conservative results ($FELA_{Mean}$=1.09). Since the effective dilatancy angle is ψ'=0°, the results are the same ($FELA_{Mean}$=1.26), when performing FELA with Davis B and Davis C. Furthermore, the upper and lower bounds are influenced by the mesh discretization, but the mean value does not depend on the number of the finite elements. When performing FELA with a coarse mesh, differences up to 10% between the bounds and the mean value become visible. However, the differences are smaller than 1% when working with a fine mesh.

$$FELA_{Mean} = \frac{|FELA_{LB} + FELA_{UB}|}{2} \tag{24}$$

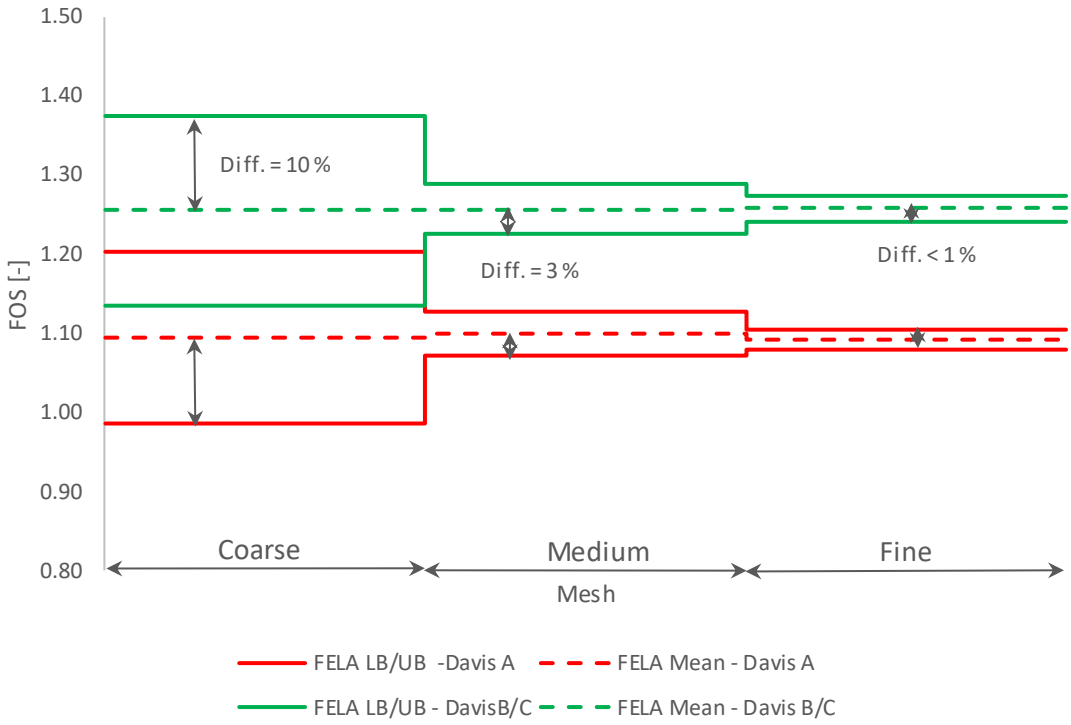

Fig. 36 Performing FELA in combination with different Davis approaches for different - ψ'=0°

4.4.2.2 Failure mechanism

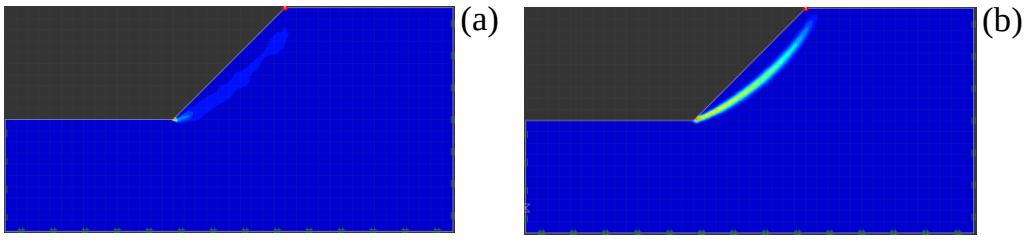

Fig. 37 Overview shear strains FELA (Davis B/C) for a fine mesh: (a) Lower elements, (b) Upper elements

Fig. 37 represents the shear strains when performing FELA with a coarse and fine mesh in combination with Davis B/C approach. The failure mechanism in combination with Davis A are shown in Fig. 101 and Fig. 102 (appendix).

4.4.3 Comparison SRFEA and FELA

Table 23 summarizes the results from SRFEA and FELA in combination with the Davis approaches for two different meshes and shape functions (for SRFEA). Performing FELA in combination with Davis A, leads to very conservative results which are not in good agreement with the results from SRFEA. Table 23 confirms that the upper and lower bounds performing FELA in combination with Davis B/C fits very well with the results from SRFEA for a 15n-fine mesh, but they are still slightly conservative. Table 24 shows the differences between SRFEA and FELA. Using a 6n-coarse mesh, the differences up to 27.2% becomes evident when performing FELA in combination with Davis B/C, compared to SRFEA. However, using a 15n elements with a fine mesh the difference between SRFEA and FELA in combination with Davis B/C is 0.8 – 10.3%.

Table 23 Comparison SRFEA and FELA (Davis approach) – ψ'=0°

	SRFEA implemented		FELA – Davis A			FELA – Davis B/C		
	Element type	FoS	LB	UB	Mean	LB	UB	Mean
Coarse	6n	1.59	0.99	1.20	1.09	1.14	1.37	1.25
	15n	1.42 – 1.48						
Fine	6n	1.42-1.50	1.08	1.11	1.09	1.24	1.27	1.26
	15n	1.27 – 1.39						

Table 24 Difference SRFEA and FELA (Davis approach) – ψ'=0°

		Difference [%]	
		Davis A	Davis B/C
Coarse	6n	45.8%	27.2%
	15n	30.3 – 35.8%	13.6 – 18.4 %
Fine	6n	30.3 - 37.6%	12.7-19.0%
	15n	16.5 – 27.5 %	0.8 – 10.3%

4.5 Influence of the flow rule on the FoS

The purpose of this section is to evaluate the influence of the flow rule, on the obtained safety factor when performing SRFEA.

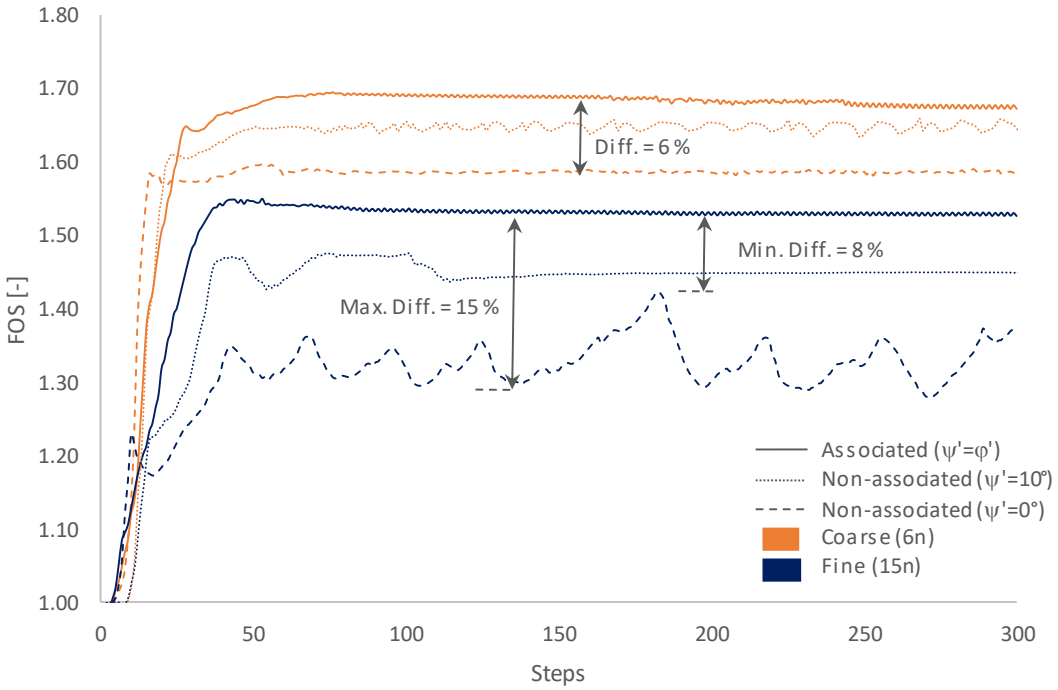

Fig. 38 Influence of the flow rule on the obtained FoS (SRFEA implemented)

Fig. 38 shows the factor of safety, calculated by means of the automatic implemented strength reduction in combination with a Mohr Coulomb soil model using 6n-coarse and 15n-fine meshes. The evaluation of the factor of safety over calculation steps clearly indicates that with decreasing the effective dilatancy angle ψ', the factors of safety are decreasing too. As already shown in chapter 4.4, a high degree of non-associativity (φ'-ψ') of the soil and the steep inclination of the slope cause an oscillation of the safety factor. It becomes evident, that this is the case when performing SRFEA with a 15n-fine mesh and an effective dilatancy angle ψ'=0°, but when using a 6n-coarse mesh, the oscillations disappear. Furthermore, it should be mentioned that the differences between associated and non-associated flow rule are smaller when performing SRFEA with a 6n-coarse mesh compared to a 15n-fine mesh. Using a 6n-coarse mesh a difference of only 6% is determined between ψ'=φ' and ψ'=0°, but for a 15n-fine mesh, the difference increases up to 15%.

4.6 Influence of the slope inclination on the FoS

The aim of this chapter is to evaluate the influence of the slope inclination on the obtained safety factor when performing SRFEA and FELA. Three different slope inclinations (20°, 30° and 45°) are part of the study. Due to the change of the model geometry, new meshes had to be generated for α=20° and α=30°. Performing SRFEA with α=20°, a 15n-fine mesh with 1,006 elements and for α=30° a 15n-fine mesh with 1,046 elements are used. A new material set MC (2) with a reduced friction angle is used for this study. All required soil parameters for the computation are summarized in Table 25.

Table 25 Material parameters of MC (2) model

MC (2)		
φ ‘	38	[°]
c'	6	[kPa]
ψ'	0°, 8°	[°]
E	40,000	[kPa]
ν	0.3	[-]

4.6.1 Effective dilatancy angle ψ’=8°

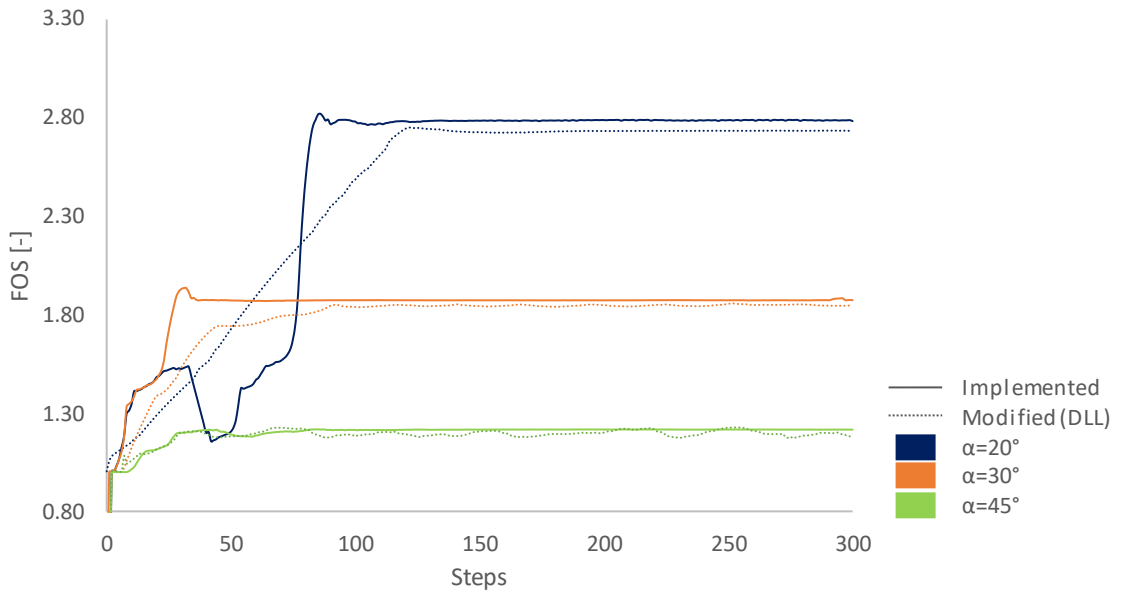

Fig. 39 Influence of the slope inclination on the obtained FoS for MC (2) and ψ’=8°

Fig. 39 shows the factor of safety, calculated by means of the automatic strength reduction performing SRFEA with three different slope inclinations. The effective dilatancy angle is ψ’=8°. The results of the implemented strength reduction

technique are represented with full lines, whereas dotted lines demonstrate the results for the modified (DLL) strength reduction. A factor of safety of 2.78 is obtained when performing SRFEA implemented with a slope inclination of 20°. Table 26 shows that the results performing FELA are in good agreement with the results from SRFEA, but still slightly conservative. The results performing FELA in combination with Davis B fits very well with the modified (DLL) strength reduction. When performing FELA in combination with Davis C, the results are in good agreement with SRFEA implemented.

Table 26 Comparison SRFEA and FELA for different slope inclinations for MC (2) - ψ'=8°

	SRFEA	FELA – Davis A			FELA – Davis B			FELA – Davis C		
	Implemented (*Modified)	LB	UB	Mean	LB	UB	Mean	LB	UB	Mean
α=20°	2.78 (*2.74)	2.35	2.39	2.37	2.70	2.75	2.73	2.74	2.79	2.76
α=30°	1.87 (*1.85)	1.62	1.65	1.63	1.81	1.85	1.83	1.84	1.88	1.86
α=45°	1.22 (*1.18-1.22)	1.08	1.11	1.09	1.13	1.16	1.14	1.14	1.17	1.15

4.6.2 Effective dilatancy angle ψ'=0°

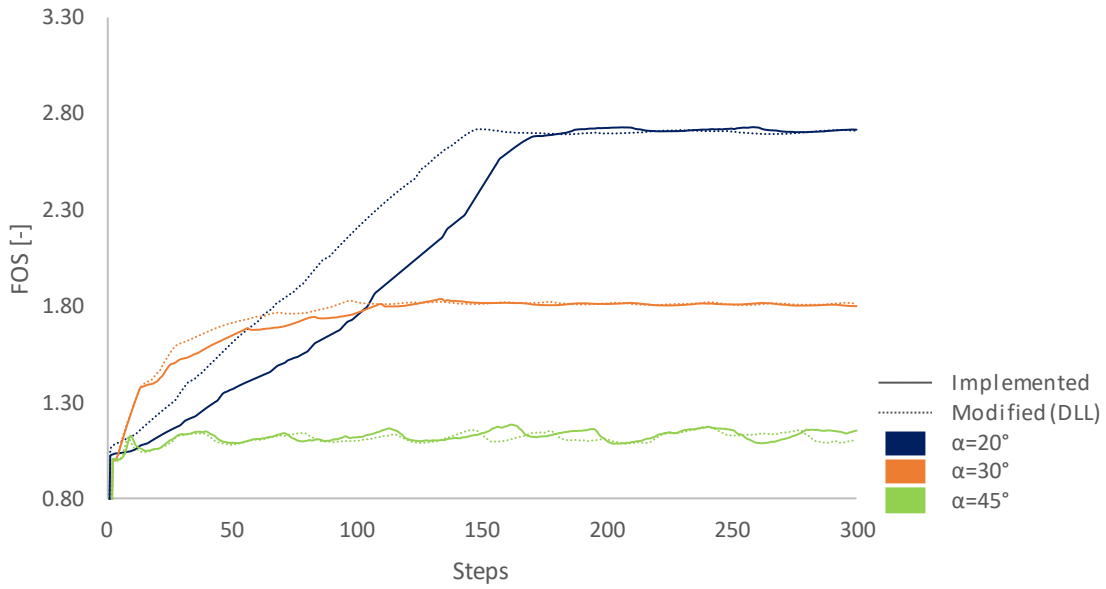

Fig. 40 Influence of the slope inclination on the obtained FoS for MC (2) - ψ'=0°

Fig. 40 shows the factor of safety, calculated by means of the automatic strength reduction technique, performing SRFEA with an effective dilatancy angle ψ'=0° for three different slope inclinations. The results of the implemented strength reduction technique are represented by full lines, whereas dotted lines show the results for the modified (DLL) strength reduction technique. The evaluation of the factor of safety over calculation steps clearly indicates that the slope inclination

influences the safety factor strongly. Since SRFEA is performed with a dilatancy angle ψ'=0°, the implemented and modified (DLL) strength reduction technique lead to the same results. A factor of safety of 2.72 is obtained when performing SRFEA with a slope inclination of 20°. Table 27 shows that the results performing FELA in combination with Davis B/C approach are in good agreement with the results from SRFEA but remain slightly conservative. It should be mentioned that performing it with slope inclinations of 20° and 30°, the oscillation of the factor of safety disappears, although the non-associativity (φ'-ψ') is still very high.

Table 27 Comparison SRFEA and FELA for different inclinations for MC (2) and ψ'=0°

	SRFEA	FELA – Davis A			FELA – Davis B/C		
	Implemented (*Modified)	LB	UB	Mean	LB	UB	Mean
α=20°	2.72 (*2.72)	2.17	2.21	2.19	2.67	2.72	2.70
α=30°	1.80–1.83 (*1.80–1.82)	1.49	1.52	1.51	1.76	1.80	1.78
α=45°	1.08-1.17 (*1.09-1.18)	1.00	1.02	1.01	1.01	1.03	1.02

4.7 Influence constitutive soil model

To evaluate the influence of the constitutive soil model on the obtained factor of safety, selected studies considering different definitions of the flow rule, are additionally performed with a Hardening soil small (HSS) model. Due to the fact, that the MC and the HSS model both deal with a Mohr Coulomb failure criterion no differences in the FoS are expected to occur when performing automatic SRFEA. But when performing manual SRFEA, differences are expected between the two constitutive models. It could be shown in previous chapters, that for ψ'=φ' and ψ'=0° SRFEA implemented and modified (DLL) lead to same results. Therefore, SRFEA modified (DLL) is here only performed for ψ'=10°. Additionally, manual SRFEA is carried out with two different values of the tolerated error (0.1% and 1%).

Table 28 Comparison of automatic and manual SRFEA using a MC and HSS model

Implemented (*Modified)	MC (1)			HSS (1)		
	ψ'=φ'	ψ'=10°	ψ'=0°	ψ'=φ'	ψ'=10°	ψ'=0°
Automatic	1.53	1.46 (*1.40-1.46)	1.27-1.39	1.53	1.46 (*-)	1.28- 1.40
Manual – Tol. err. = 1%	1.57	1.43 (*1.41)	1.36	1.58	1.51 (*1.47)	1.40
Manual – Tol. err. =0.1%	1.54	1.40 (*1.36)	1.30	1.54	1.43 (*1.38)	1.25

Due to the Mohr Coulomb failure criterion, the safety factors, shown in Table 28, using a Mohr Coulomb and Hardening soil small model are similar when performing automatic SRFEA. As shown in Table 28, when carrying out manual SRFEA, a reduction of the tolerated error leads to lower factors of safety. Apart from that, the factor of safety is less influenced by the tolerated error when performing automatic SRFEA. However, performing manual SRFEA for associated plasticity (ψ' = φ') with a HSS model, the factor of safety increases slightly. For non-associated plasticity (ψ' = 10°, ψ' = 0°), no trend can be observed, because the failure mechanisms vary slightly for different sets of FEA. These minor changes of the slip surface during the manual SRFEA can be attributed again to the high amount of non-associativity.

5 3D Slope stability for drained material behavior

5.1 Introduction

5.1.1 Problem description

In this section, automatic 3D SRFEA are performed as drained analysis, using a linear elastic-perfectly plastic model including a Mohr Coulomb failure criterion (MC (1)). All computations in this section are performed with Plaxis 3D Version 2018 with the implemented and the modified (DLL) strength reduction technique. The results of 2D and 3D SRFEA are compared in subchapter 5.4.

5.1.2 Model, material and construction steps

To obtain comparable results according to 2D SRFEA (see chapter 4) same conditions regarding the geometry, the constitutive model and the construction steps are used for 3D SRFEA. As, it is a 3D analysis, the geometry has to be extended in the y-direction (model depth). Therefore, the same homogeneous slope, as presented in Fig. 10 is analyzed for two different model depths (2m and 50m). The properties of the used constitutive soil model MC (1) are summarized in Table 3. The calculation steps are also equal to 2D SRFEA, which are shown in subchapter 4.1.5 (1. K_0 procedure 2. Plastic phase 3. Safety analysis).

5.1.3 Meshes

Two different model depths (2m and 50m) with two different mesh discretization, namely coarse and very fine mesh discretization, are part of the 3D study. The meshes for 2m model depth, shown in Fig. 41 (a) consists of 2,003 (coarse) and 773,811 (very fine) 10n-finite elements. The meshes for 50m model depth are shown in Fig. 41 (b). It consists of 6,300 (coarse) and 1,003,359 (very fine) 10n-finite elements.

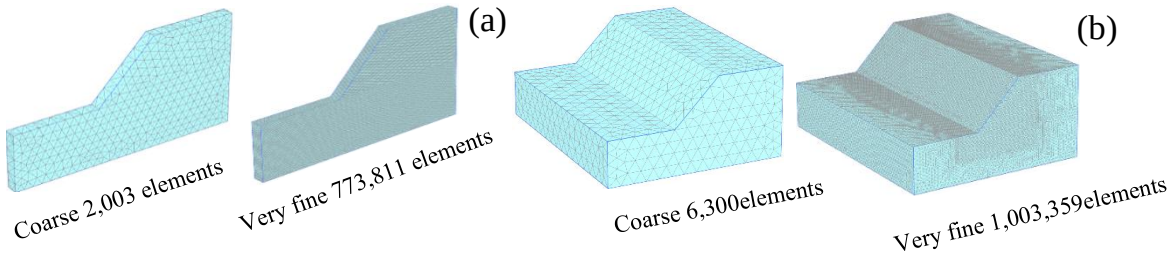

Fig. 41 Meshes for 3D SRFEA: (a) model depth 2m, (b) model depth 50m

5.2 Model depth 2m

5.2.1 Associated flow rule (ψ'=φ')

The purpose of this subchapter is to evaluate the influence of the mesh discretization on the obtained safety factor in combination with associated plasticity (ψ'=φ'). 3D SRFEA are performed with the implemented and modified (DLL) technique. Nevertheless, the results are expected to be in the same range for ψ'=φ'.

5.2.1.1 Mesh discretization

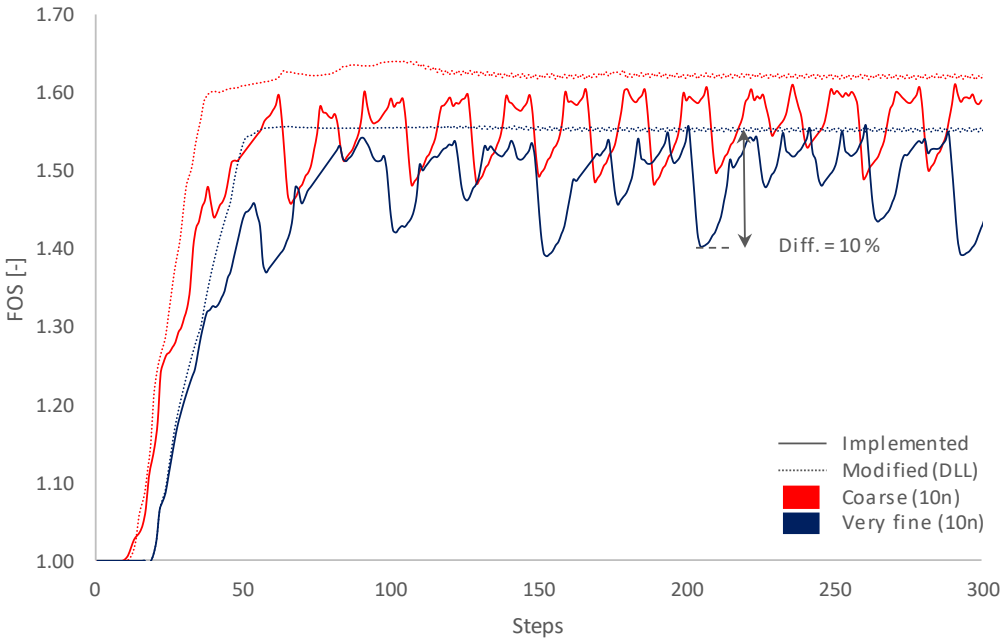

Fig. 42 Computed FoS for MC model: Comparison of implemented and modified (DLL) SRFEA for ψ'=φ'

In Fig. 42, the factor of safety is determined by means of effective stresses for two different meshes. Full lines represent the implemented, dotted lines the modified (DLL), strength reduction technique. As already elaborated in 2D SRFEA, the number of finite elements has a substantial influence on the obtained factor of safety. It becomes evident, that the modified (DLL) strength reduction technique leads to satisfactory results; a factor of safety of 1.62 when performing SRFEA with a coarse mesh, and 1.54 with a very fine mesh, are obtained. Since, the computation performs with an associated flow rule, the implemented and modified (DLL) SRFEA should lead to the same results. But performing implemented SRFEA, causes a heavy oscillation of the safety factor for the coarse as well for the very fine meshes in 3D. Since, this scatter is usually only noticeable for steep slopes with a high degree of non-associativity (φ'-ψ'), further studies are hereby conducted to investigate the cause of this heavy oscillation. A parameter study of

the effective dilatancy angle ψ' (subchapter 5.2.1.3), and a sensitivity analysis of numerical control parameters (subchapter 5.2.1.4) are described in the following.

5.2.1.2 Failure mechanism

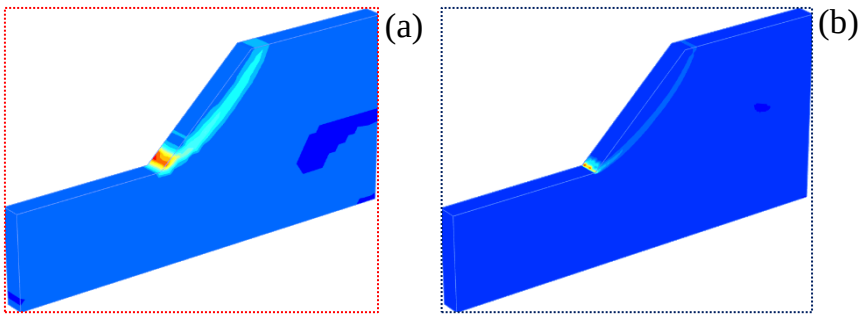

Fig. 43 Failure mechanism SRFEA modified (DLL): (a) Coarse (10n), (b) Very fine (10n)

Fig. 43 represents the incremental deviatoric strains performing SRFEA with a 10n-coarse and 10n-very fine mesh for the modified (DLL) technique. The failure mechanism for both meshes looks similar but the number of finite elements influences the extent of the slip surface strongly (as already elaborated in 2D SRFEA).

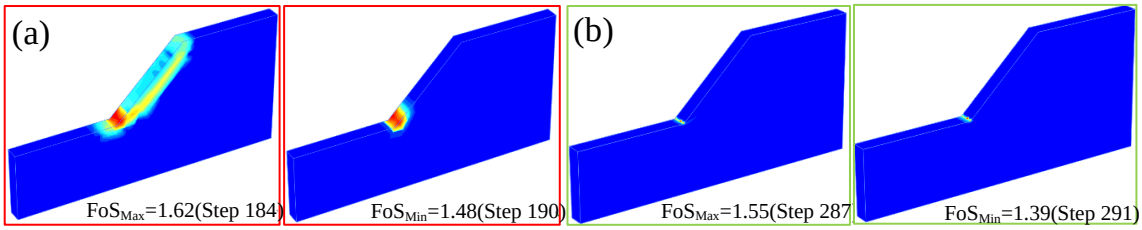

Fig. 44 Failure mechanism SRFEA implemented: (a) Coarse (10n), (b) Very fine (10n)

As shown in Fig. 44 (incremental deviatoric shear strains), no failure mechanism is visible when performing SRFEA implemented. However, in Fig. 107 (appendix) it can be seen, that plastic points are primary located in the expected slip surface. Also, the total displacements (Fig. 108) indicate the expected slip surface. The development of the relative shear stress is shown in Fig. 109.

5.2.1.3 Variation of the effective dilatancy angle ψ'

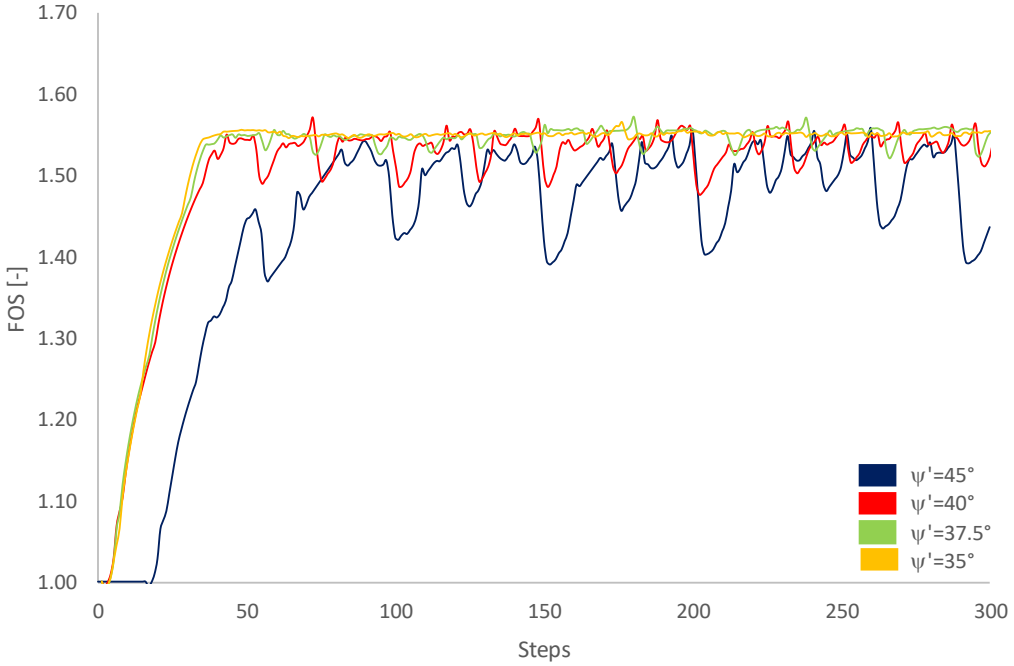

Fig. 45 Variation of the effective dilatancy angle ψ'

As already shown in Fig. 42, heavy oscillations of the obtained safety factor occur, when performing automatic 3D SRFEA implemented in combination with an associated flow rule (ψ'=φ'). Hence, a study with altered effective dilatancy angles ψ' is carried out to investigate when the oscillations disappear. Effective dilatancy angles ψ' of 40°, 37.5° and 35° are used for this analysis. Fig. 45 shows that the oscillations disappear for dilatancy angles ψ'<35°.

However, when performing 2D SRFEA in combination with an associated flow rule (ψ'=φ'), no oscillations occur. Further studies have to be conducted to investigate the reason for this problem. Therefore, a sensitivity analysis of numerical control parameters was performed and described in the next section.

5.2.1.4 Numerical control parameter

A sensitivity analysis is performed to evaluate, if numerical control parameters cause the heavy oscillation of the obtained factor of safety. All calculations are performed with a very fine mesh and a model depth of 2m. The following parameters are part of the analysis, the default values in Plaxis 3D are:

Incremental Multiplier:	M_{SF}=0.1
Updated Mesh:	OFF
Tolerated error:	1%
Over relaxation factor:	1.2
Arc length control:	ON
Desired iterations:	Min: +6, Max: +15

- Incremental multiplier M_{SF}

The numerical control parameter *incremental multiplier* controls the increment of the first calculation step, when performing an automatic strength reduction (safety analysis) in Plaxis 3D. The effective strength parameters of the soil are reduced automatically until 300 calculation steps are reached. As shown in Eq. (25), the factor of safety is then defined as the sum of the incremental multiplier at failure. The default setting for the incremental multiplier is 0.1 (Brinkgreve, 2018). To prove if this numerical control parameter influences the heavy oscillation of the factor of safety, the same calculation is performed with reduced values.

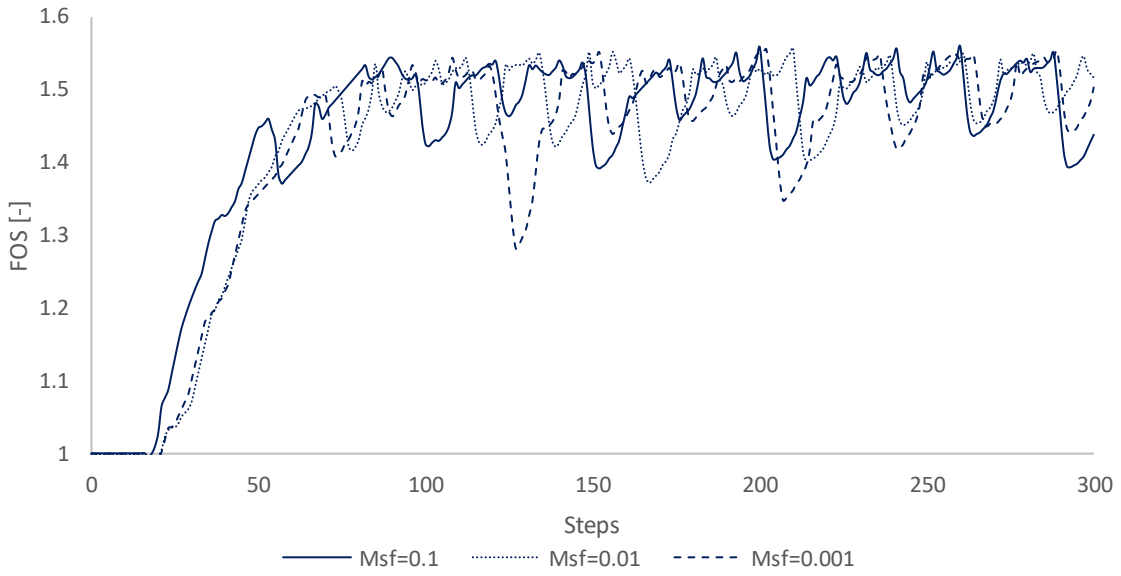

Fig. 46 Influence of the numerical control parameter incremental multiplier on the obtained FoS – ψ'=φ'

Incremental multipliers of 0.01 and 0.001 are used for the analysis. Fig. 46 shows the results. It becomes evident that this numerical control parameter does not improve the heavy oscillation. It should be mentioned that a value of 0.001 leads to some strong outliers (e.g. step 130). Therefore, it is recommended not using this value, when performing an automatic strength reduction in Plaxis 3D.

$$FoS = \sum M_{SF} \tag{25}$$

- Updated mesh

The numerical control parameter *updated mesh* considers the influence of the geometry changing after the plastic phase. Hence, this parameter may become effective when large deformations of the soil occur. If large deformations occur, additional terms in the structure stiffness matrix must be considered (Brinkgreve, 2018). A maximum total displacement of 5.5 cm is computed for this analysis.

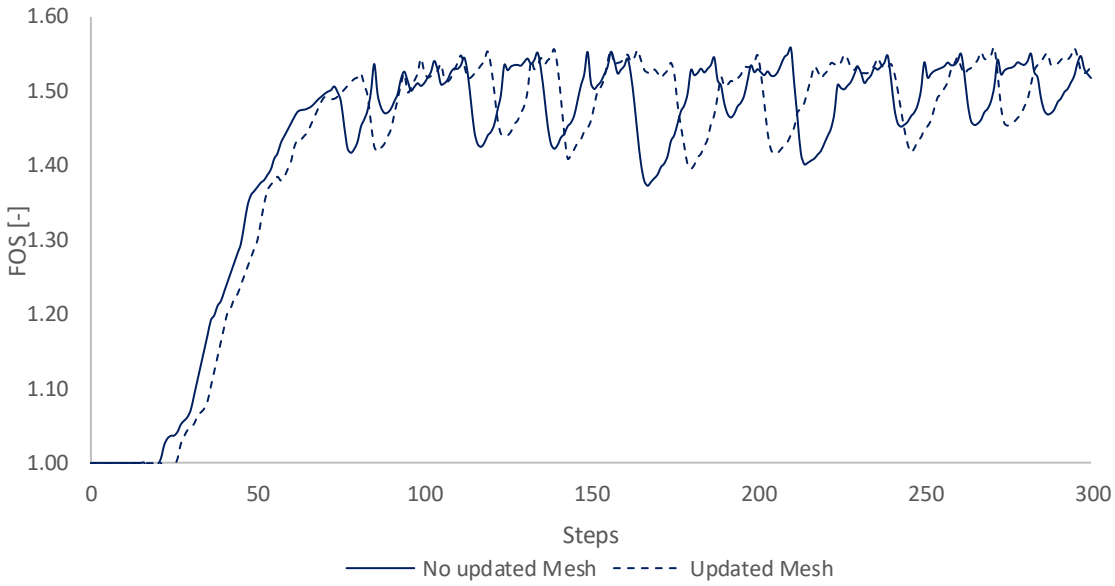

Fig. 47 Influence of the numerical control parameter updated mesh on the obtained FoS - ψ'=φ'

Fig. 47 shows the results performing the analysis with an updated mesh. It becomes clear that this numerical control parameter has no significant influence on the safety factor. With an updated mesh analysis, the FoS still scatters in the same range as in the previous analysis.

- Tolerated error

Since every non-linear numerical analysis is just an approximation to the exact solution, deviations, as shown in Fig. 48, between the numerical and exact solutions occur. These deviations are controlled by the solution algorithm with the numerical control parameter *tolerated error*. The algorithm ensures that the equilibrium errors remain with acceptable limits. During the safety analysis, the program carries out iterations until the calculated error is smaller than the selected tolerated error. It should be noted that high tolerated errors may lead to inaccurate results (Brinkgreve, 2018).

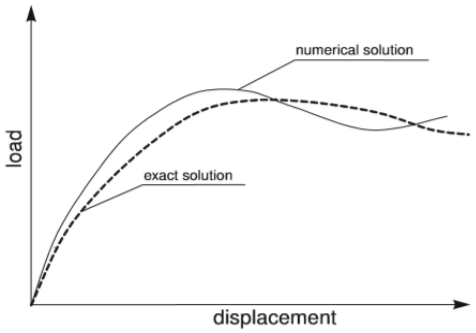

Fig. 48 Numerical solution vs. exact solution (Brinkgreve, 2018)

The default setting in Plaxis 3D for the tolerated error is 1%. To prove if this numerical control parameter influences the oscillations, an analysis with a tolerated error of 0.1% is performed. In the following Fig. 49, it becomes evident that a reduced tolerated error of 0.1% leads to a substantially improvement of the curve and the heavy oscillation. After about 700 calculation steps a safety factor of approximately 1.54 is obtained.

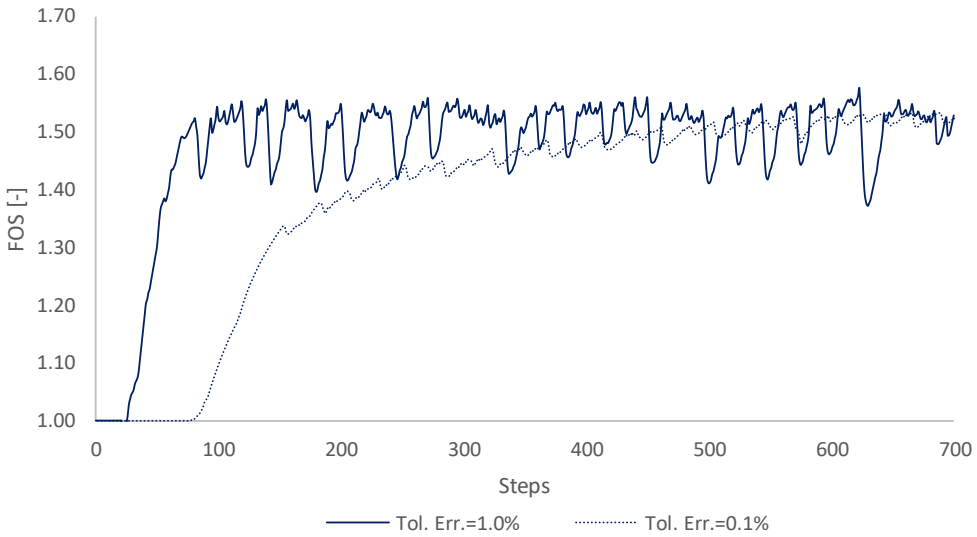

Fig. 49 Influence of the numerical control parameter tolerated error on the obtained FoS – ψ'=φ'

- Over relaxation factor

The numerical control parameter *over relaxation* is used to reduce the number of iterations that are necessary for convergence to speed up the calculation process. As shown in Fig. 50 a purposely overestimation, due to the reduced number of iterations, of the equilibrium error is assumed. The calculation is performed under the condition that the subsequent iteration is still far away from equilibrium. The degree of the overestimation corresponds to the over relaxation factor, where the default setting in Plaxis 3D is 1.2 (Brinkgreve, 2018).

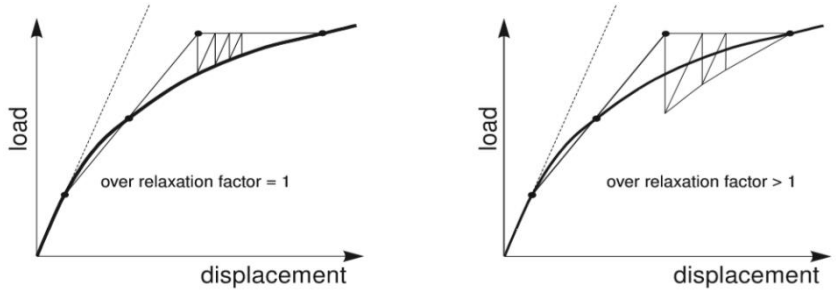

Fig. 50 Influence of over-relaxation (Brinkgreve, 2018)

To prove, if this numerical control parameter influences the heavy oscillation of the FoS, considering associated flow rule, the calculation is performed with an over relaxation factor of 1.0. Fig. 51 clearly illustrates, that this numerical control parameter has no significant influence on the obtained factor of safety and the scatter is still in the same range as for a standard over-relaxation factor of 1.2.

Fig. 51 Influence of the numerical control parameter over relaxation factor on the obtained FoS - ψ'=φ'

- Arc length control

It is well known, that for load-controlled calculations the numerical control parameter *arc length control* influences the obtained failure load. If the setting arc length control is activated, the remaining portion of external load for collapse is automatically evaluated, as shown in Fig. 52 and an accurate factor of safety can be determined. Since the setting leads to more accurate results, it is recommended activating it when performing safety analysis (Brinkgreve, 2018).

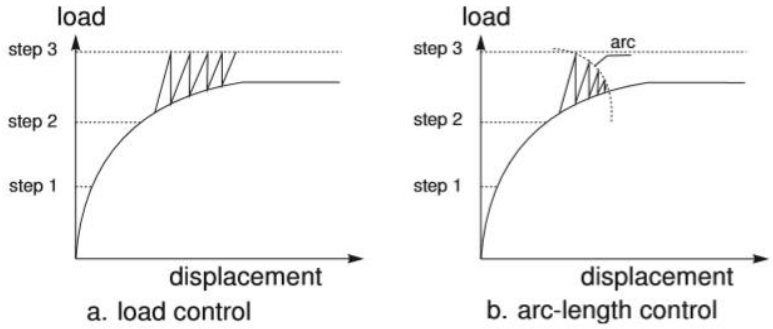

Fig. 52 Influence of arc length control (Brinkgreve, 2018)

However, the calculation is performed with arc length control off to prove if this numerical control parameter influences the heavy oscillation of the obtained factor of safety. As shown in Fig. 53, a deactivation of the setting influences the obtained safety factor. Obviously, no solution of the failure load is found which leads to an increase of the obtained factor of safety by steps. Therefore, arc length should always be switched on when performing SRFEA in Plaxis 3D.

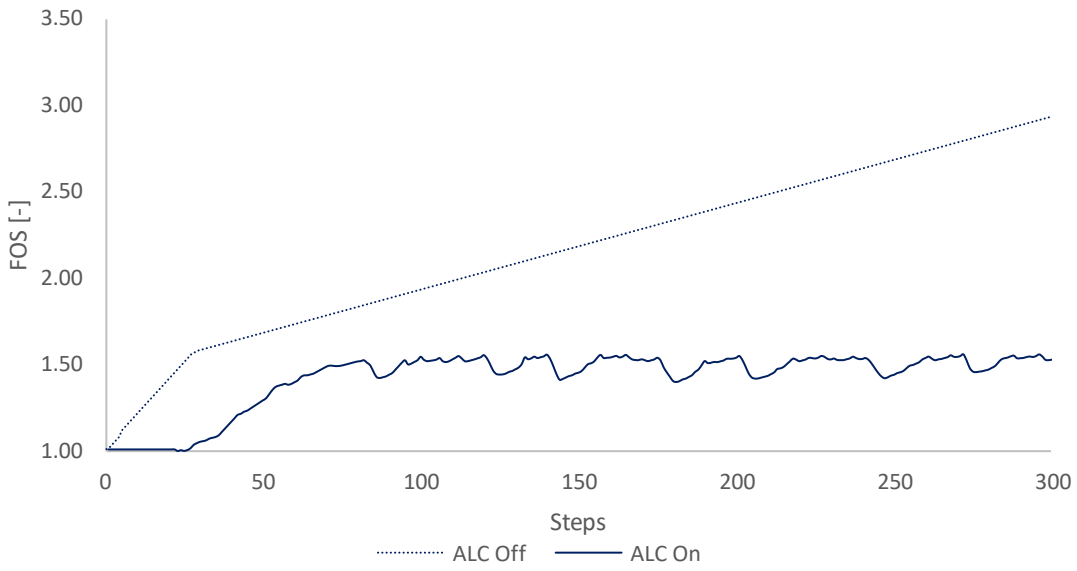

Fig. 53 Influence of the numerical control parameter arc length control on the obtained FoS - ψ'=φ'

- Desired min and desired max number of iterations

Since Plaxis 3D deals with an automatic step size algorithm, the numerical control parameters *desired min number of iterations and desired max number of iterations* control the number of iterations per step. The default setting in Plaxis 3D considers a desired minimum of 6 and a desired maximum of 15 iterations. In order to obtain more accurate results, especially for high effective friction angles, it is recommended reducing the desired minimum and increasing the desired maximum of iterations (Brinkgreve, 2018). Since the effective friction angle of the material set of φ'=45° is very high, a calculation with a desired minimum of 3 and a desired maximum of 25 iteration is performed. It becomes clear in Fig. 54 that the desired min/max number of iterations does not lead to any improvement of the heavy oscillations. The scatter is still in the range as in previous analysis with the default settings.

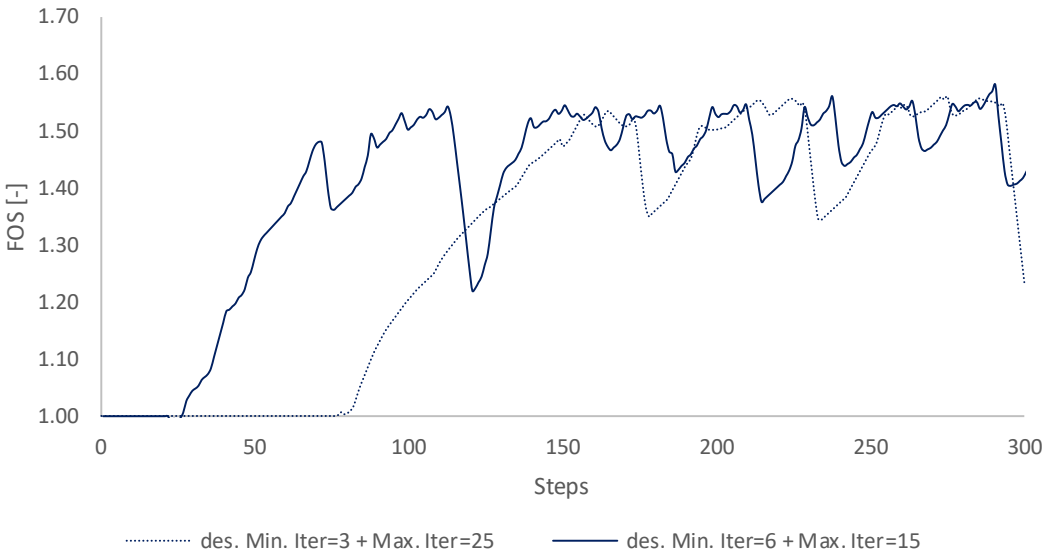

Fig. 54 Influence of the numerical control parameter desired min/max number of iterations on the obtained FoS - ψ'=φ'

5.2.2 Non-associated flow rule (ψ'=10°)

The purpose of this chapter is to evaluate the influence of the mesh discretization on the obtained safety factor for non-associated plasticity (ψ'=10°), when performing 3D SRFEA.

5.2.2.1 Influence mesh discretization

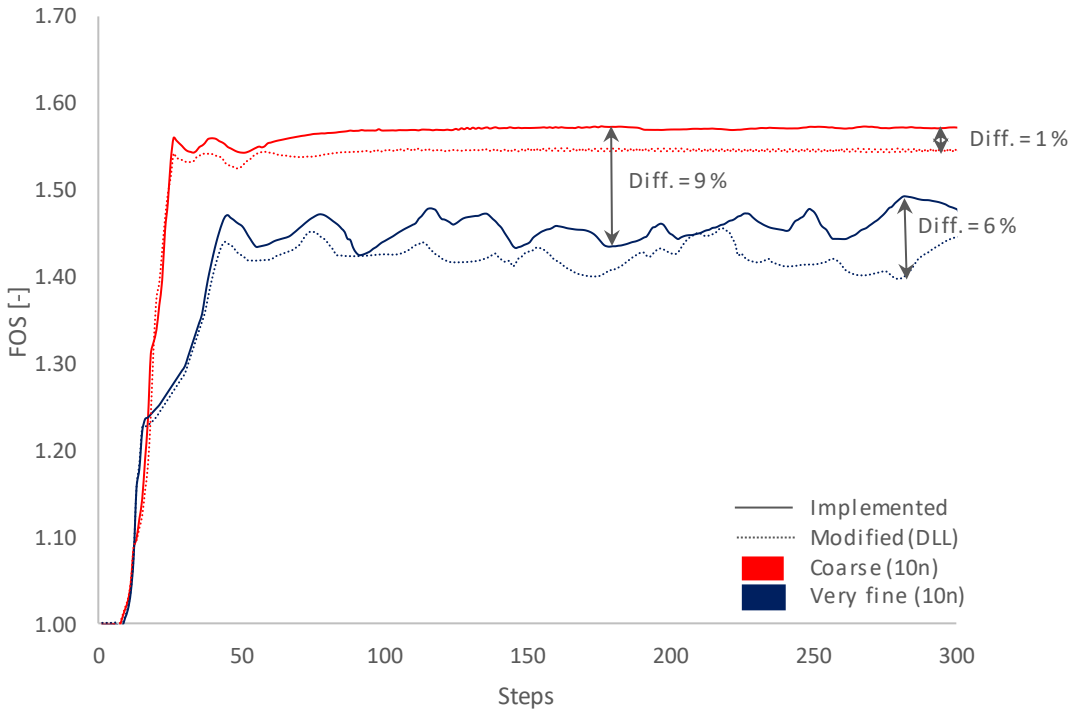

Fig. 55 Computed FoS for MC model: Comparison of implemented and modified (DLL) SRFEA for ψ'=10°

Fig. 55 shows the obtained factor of safety for two different meshes. Full lines represent the implemented, whereas dotted lines the modified (DLL) strength reduction technique. As already elaborated for 2D SRFEA, the number of elements influence the safety factor strongly. Performing modified (DLL) SRFEA leads to lower safety factors, compared to the implemented strength reduction technique with a maximum difference of 6%. For a very fine mesh a slightly scatter of the safety factor occurs in the range of 1.45-1.49 when performing implemented SRFEA (1.40-1.46 for the modified (DLL) SRFEA). The presented results are performed with default settings in PLAXIS 3D (no altered values of numerical control parameters).

5.2.2.2 Failure mechanism

Fig. 56 and Fig. 57 demonstrate the incremental deviatoric strains performing SRFEA with a 10n-coarse and a 10n-very fine mesh for the implemented and modified (DLL) strength reduction technique. Since, the factor of safety for the very fine mesh scatters slightly, the shape of the failure mechanism also changes for different calculation steps. The failure mechanisms for the maximum and minimum obtained safety factors are shown below.

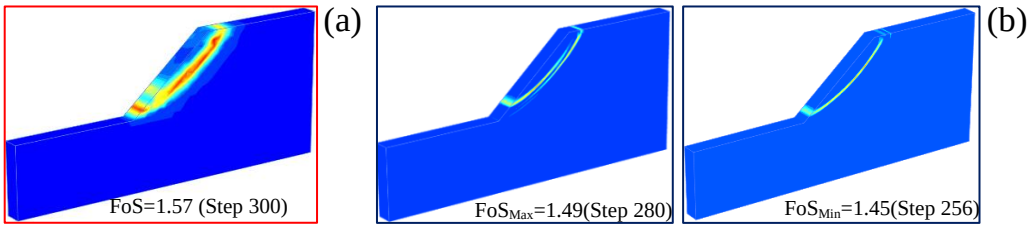

Fig. 56 Failure mechanism SRFEA implemented: (a) Coarse (10n), (b) Very fine (10n)

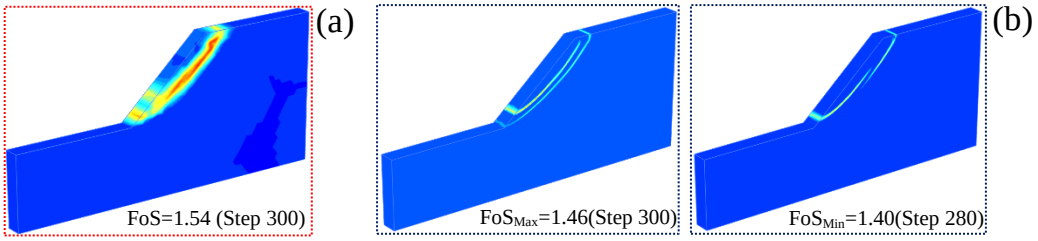

Fig. 57 Failure mechanism SRFEA modified (DLL): (a) Coarse (10n), (b) Very fine (10n)

5.2.3 Non-associated flow rule (ψ'=0°)

In the subject chapter 3D SRFEA is performed with an effective friction angle ψ'=0°. As already in the previous section, two meshes (coarse and very fine) and two strength reduction techniques (implemented and modified (DLL)) are used for the analysis.

5.2.3.1 Mesh discretization

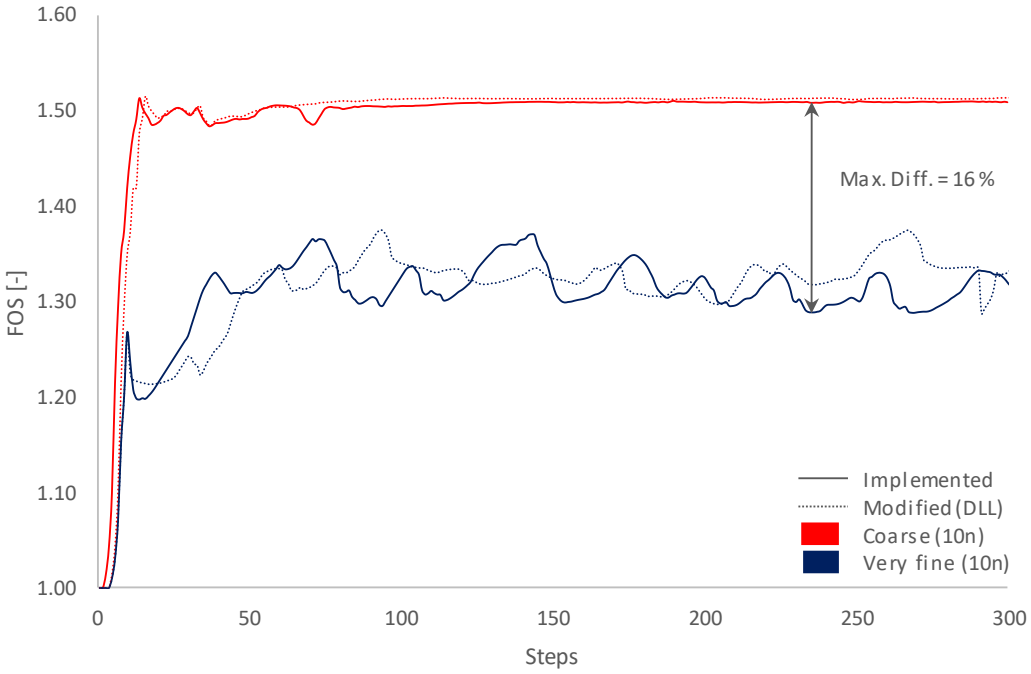

Fig. 58 Computed FoS for MC model: Comparison of implemented and modified (DLL) SRFEA for ψ'=0°

The results performing 3D SRFEA with an effective dilatancy angle ψ'=0° are shown in Fig. 58. Full lines represent the implemented, dotted lines the modified (DLL) strength reduction technique. As already seen when performing 2D SRFEA, the number of finite elements has a strong influence on the FoS. Since the effective dilatancy angle ψ'=0°, the implemented and modified (DLL) strength reduction technique leads to the same results. Due to the high degree of non-associativity (φ'-ψ') and the steep slope, a scatter of the factor of safety occurs when performing SRFEA with a very fine mesh. The range of the scatter is the same for both strength reduction techniques. A maximum factor of safety of 1.50 is obtained when performing SRFEA with a 10n-coarse mesh. The minimum factor of safety of 1.28 is achieved when performing SRFEA with a 10n-very fine mesh, which is a resulting difference of about 16%. Furthermore, it also should be noted that when performing SRFEA with 10n-coarse mesh, no oscillation of the safety factor occurs. The presented computations are performed with default settings in PLAXIS 3D (no altered values of numerical control parameters).

5.2.3.2 Failure mechanism

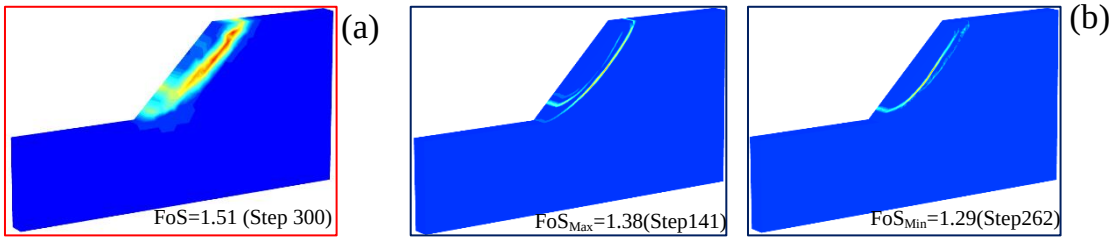

Fig. 59 Failure mechanism SRFEA implemented: (a) Coarse (10n), (b) Very fine (10n)

Fig. 59 demonstrates the incremental deviatoric strains performing 3D SRFEA (implemented SRFEA technique) for different meshes. Since, SRFEA implemented and modified (DLL) lead to same results for ψ'=0°, also the failure mechanism looks similar. As already seen when performing 2D analysis, the high non-associativity (φ'-ψ') and the steep slope lead to an oscillation of the obtained factor of safety (shown in Fig. 58). Therefore, the shape of the failure mechanism changes with each calculation step. The figures presenting the incremental deviatoric strains for the minimum and maximum obtained FoS.

5.3 Model depth 50m

The purpose of this chapter is to evaluate the influence of the mesh discretization on the obtained safety factor and failure mechanism, considering different definitions of the flow rule and strength reduction techniques. The model depth (y-direction) for all analyzes is equal to 50m. Since, the results are very similar as for a model depth of 2m no detailed evaluation and interpretation of the results will be provided here. All required figures are attached. The influence of the mesh discretization for associated flow rule (ψ'=φ') is shown in Fig. 110. The results for non-associated flow rule (ψ'=10°) are given in Fig. 111. The results performing 3D SRFEA with ψ'=0° are shown in Fig. 112.

5.4 Comparison of 2D SRFEA and 3D SRFEA

Fig. 60 shows the comparison of 2D SRFEA, optimized (tolerated error of 0.1% for associated plasticity) 3D SRFEA for associated plasticity (ψ'=φ') and 3D SRFEA for non-associated plasticity (ψ'=0°). Full lines represent the results performing 2D SRFEA, dashed lines show the results performing 3D SRFEA with 2m model depth. Dotted lines represent the results performing 3D SRFEA considering a model depth of 50m. The following comparison is shown for the implemented strength reduction technique. It was previously explained that, when performing SRFEA in combination with an associated flow rule (ψ'=φ') a tolerated error of 0.1% is required to obtain satisfactory results without oscillations. For non-associated plasticity (ψ'=0°), the default settings from Plaxis 3D (tolerated error 1%) are used for the computation. Additionally, the number of calculation steps during the φ'/c' reduction have been increased. It can be seen very well that after around 600 calculation steps, the obtained safety factors for 2D and 3D SRFEA are in good agreement when performing SRFEA with associated plasticity (ψ'=φ') and the obtained FoS is approximately 1.54. When performing SRFEA with non-associated plasticity (ψ'=0°), the results from 2D and 3D SRFEA are in good agreement as well, and the obtained FoS is in a range of 1.28-1.39. When performing 3D SRFEA with a model depth of 50m slightly higher safety factors are obtained compared to 2D SRFEA and 3D SRFEA with a model depth of 2m. Even though the mesh has approximately 1,000,000 elements (with mesh refinement) more elements would be required to obtain similar FoS as for 2D SRFEA and 3D SRFEA with 2m model depth.

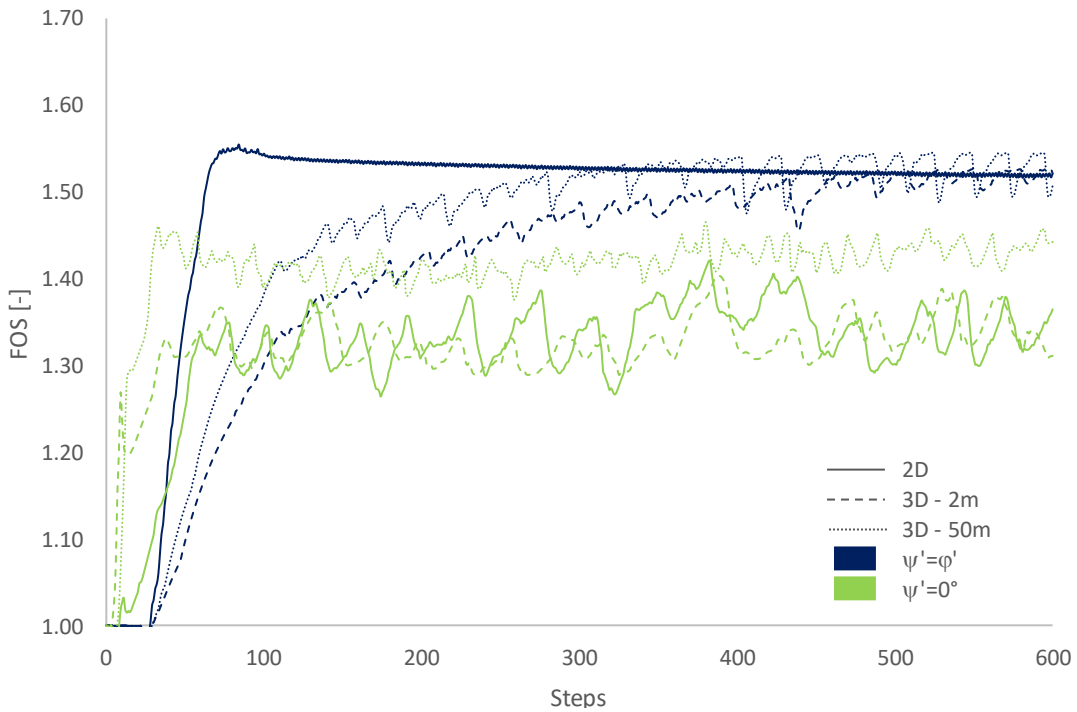

Fig. 60 Comparison of 2D and 3D SRFEA for different flow rules

6 2D Slope stability for undrained material behavior

6.1 Introduction and overview

6.1.1 Problem definition and tasks

To study the impact of undrained conditions on the obtained factor of safety, 2D SRFEA using drained and undrained material behavior are compared in the following. The undrained analyzes are performed by using effective strength and stiffness parameters, denoted as Undrained (A). The same slope geometry is analyzed, as already elaborated for 2D SRFEA with drained material behavior, presented in Fig. 10, with a different material set MC (3) and HSS (3). Ten excavation steps are considered to model the geometry of the slope. Additionally, the influence of ignoring the undrained material behavior during safety analysis is part of the investigation. The φ'/c' reduction is performed automatically and manually using the implemented strength reduction technique. Since it is an undrained analysis, the effective dilatancy angle ψ'=0°. As already shown in chapter 4.4, both strength reduction techniques lead to the same results for ψ'=0°. Therefore, no calculations are performed with the modified (DLL) strength reduction technique for the subsequent studies. All calculations are performed and compared with two different constitutive models. The material parameters for the Mohr Coulomb (MC) and Hardening soil small (HSS) model are shown in subchapter 6.1.2. Due to the excavation of the slope, negative pore water pressures may occur. Therefore, the influence of cavity as well the effect of suction is part of the subsequent analysis. The development of stress paths, excess pore pressures and volumetric strains are evaluated.

6.1.2 Constitutive models and material set

The unit weight of the saturated soil is 19 kN/m³. Two different constitutive models, namely a MC (3) and HSS (3), are used and then compared. All required material properties of the linear elastic-perfectly plastic Mohr Coulomb (MC) and the Hardening soil small (HSS) model are summarized in Table 29. According to the flow rule, presented in Fig. 7, the corresponding effective dilatancy angle is ψ'=0°.

Table 29 Material parameters of MC (3) and HSS (3) model

MC (3)		HSS (3)	
E’	20,000 kPa	E_{oed}^{ref}	15,000 kPa
ν’	0.3	E_{50}^{ref}	20,000 kPa
φ’	25 °	E_{ur}^{ref}	60,000 kPa
ψ’	0°	p^{ref}	100 kPa
c’	20 kPa	ν_{ur}	0.2
		φ'	25°
		ψ’	0°
		c’	20 kPa
		G_0	90,000 kPa
		$\gamma_{0.7}$	0.00015

6.1.3 Mesh

It was shown in section 4 that the number of finite elements has a substantial influence on the obtained factor of safety. Therefore, a mesh study is not part of the subject chapter and a very fine mesh is used to perform the analysis. Fig. 61 represents the very fine mesh with 3,371 15n-finite elements. The mesh is refined in the area of the expected slip surface.

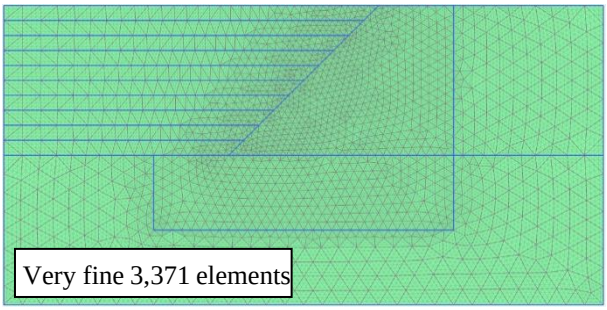

Fig. 61 Mesh for undrained analysis

6.1.4 Construction steps

The initial stresses are determined with the K_0 procedure as a first “calculation” phase. The computation is the same as for drained conditions. The required equations and the explanation to perform the K_0 procedure are shown in 4.1.5.1. Subsequently 10 excavation steps, as presented in Fig. 62, à 1m are considered to reach the geometry with an excavation depth of 10m. The φ’/c’ reduction as a last “calculation phase” is performed by means of the implemented strength reduction technique automatically and manually.

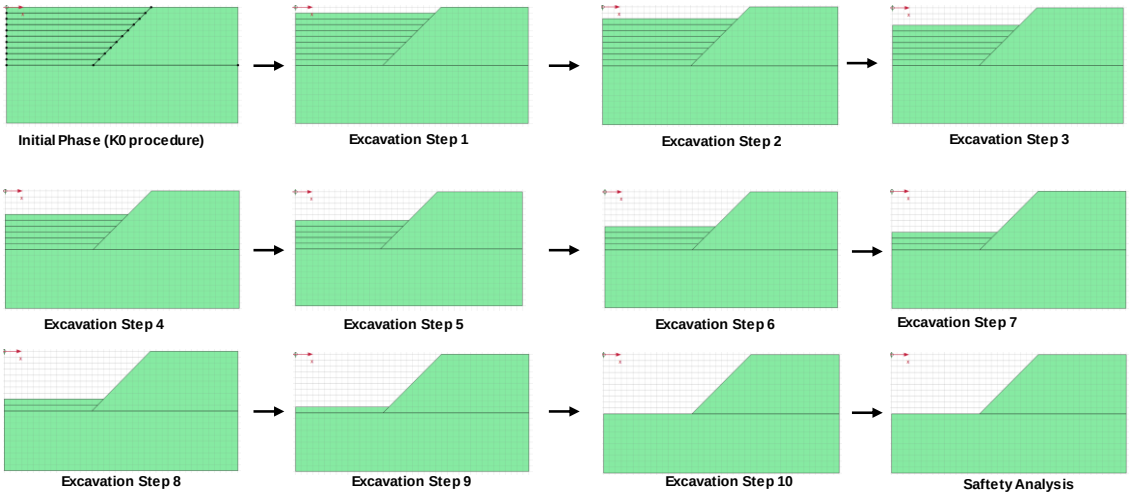

Fig. 62 Construction steps of the excavation

6.2 No cavitation cut off

The purpose of this chapter is to evaluate the factor of safety considering no cavitation cut off for drained, undrained (A) and undrained (A) - ignore undrained (in safety analysis) conditions. Furthermore, the evaluation and development of stress paths, excess pore pressures and volumetric strains are subject of this chapter. With the setting "No cavitation cut off", infinite tensile excess pore pressures are allowed in the calculation.

6.2.1 Influence constitutive model and drainage conditions

Fig. 63 represents the obtained safety factor, for the Mohr Coulomb (MC) and the Hardening soil small (HSS) FEA. Full lines represent the results for undrained conditions and dotted lines the results for ignoring undrained behavior during safety analysis. Dashed lines demonstrate the results for the fully drained analysis. As illustrated in the figure, the drainage conditions and the constitutive model influence the computed factor of safety significantly. It was previously shown in Table 28 that the MC and HSS models reach the same factors of safety for drained conditions when performing automatic strength reductions (safety analysis) because both models consider a Mohr Coulomb failure criterion. This fact can also be observed in the following figure, where a factor of safety of about 1.38 is reached for fully drained conditions performing SRFEA with a MC and HSS model. Aside from that, the factor of safety increases strongly for undrained behavior due to the development of negative pore pressures during the excavation phases of the embankment. The undrained analysis considering a MC model calculates a higher factor of safety than the HSS model because of different developments of the excess pore water pressure. A detailed evaluation of the development of the excess pore water pressure is discussed in subchapter 6.2.4. Compared to the fully undrained analysis, ignoring undrained material behavior during the safety analysis leads to slightly lower safety factors for HSS but to higher safety factors for the MC model. The factor of safety performing manual strength reduction is only determined for fully undrained conditions. Performing SRFEA with the MC model, a higher safety factor is obtained compared to the automatic strength reduction. It becomes evident that the result from manual SRFEA manual corresponds approximately to the upper peak of the automatic strength reduction for a MC model. Performing undrained SRFEA using the HSS model, slightly lower manual safety factor, are obtained.

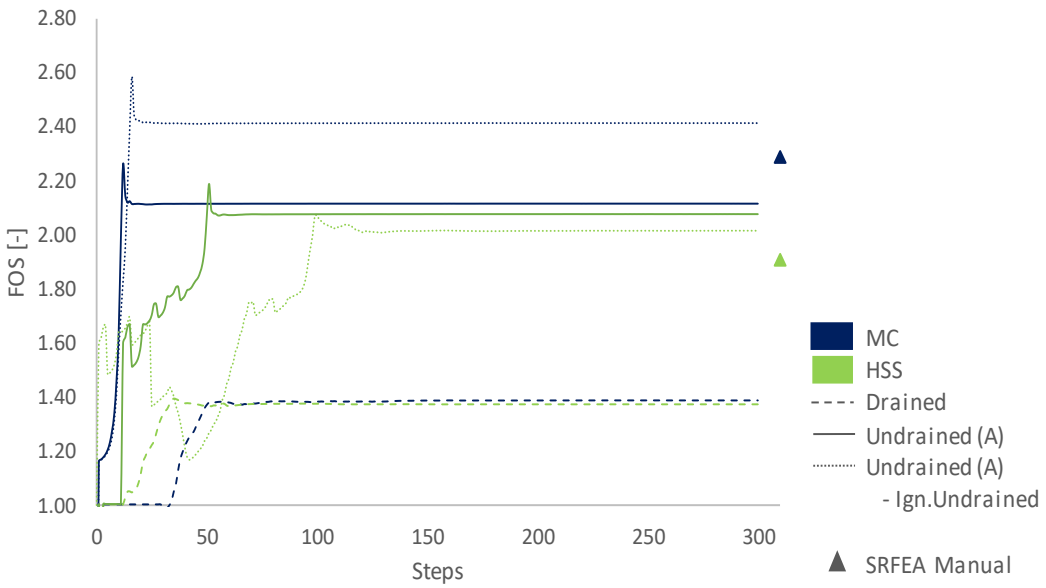

Fig. 63 Overview of FoS – Comparison of MC and HSS model for different drainage conditions

6.2.2 Failure mechanism

Fig. 64 and Fig. 65 represent the incremental deviatoric strains performing SRFEA with the MC and the HSS model for fully drained and undrained conditions as well as for ignoring the undrained material behavior during safety analysis. It reveals that the shape of the slip surface performing SRFEA with the HSS and MC looks similar for fully undrained conditions. The impact of ignoring undrained behavior leads to a slight change of the failure mechanism. It should be remarked that two stress points are selected, one in the lower part (SP A) and one in the upper part (SP B) of the failure mechanism. The following evaluation of the development of the stress paths, the excess pore pressures and the volumetric strains is done for these stress points.

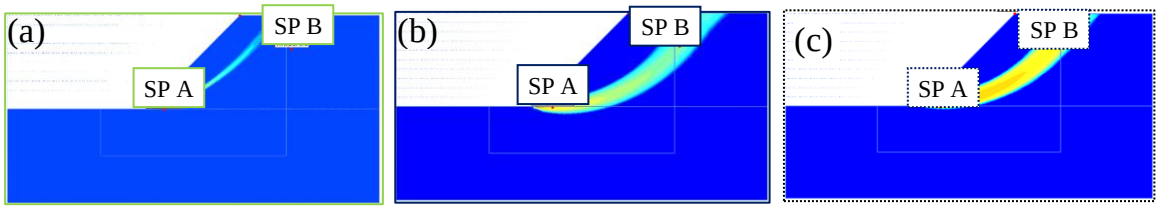

Fig. 64 Overview incremental deviatoric strains MC model: (a) Drained, (b) Undrained (A), (c) Undrained (A) – Ign. undrained

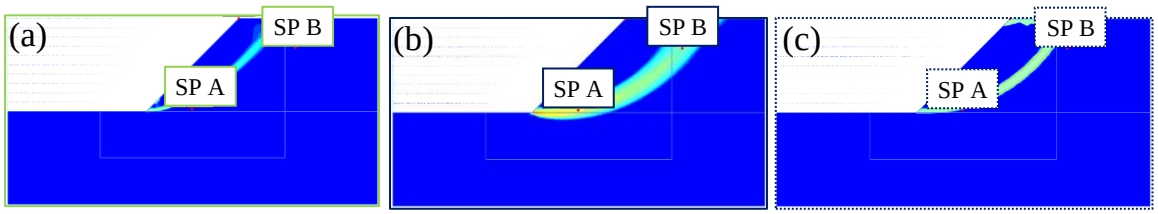

Fig. 65 Overview incremental deviatoric strains HSS model: (a) Drained (A), (b) Undrained (A), (c) Undrained (A) – Ign. undrained

6.2.3 Stress paths

Fig. 66 shows the development of the stress paths of stress point A for drained FEA, undrained FEA and undrained analysis with ignored undrained material behavior in the safety analysis for MC and HSS model. Blue lines represent the stress paths for undrained analysis (dotted blue line for ignoring undrained in safety analysis) and the green line represents the fully drained calculation. Since the initial stresses are computed in the same way for all FEA, all stress paths start at the same point. It becomes evident, that for undrained material behavior the effective mean stress p' remains constant for the excavation as well for the φ'/c' reduction. The deviatoric stresses q on the other hand changes significantly. For ignoring undrained material behavior (in the φ'/c' reduction), the effective mean stresses p' as well the deviatoric stresses q increase during the strength reduction phase. Performing SRFEA with drained material behavior, the effective mean stresses p' as well as the deviatoric stresses q decrease at the beginning. But after reaching half of the excavation q increases. However, all stress paths look similar for both constitutive models. In Fig. 64 and Fig. 65, it can be seen that stress point A is located within the failure mechanism of the slope, hence the stress paths end at the MC failure line (undrained and ignore undrained in safety analysis). It should be pointed out that the failure mechanism for drained analysis looks slightly different and as a consequence the same stress point A is not located within the failure mechanism. For this reason, the stress paths for drained FEA do not end at the MC failure line. The development of the stress paths for stress point B are shown in Fig. 113 (appendix). The trend of the development of the stress path is similar to stress point A.

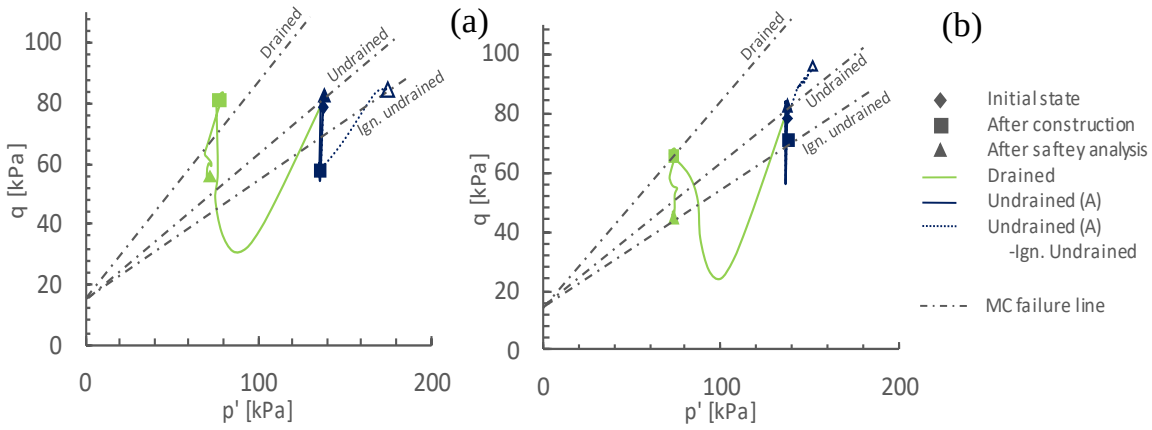

Fig. 66 p'q-diagram for different drainage conditions and Stress point A: (a) MC, (b) HSS

6.2.4 Excess pore water pressures

Fig. 67 represents the development of the excess pore water pressure of stress point A for different drainage conditions performing SRFEA with a MC and a HSS model. Blue lines demonstrate the development of the undrained FEA (dotted blue line for ignoring undrained in safety analysis), green lines for the fully drained calculations. Since the initial stresses are computed similarly for all FEA, the starting point is the same for all calculations. As no pore water pressures are generated for drained analysis, only a change of the effective mean stress p' is noticeable. It can be seen, that negative excess pore pressures are generated during the excavation for both constitutive models (because no cavitation cut off is considered). Performing SRFEA with the MC model a higher excess pore pressure is generated as when using the HSS model. As already shown in Fig. 63 this difference of the excess pore pressures leads to different safety factors. By ignoring the undrained behavior during safety analysis, the excess pore pressure remains constant but the effective mean stress changes significantly. For undrained FEA p' remains constant in the φ'/c' reduction phase but the excess pore pressures decrease. Fig. 114 (appendix) shows the development of the excess pore pressure of stress point B. Since the stress point is located very close to the surface, very less excess pore pressures are generated but the trend is similar to stress point A for all drainage conditions. Fig. 68 represents the contour plots of the development of the excess pore pressure for different calculation phases performing SRFEA with the MC model. Fig. 115 (appendix) shows the development of the excess pore pressure by using the HSS model. It is here well illustrated that when ignoring the undrained material behavior in φ'/c' reduction phase, the excess pore pressure does not change after construction. For undrained FEA a slightly change of the excess pore pressure is visible.

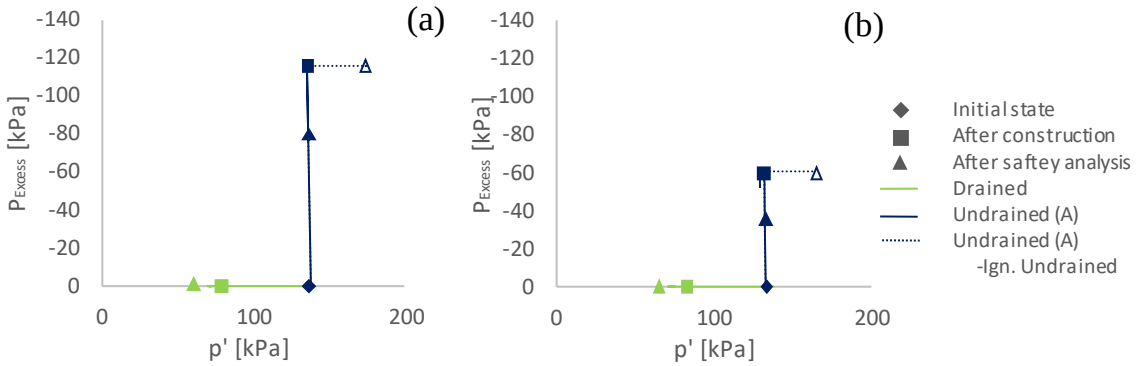

Fig. 67 Development excess pore water pressures for stress point A: (a) MC, (b) HSS

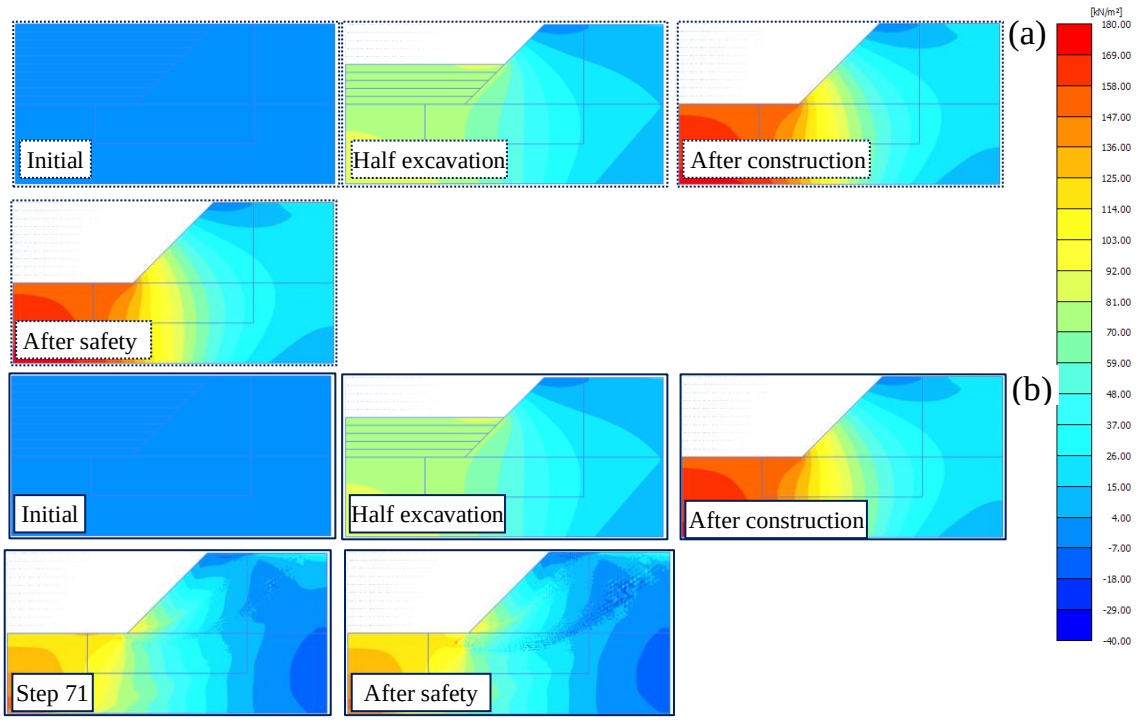

Fig. 68 Development of excess pore water pressures for MC – model: (a) Undrained (A) - Ign. Undrained, (b) Undrained (A)

6.2.5 Total volumetric strains

Fig. 69 shows the development of the total volumetric strains ε_{Vol} of stress point A. Blue lines represent the undrained FEA, dotted blue lines shows the undrained FEA with ignoring undrained in safety analysis, and green lines illustrate the fully drained analysis. Since for the initial state no volumetric strains occur all three lines starts at the same point (ε_{Vol}=0). For drained analysis positive volumetric strains occur during the excavation phase as well as in the φ'/c' reduction. Since the bulk modulus of undrained material is very high, no volumetric strains occur during the excavation phase for undrained conditions as well as for ignoring undrained material behavior during safety analysis. During the strength reduction analysis using undrained material behavior, ε_{Vol} remains zero but the pore pressures are changing. Negative total volumetric strains develop during the safety analysis by ignoring the undrained material behavior. Fig. 116 (appendix) shows the development of the volumetric strains for stress point B. The trend of the development is the same as for stress point A, but the magnitude of the volumetric strains is less. Fig. 70 shows the contour plots of the volumetric strains for different calculation steps performing SRFEA with the MC model. It is apparent, that for undrained conditions no volumetric strains occur, for ignoring undrained material behavior during safety analysis volumetric strains occur after construction. The contour plots of the volumetric strains performing SRFEA with the HSS model is shown in Fig. 117 (appendix).

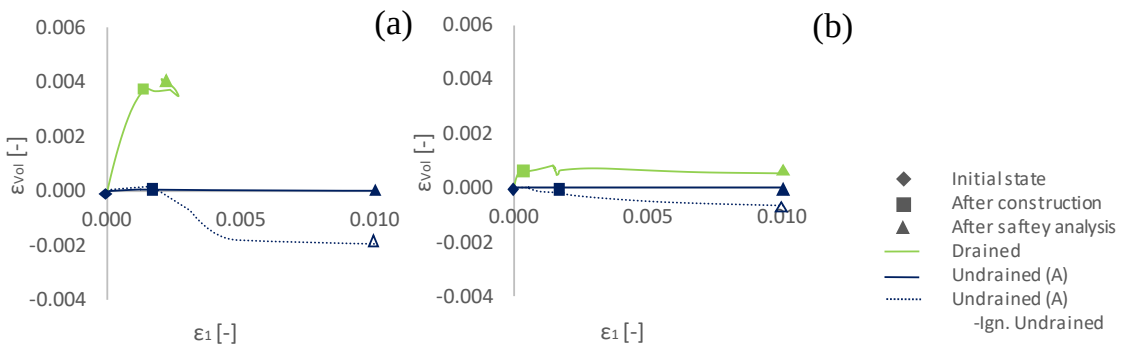

Fig. 69 Development of the volumetric strains for stress point A: (a) MC, (b) HSS

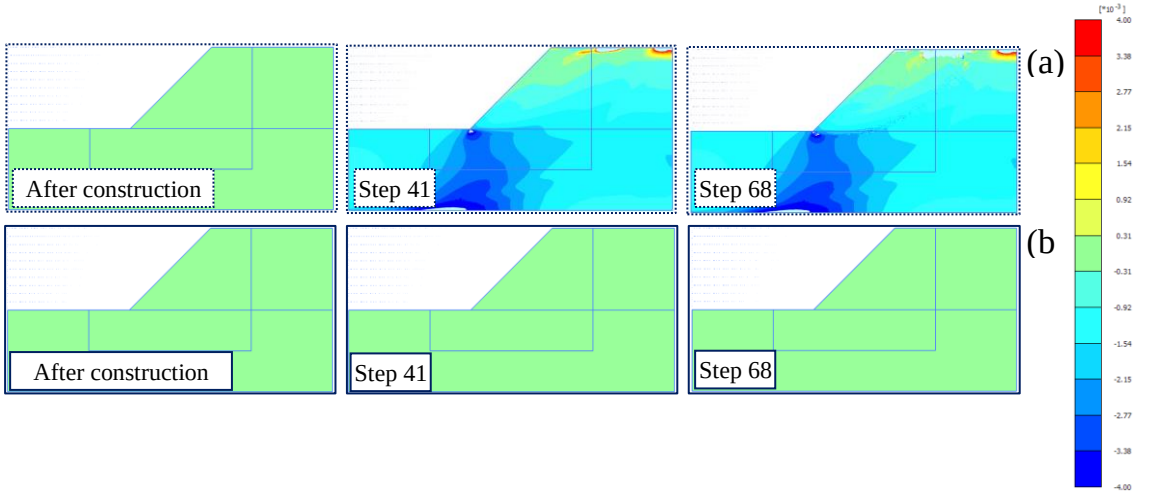

Fig. 70 Development total volumetric strains MC model: (a) Undrained (A) – Ign. Undrained, (b) Undrained (A)

6.3 Cavitation cut off stress 0 kPa

The purpose of this chapter is to investigate the safety factor considering a cavitation cut off stress of 0 kPa (in all calculation steps) for different drainage conditions. Furthermore, the evaluation and development of the incremental deviatoric strains, stress paths, excess pore pressures and volumetric strains is subject of this chapter. In the following figures full blue lines represent the results for undrained conditions, dotted blue lines the results for ignoring undrained behavior during safety analysis. Green lines illustrate the fully drained FEA.

6.3.1 Influence drainage conditions

Fig. 71 represents the obtained safety factors using the Mohr Coulomb (MC) model. Considering drained material behavior, a safety factor of about 1.38 is obtained. The safety factors, performing undrained analysis (considering a cavitation cut of stress of 0 kPa), differ only a little bit from the results from drained analysis. The corresponding FoS is slightly lower when performing undrained analysis (FoS=1.34) as well as for ignoring undrained during safety analysis (FoS=1.36). The manual strength reduction is in good agreement in terms to the automatic SRFEA. Since no negative excess pore pressures are generated during this analysis (because the cavitation cut off stress is 0kPa), the results of the undrained analysis are very similar to the results concerning drained material behavior. The development of the stress paths and the development of the excess pore pressure will be subsequently elaborated.

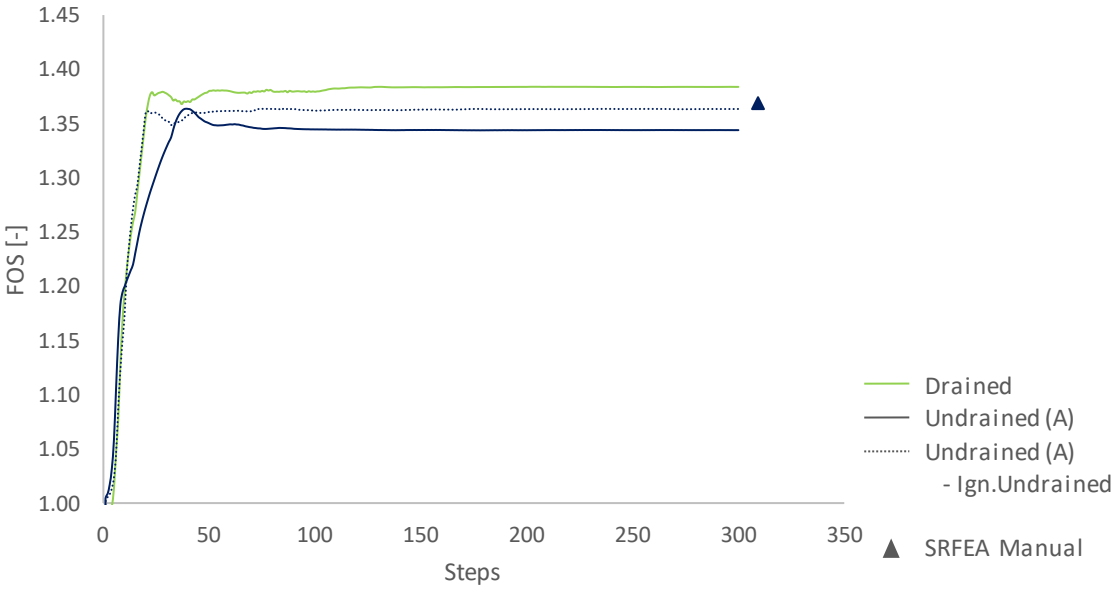

Fig. 71 Influence drainage condition on the obtained FoS for a cavitation cut off stress of 0 kPa

6.3.2 Failure mechanism

Fig. 72 shows the incremental deviatoric strains performing SRFEA with the MC model for drained FEA, undrained FEA and undrained analyzes with ignore undrained behavior in the strength reduction phase. It can be seen, that all failure mechanisms look very similar. The impact of undrained material behavior (cavity cut off stress 0 kPa) does not lead to a different shape of the failure mechanism. Two stress points, namely stress point A and stress point B, are selected for the evaluation of stress paths, excess pore pressures and volumetric strains. The results are presented in the following subchapters.

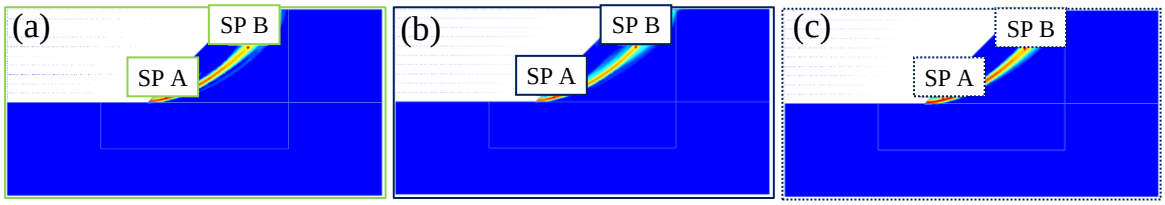

Fig. 72 Overview incremental deviatoric strains MC model: (a) Drained, (b) Undrained (A), (c) Undrained (A) – Ign. undrained

6.3.3 Stress paths

Fig. 73 (a) represents the stress path for stress point A, Fig. 73 (b) shows the stress path for stress point B, for different drainage conditions. Since the initial stresses are computed in the same way for all FEA, all stress paths start thereby at the same point. Apparently, all stress paths look similar and end at the drained MC failure line. But the effective mean stresses p' changes for the undrained analysis as well (in general p' must be constant when performing undrained analysis). However, the impact of a cavity cut off stress of 0 kPa influences the stress paths, as already the safety factor, significantly.

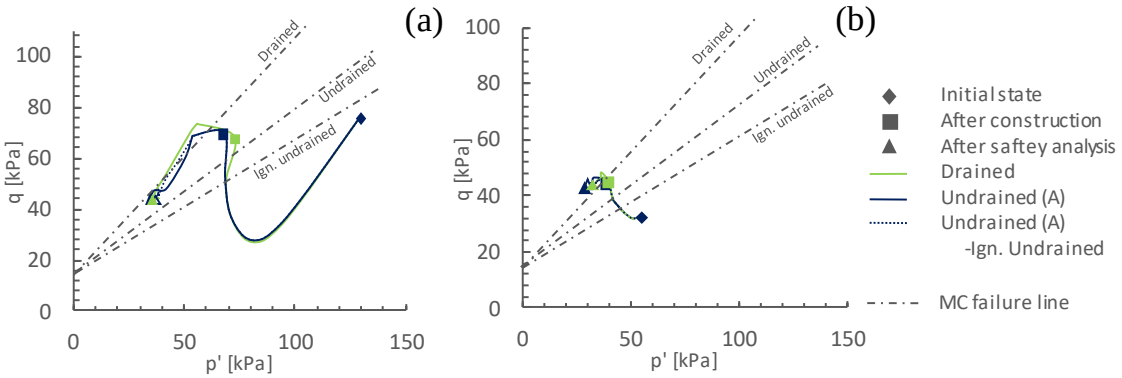

Fig. 73 p'q-diagram for MC model: (a) Stress point A, (b) Stress point B

6.3.4 Excess pore water pressures

Fig. 74 (a) shows the development of the excess pore pressures of stress point A, Fig. 74 (b) presents the results of stress point B for different drainage conditions. As, no pore water pressures are generated for drained analysis, only a change of the effective mean stress p' is observed. However, no significant excess pore pressures are generated for the undrained analysis. Consequently, for a cavitation cut off stress of 0 kPa, the results of all FEA are similar for all drainage conditions. This is the reason why the safety factors as well as the stress paths are very similar for all drainage conditions. However, this analysis with a cavitation cut off stress of 0 kPa does not represent realistic undrained material behavior.

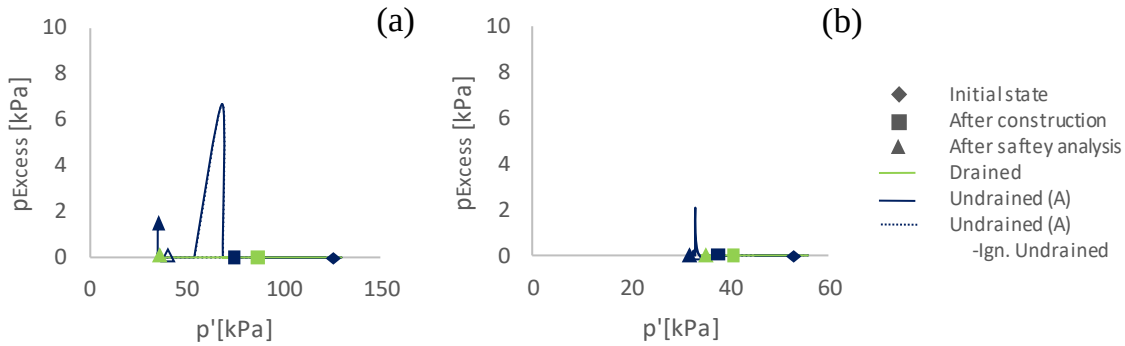

Fig. 74 Development of excess pore water pressures MC model: (a) Stress point A, (b) Stress point B

6.3.5 Total volumetric strains

Fig. 75 (a) shows the development of the total volumetric strains ε_{Vol} for stress point A and Fig. 75 (b) for stress point B. As for the initial state no volumetric strains occur, all three lines start at the same point ($\varepsilon_{Vol}=0$). Since the drained and undrained FEA are very similar for this case, the volumetric strains are also in the same range.

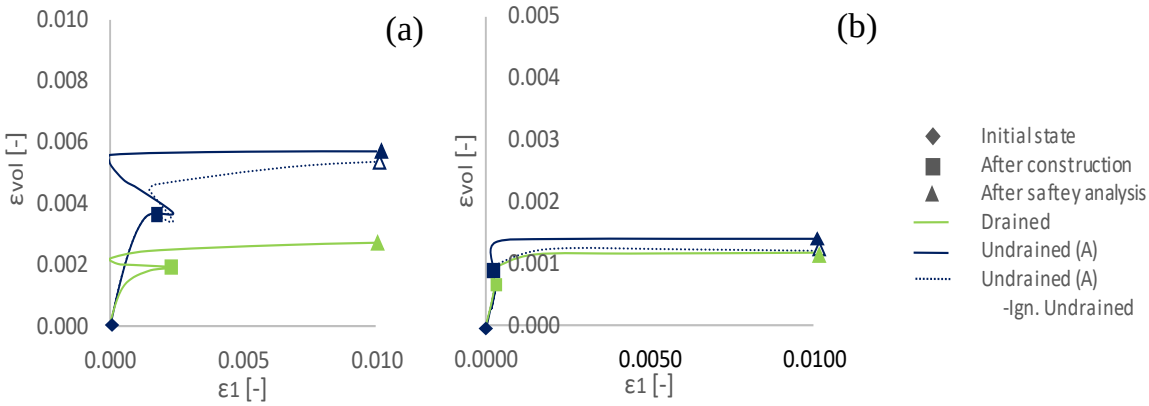

Fig. 75 Development total volumetric strains MC model: (a) Stress point A, (b) Stress point B

6.4 Cavitation cut off stress 100 kPa

The purpose of this chapter is to evaluate the factor of safety performing SRFEA with a cavitation cut off stress of 100 kPa for drained, undrained (A) and undrained (A) - ignoring undrained (in safety analysis) conditions. Furthermore, the evaluation and development of stress paths, excess pore pressures and volumetric strains is discussed. In the following figures full blue lines represent the results for undrained conditions, dotted blue lines the results for ignoring undrained behavior during safety analysis. Green lines illustrate the fully drained FEA.

6.4.1 Influence drainage conditions

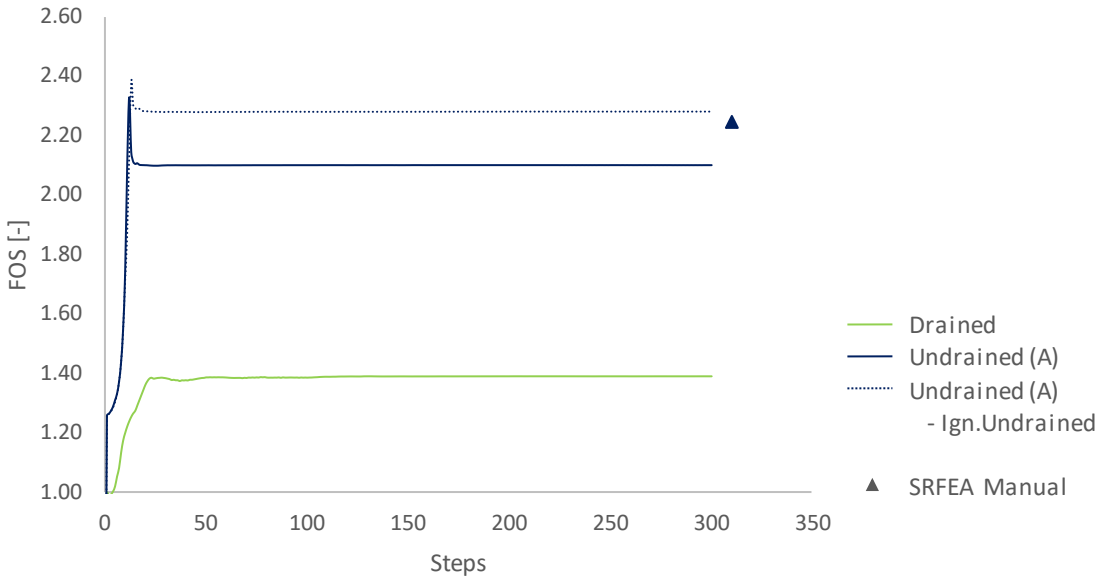

Fig. 76 Influence drainage conditions on the obtained FoS for a cavitation cut off stress of 100 kPa

Fig. 76 shows the obtained safety factor for the Mohr Coulomb (MC) constitutive model. As shown in the figure, the drainage conditions as well as the cavity cut off stress of 100 kPa influence the results strongly. A safety factor of 1.38 is obtained when performing SRFEA for drained conditions. For undrained conditions, the factor of safety increases strongly due to the development of negative excess pore pressures during the excavation phase of the embankment. Manual SRFEA is only performed for undrained material behavior. The result is in good agreement with the automatic SRFEA and corresponds approximately the upper peak of the automatic strength reduction. However, the results are similar to the results where no cavitation cut off was defined. A comparison of the influence of cavity is given later in chapter 6.5.

6.4.2 Failure mechanism

Fig. 77 represents the incremental deviatoric strains developed during SRFEA for different drainage conditions. It can be seen, that the impact of undrained material behavior and the cavitation cut off stress of 100 kPa significantly influences the shape of the slip surface. Two stress points A and B, as already treated in previous chapters, are selected for the further evaluation of stress paths, excess pore pressures and the volumetric strains.

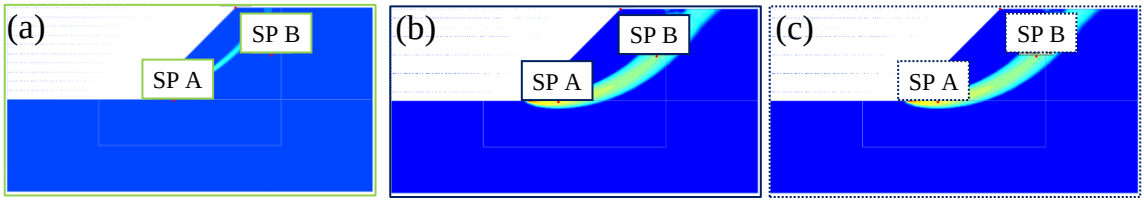

Fig. 77 Overview incremental deviatoric strains MC model: (a) Drained, (b) Undrained, (c) Undrained (A) – Ign. undrained

6.4.3 Stress paths

Fig. 78 (a) demonstrates the stress path of stress point A, Fig. 78 (b) for stress point B, considering different drainage conditions. Since the initial stresses are computed in the same way for all FEA, all stress paths start at the same point. It becomes apparent that for a cavitation cut off stress of 100 kPa, the stress paths correspond to the expectation of an undrained analysis. The effective mean stresses p' remains constant during the excavation as well as for the φ'/c' reduction. Ignoring undrained material behavior during safety analysis leads to a change of p'. For the drained analysis p' already changes during the excavation phase. It should be mentioned that the development of the stress paths looks very similar to the stress paths where no cavitation cut off was defined.

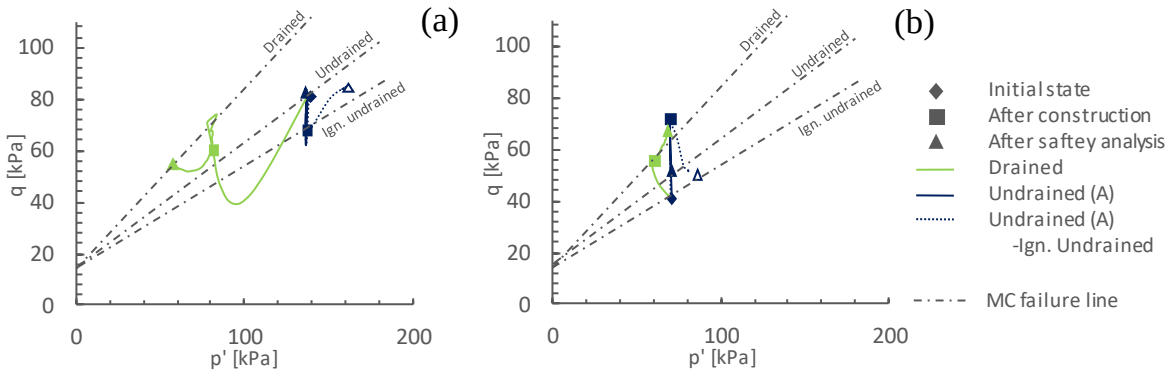

Fig. 78 p'q-diagram for MC model: (a) Stress point A, (b) Stress point B

6.4.4 Excess pore water pressures

Fig. 79 (a) represents the development of the excess pore water pressure for stress point (A), Fig. 79 (b) for stress point B. Since the initial stresses for all FEA are computed with the K_0 procedure, the starting point is the same for all analyzes. For the drained analysis, no pore water pressure is generated, just a change of the effective mean stress p' is noted. For the undrained analysis negative excess pore pressures are build up during the excavation phase. For the undrained analysis p' remains constant during the entire calculation. By ignoring undrained material behavior, the excess pore pressures remain constant after the construction but p' changes. It should be noted that the development of the excess pore pressures is very similar compared to the computation where no cavitation cut off was defined.

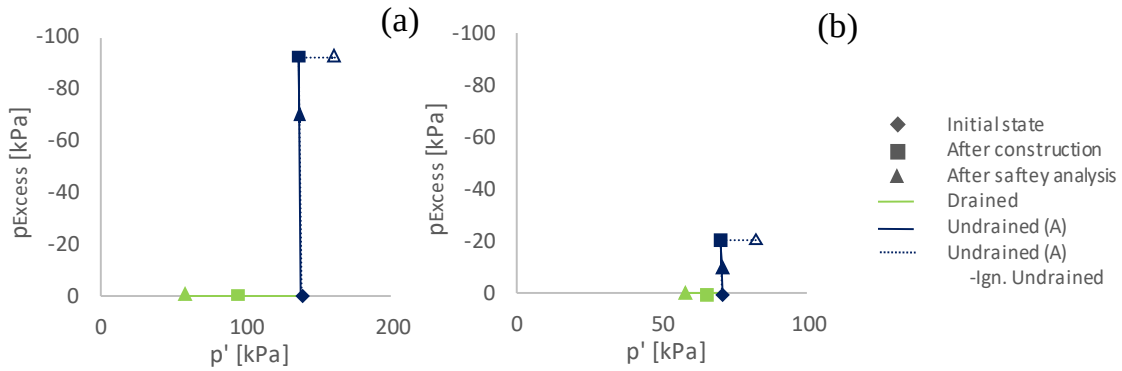

Fig. 79 Development excess pore water pressures Stress MC model: (a) Stress point A, (b) Stress point B

6.4.5 Total volumetric strains

In Fig. 80 (a) the total volumetric strains of stress point A and in Fig. 80 (b) for stress point B, are shown. Since for the initial state no volumetric strains occur all three lines starts at the same point ($\varepsilon_{Vol}=0$). The development of the volumetric strains is similar for all FEA, where no cavitation cut off criterion was defined. For drained analysis positive volumetric strains occur during the entire calculation. When performing undrained analysis, no volumetric strains occur because the bulk modulus is very high for undrained material behavior. By ignoring undrained material behavior during safety analysis, negative volumetric strains occur after construction.

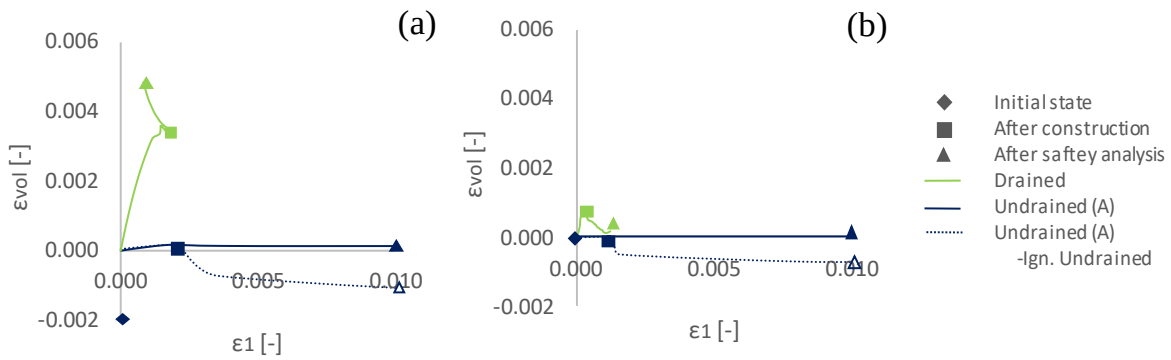

Fig. 80 Development total volumetric strains MC model: (a) Stress point A, (b) Stress point B

6.5 Influence of cavity

The comparison of the influence of the cavitation cut off stress for undrained material behavior is shown in Fig. 81. It is noticeable, that for the case, where a cavitation cut off equal to 0 kPa is defined, the obtained safety factor corresponds approximately the results from drained FEA. Nevertheless, the results when performing with no cavitation off and a cavitation cut off of 100 kPa are very similar. However, a slight difference occurs by ignoring undrained material behavior during φ'/c' reduction. However, the impact of cavity has an essential influence on the obtained safety factor. A cavitation cut off stress of 0 kPa should never be used for undrained FEA in combination with unloading stress paths because no excess negative pore pressures are generated.

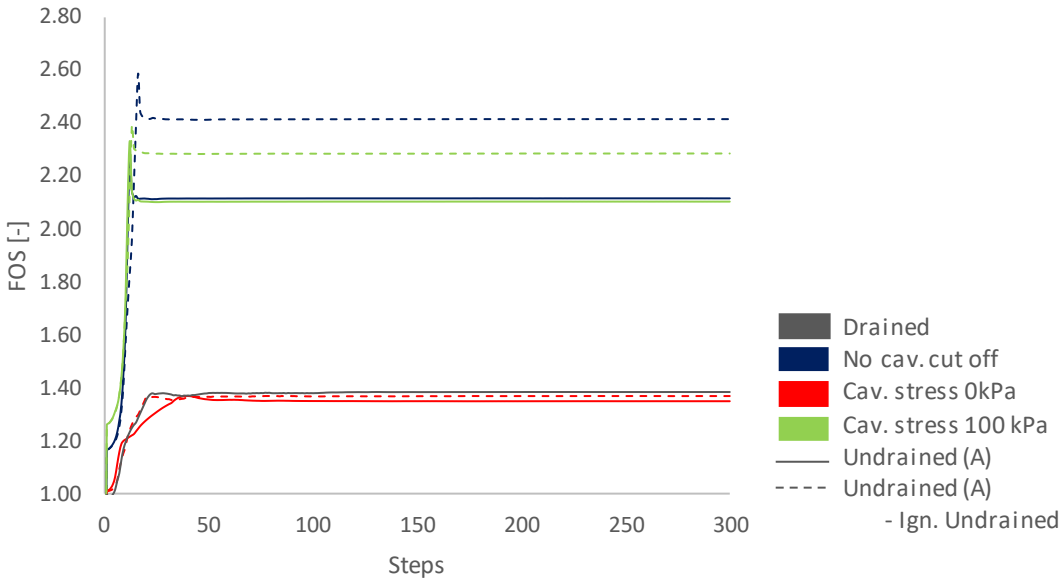

Fig. 81 Influence of the cavitation cut of stress on obtained FoS

6.6 Influence of suction

The purpose of this chapter is the evaluation of the influence of suction on the obtained factor of safety for undrained material behavior. In the following, blue lines represent the calculation with the default setting *"Ignore suction"* during the plastic phase and the safety analysis, orange lines demonstrate the results of the undrained analysis where suction is allowed. Dotted lines represent the obtained safety factor for undrained material behavior with ignoring undrained material behavior during φ'/c' reduction. The entire calculation is performed with no cavitation cut off.

6.6.1 Influence drainage conditions

Fig. 82 shows the impact of suction on the obtained factor of safety. It is evident, that suction influences the factor of safety for the considered boundary value problem. Performing undrained analysis, where suction is allowed, the factor of safety is in the same range as for drained conditions but slightly higher. For the case where suction is allowed, for ignoring undrained material behavior during the safety analysis leads to a lower safety factor compared to the computation with fully undrained conditions.

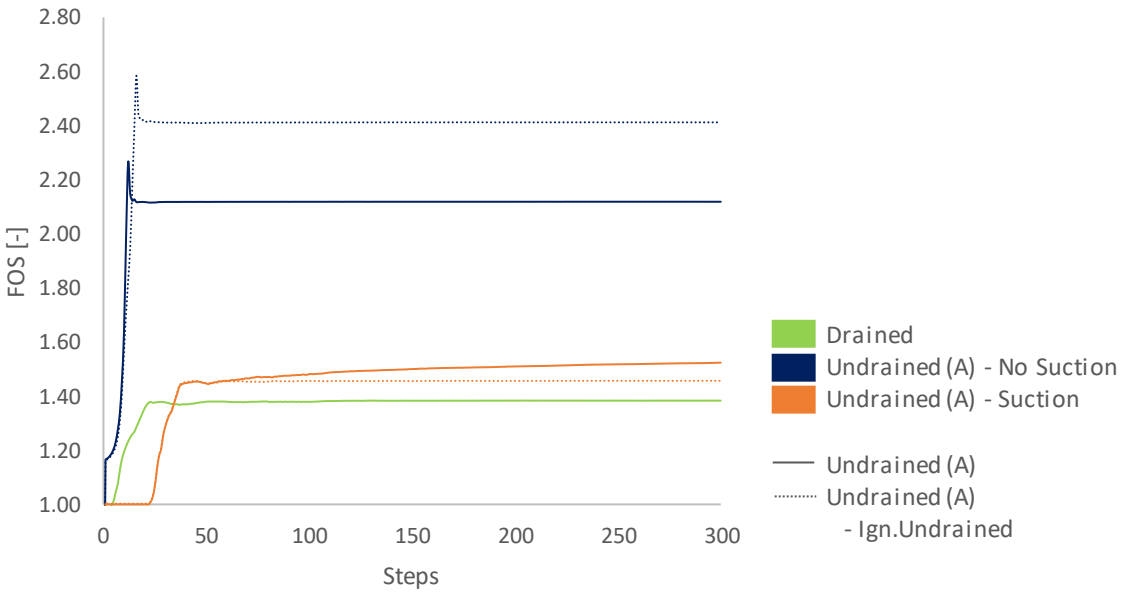

Fig. 82 Influence of suction on obtained FoS

6.6.2 Failure mechanism

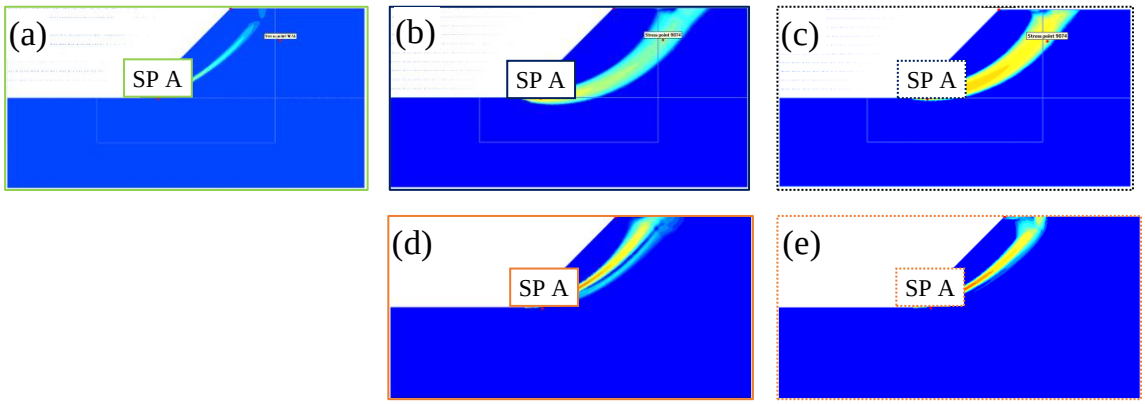

Fig. 83 Overview failure mechanism: (a) Drained, (b) Undrained (A), (c) Undrained (A) – Ign. Undrained, (d) Undrained (A) – Suction, (e) Undrained (A) – Ign. Undrained – Suction

Fig. 83 shows the failure mechanism for different drainage conditions and the influence of suction. Fig. 83 (d) and Fig. 83 (e) clearly demonstrate that the effect of suction strongly influences the shape of the failure mechanism. Stress point A in the lower area of the slip surface is chosen for the further evaluation of the stress paths, the development of the excess pore pressures and the volumetric strains.

6.6.3 Stress paths

Fig. 84 represents the development of the stress paths of stress point A for different drainage conditions and the influence of the effect of suction. The influence of suction effects leads to a similar development of the stress paths as for drained conditions. Although it is an undrained analysis the effective mean stresses p' does not remain constant during the excavation and the safety analysis.

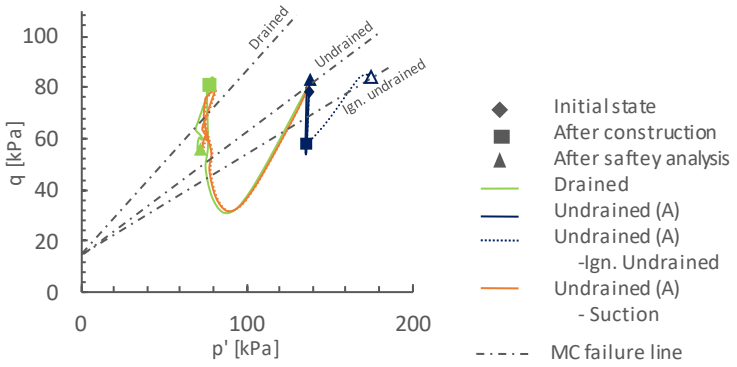

Fig. 84 Influence of suction on stress path

6.6.4 Excess pore water pressures

Fig. 85 shows the development of excess pore water pressures of stress point (A). It has already been shown with the stress paths that the effect of suction during an undrained analysis significantly influences the factor of safety and the stress paths behave very similar to drained material behavior. This fact can also be observed in the development of the excess pore pressures. The effect of suction considering undrained material behavior leads to a heavy reduction of excess pore pressures.

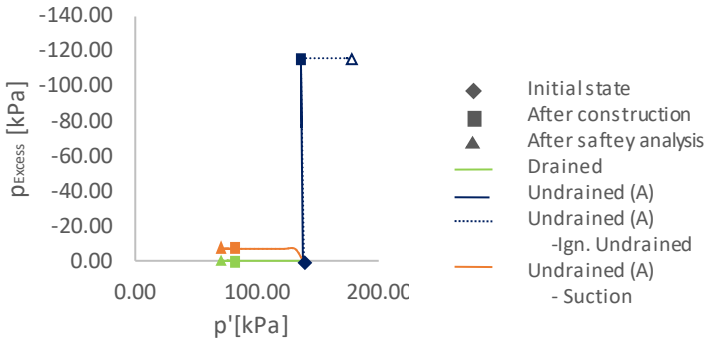

Fig. 85 Influence of suction on excess pore water pressures

6.6.5 Total volumetric strains

Fig. 86 shows the development of the total volumetric strains considering the effect of suction during an undrained analysis. It can be seen very well that the development of the total volumetric strains behaves similar to drained material behavior.

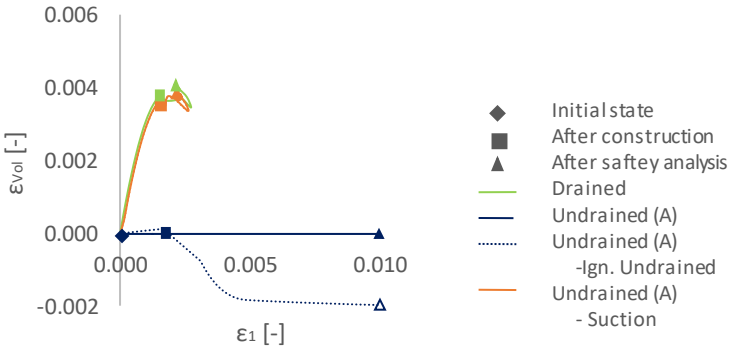

Fig. 86 Influence of suction on total volumetric strains

7 Conclusion

The results presented in this thesis confirm that two different approaches of FEA for slope stability analysis, namely SRFEA and FELA are in good agreement for associated plasticity ($\psi'=\varphi'$). Since FELA is limited to associated plasticity, the necessity of the Davis approach came up to model non-associated plasticity. It is shown, that the results, considering non-associated plasticity, from FELA (with Davis approach) compared to SRFEA are still in good agreement but remain slightly conservative. When performing SRFEA implemented, the effective dilatancy angle ψ' is kept constant. A couple of studies have been carried out with the modified (DLL) strength reduction technique, where the effective dilatancy angle ψ' is reduced in the same way than the effective friction angle φ' (for ($\psi' < \varphi'_{reduced}$). It could be shown that for associated plasticity ($\psi'=\varphi'$) as well as for the case that $\psi'=0°$, both strength reduction techniques lead to very similar FoS. However, for $0°<\psi'<\varphi'$, the implemented strength reduction technique slightly overestimates the safety factor. It is recommended performing SRFEA with the modified (DLL) technique. It is well known that the mesh discretization and the shape function have a significant influence on the obtained factors of safety. This was also confirmed in a couple of examples of this thesis. Furthermore, it was shown that a high degree of non-associativity (φ'-ψ') in combination with steep slopes leads to oscillations on the obtained FoS. An important outcome of the studies is, that the automatic and manual strength reduction, for drained and undrained conditions, are in good agreement and that a reduction of the tolerated error leads to lower FoS when performing manual SRFEA. Nevertheless, the factor of safety is less influenced by the tolerated error when performing an automatic SRFEA. Furthermore, it could be shown that the setting of the incremental multiplier has a very small influence on the obtained safety factor (performing an automatic strength reduction). Since the MC and HSS model use a Mohr Coulomb failure criterion, it was shown (for automatic SRFEA) that the same safety factors are obtained for drained material behavior. However, for manual SRFEA, differences between these constitutive models occur. Furthermore, this thesis has proven that the results, when performing 3D SRFEA are in good agreement with the results from 2D FEA for non-associated plasticity. It could also be shown that the oscillations are in the same range. For associated plasticity ($\psi'=\varphi'$) the overall trend of the obtained results is similar to 2D SRFEA, but for 3D SRFEA strong oscillation occurred and no clear failure mechanism of the soil body was obtained. A sensitivity analysis of some numerical control parameters was performed for associated plasticity ($\psi'=\varphi'$). The numerical parameters over-relaxation factor, updated mesh, desired min/max number of iterations, arc length control, solver type and the incremental multiplier lead to no improvement. At the same time, it could be shown that for a reduced tolerated error equal to 0.1%, the strong oscillations decrease significantly. To study the impact of the drainage conditions on the factor of safety, 2D SRFEA using effective strength and stiffness parameters were performed. Drained FEA, undrained FEA and undrained analysis with ignore

undrained behavior in the strength reduction phase were part of the investigation. The results revealed that due to an unloading negative excess pore water pressures occur, which lead to higher safety factors. Compared to drained analysis, it could be shown that the obtained factors of safety for MC and HSS for undrained material behavior differ, because of different developments of the excess pore pressures. A further important outcome of the undrained studies is that the cavitation cut off stress and the effect of suction strongly influence the safety factors.

8 List of tables

9 List of figures

10 References

[1] Brinkgreve R.B.J., Kumarswamy S., Swolfs W.M., Foria F., Plaxis 2D 2018-User Manual, Delft, The Netherlands: Plaxis bv; 2018

[2] Brinkgreve R.B.J., Kumarswamy S., Swolfs W.M., Plaxis 2D 2016-User Manual, Delft, The Netherlands: Plaxis bv; 2016

[3] Brinkgreve R.B.J., Kumarswamy S., Swolfs W.M., Plaxis 3D 2018-User Manual, Delft, The Netherlands: Plaxis bv; 2018

[4] Krabbenhoft K., Optum G2: Theory, Optum Computational Engineering; 2018

[5] Tschuchnigg, F., Schweiger, H.F. and Sloan, S.W. (2015). Slope stability analysis by means of finite element limit analysis and finite element strength reduction techniques. Part l: Numerical studies considering non-associated plasticity. Computers and Geotechnics 70: 169-177

[6] Oberhollenzer, S., Tschuchnigg, F. and Schweiger, H.F. (2018). Finite element analyses of slope stability problems using non-associated plasticity. Journal of Rock Mechanics and Geotechnical Engineering 10 (2018) 1091-1101

[7] Tschuchnigg, F., Schweiger, H.F., Sloan, S.W., Lyamin, A.V. and Raissakis I. (2015). Comparison of finite-element limit analysis and strength reduction techniques. Geotechnique 65, No. 4. 249-257 [http://dx.doi.org/10.1680/geot.14.P02]

[8] Davis, E.H. (1968). Theories of plasticity and failure of soil masses. In Soil mechanics: selected topics. (ed. I. K. Lee), pp.341–354. New York, NY, USA: Elsevier.

[9] Oberhollenzer, S. (2017), Numerical studies on slope stability analysis, Master´s thesis, Institute of Soil Mechanics, Foundation Engineering and Computational geotechnics, Graz University of technology

[10] Egger, D. (2012), Untersuchung zur Böschungsstabilität mittels FE-Methode. Master´s thesis, Institute of Soil Mechanics, Foundation Engineering and Computational geotechnics, Graz University of technology

[11] Schweiger, H.F. (2018), Computational Geotechnics: Lecture notes, Institute of Soil Mechanics, Foundation Engineering and Computational geotechnics, Graz University of technology

[12] Schweiger, H.F. (2017), Marte, R. (2017), Soil mechanics and Foundation Engineering: Lecture notes, Institute of Soil Mechanics, Foundation Engineering and Computational geotechnics, Graz University of technology

[13] Marte, R. (2015), Boden- u. Felsmechanik Grundlagen: Lecture notes, Institute of Soil Mechanics, Foundation Engineering and Computational geotechnics, Graz University of technology

[14] Hill, R. (1950). The Mathematical Theory of Plasticity. Oxford University Press, London, U.K.

[15] Schanz, T., Vermeer, P.A., Bonnier, P.G. (1999). The hardening-soil model: Formulation and verification. In R.B.J. Brinkgreve, Beyond 2000 in Computational Geotechnics, Balkema, Rotterdam. 281-290

[16] Benz, T. (2006). Small-Strain Stiffness of Soils and its Numerical Consequences. Ph.d. thesis, Universität Stuttgart.

11 Appendix

4.2.1.3 Failure mechanism SRFEA associated flow rule (ψ'=φ')

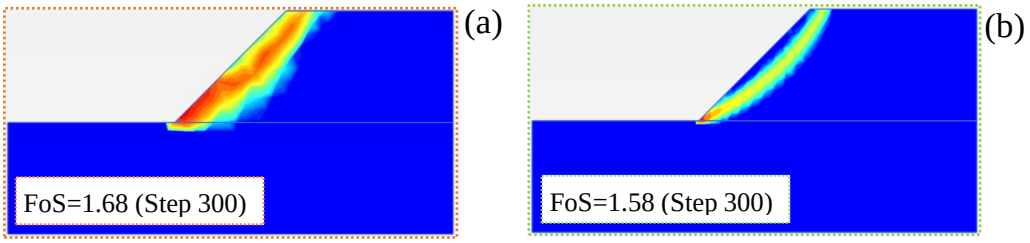

Fig. 87 Overview failure mechanism SRFEA modified (DLL): (a) Coarse (6n), (b) Fine (6n)

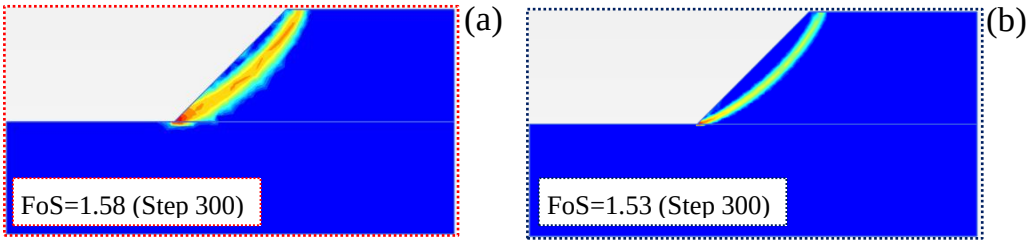

Fig. 88 Overview failure mechanism SRFEA modified (DLL): (a) Coarse (15n), (b) Fine (15n)

4.3.1.3 Failure mechanism SRFEA non-associated flow rule (ψ'=10°)

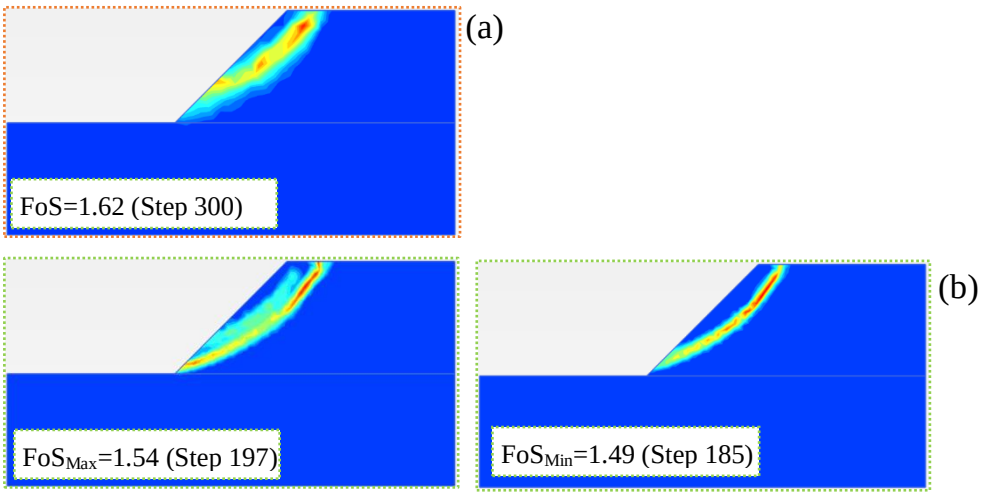

Fig. 89 Overview failure mechanism SRFEA modified (DLL): (a) Coarse (6n), (b) Fine (6n)

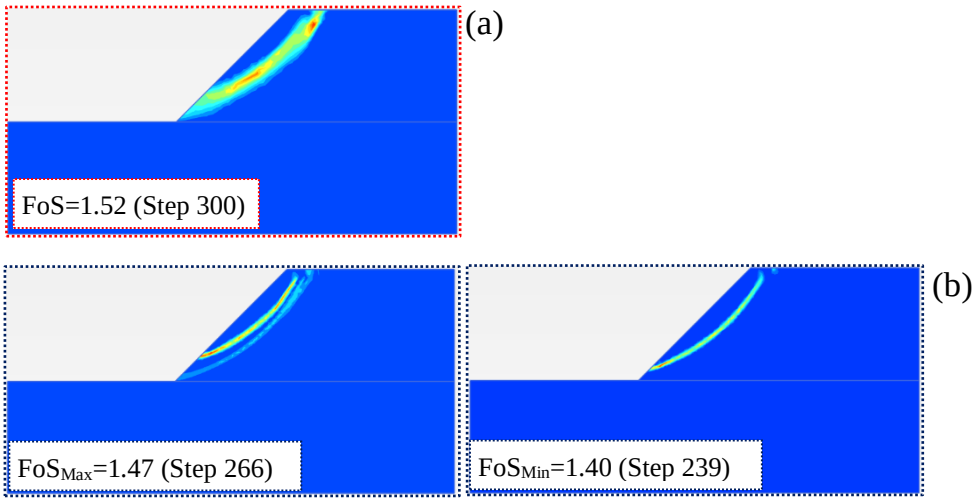

Fig. 90 Overview failure mechanism SRFEA modified (DLL): (a) Coarse (15n), (b) Fine (15n)

4.3.2.2 Failure mechanism FELA non-associated flow rule ψ'=10°

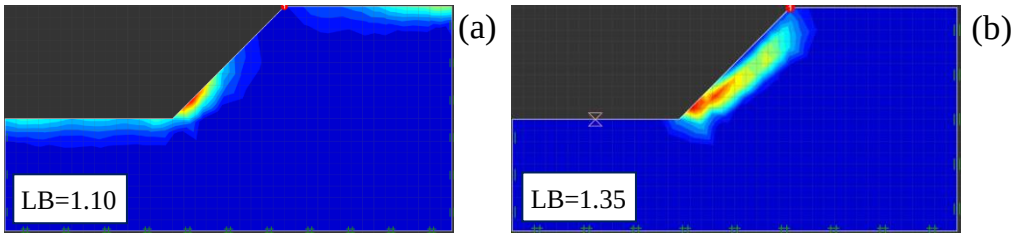

Fig. 91 Overview shear strains FELA (Davis A) for a coarse mesh (a) Lower elements, (b) Upper elements

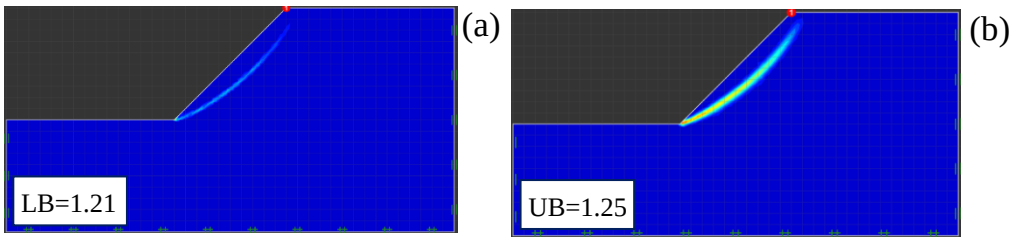

Fig. 92 Overview shear strains FELA (Davis A) for a fine mesh (a) Lower elements, (b) Upper elements

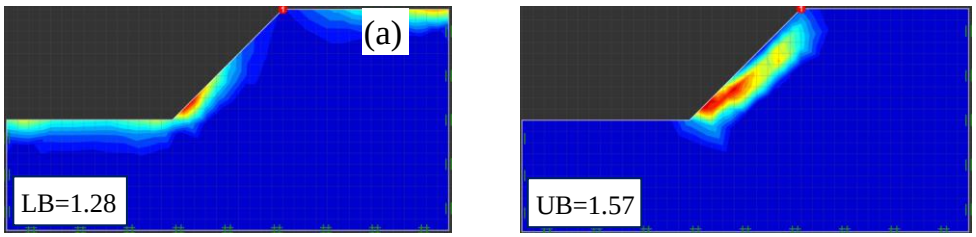

Fig. 93 Overview shear strains FELA (Davis C) for a coarse mesh (a) Lower elements, (b) Upper elements

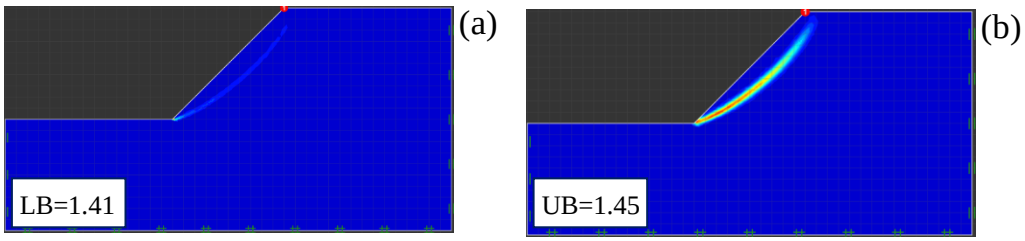

Fig. 94 Overview shear strains FELA (Davis C) for a fine mesh (a) Lower elements, (b) Upper elements

4.3.1.4 Numerical settings for non-associated flow rule (ψ'=10°)

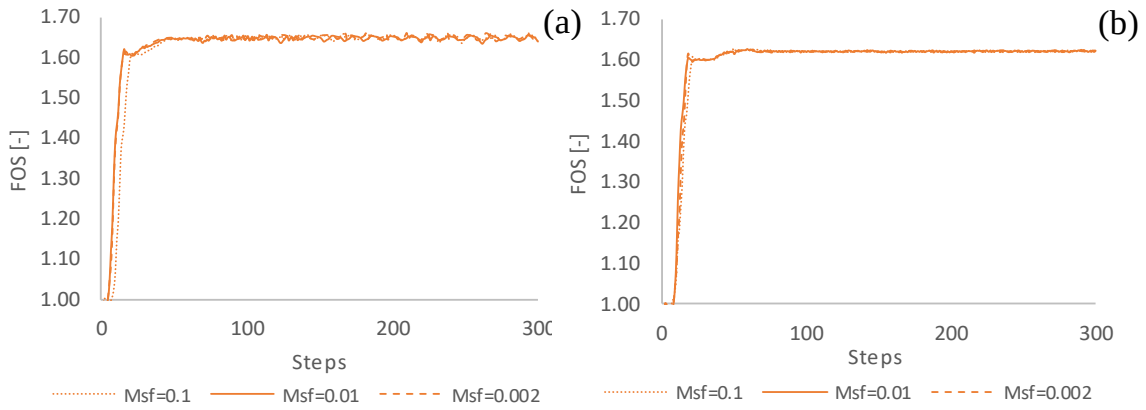

Fig. 95 Comparison influence M_{SF} for 6n-coarse mesh and ψ'=10°: (a) SRFEA implemented, (b) SRFEA modified (DLL)

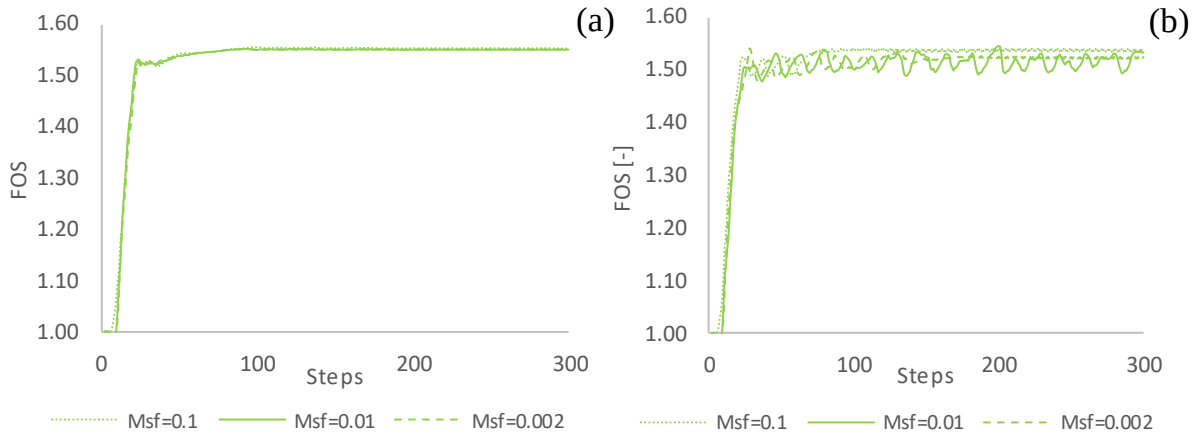

Fig. 96 Comparison influence M_{SF} for 6n-fine mesh and ψ'=10°: (a) SRFEA implemented, (b) SRFEA modified (DLL)

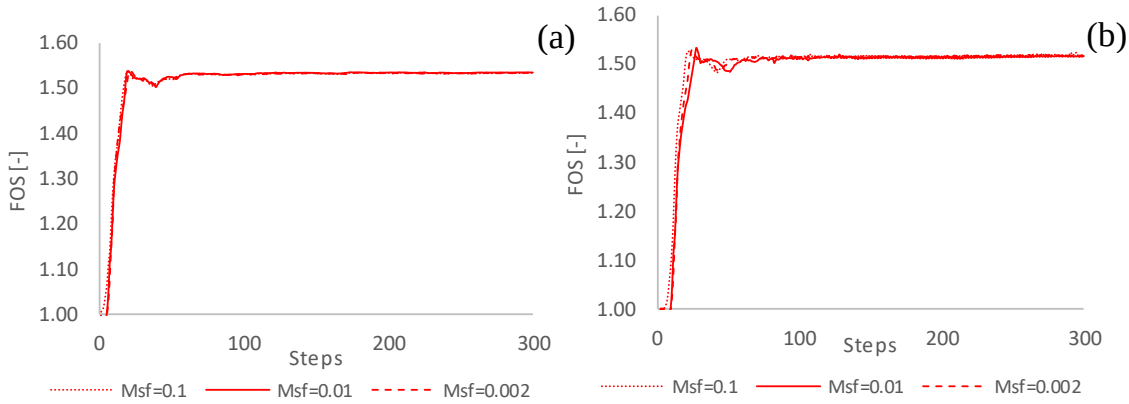

Fig. 97 Comparison influence M_{SF} for 15n-coarse mesh and ψ'=10°: (a) SRFEA implemented, (b) SRFEA modified (DLL)

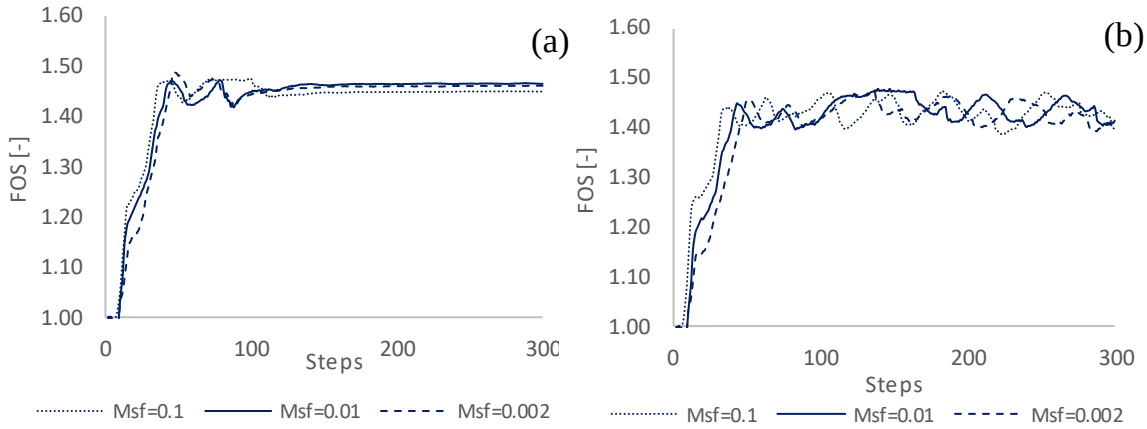

Fig. 98 Comparison influence M_{SF} for 15n-fine mesh and ψ'=10°: (a) SRFEA implemented, (b) SRFEA modified (DLL)

4.4.1.3 Failure mechanism SRFEA non-associated flow rule (ψ'=0°)

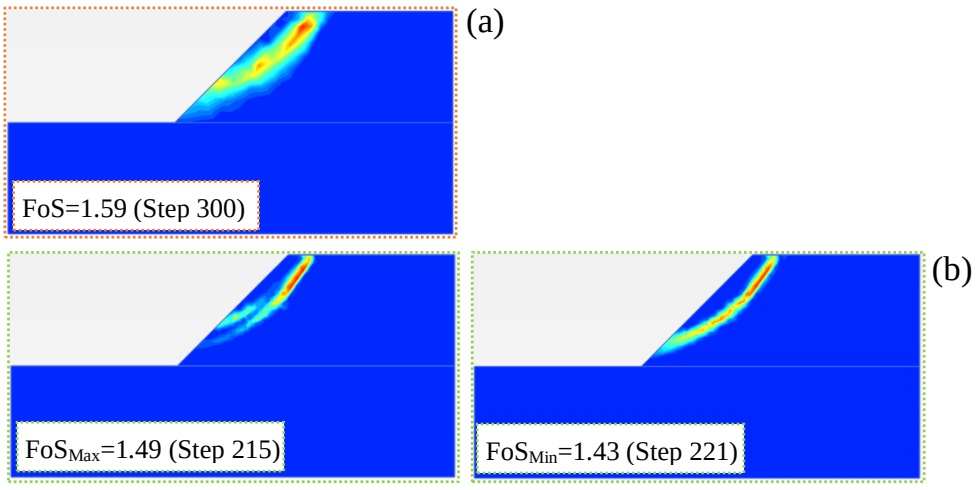

Fig. 99 Overview failure mechanism SRFEA modified (DLL): (a) Coarse (6n), (b) Fine (6n)

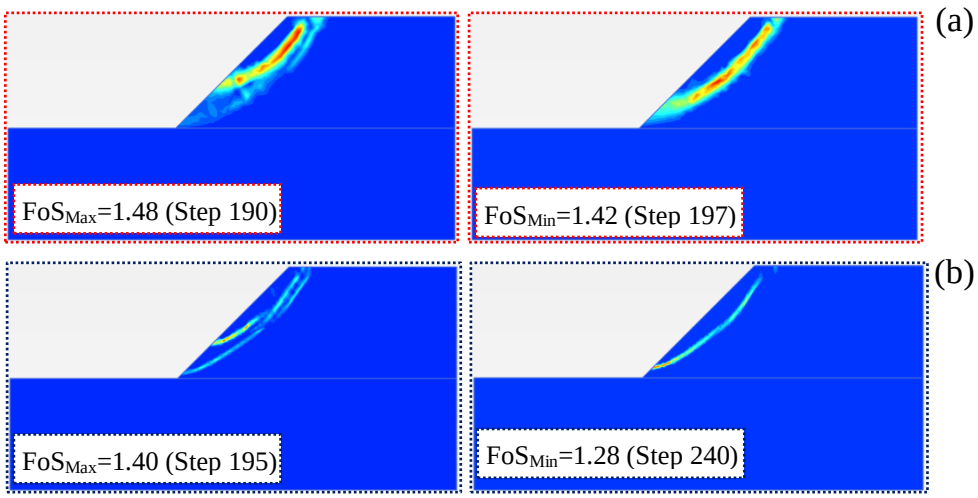

Fig. 100 Overview failure mechanism SRFEA modified (DLL): (a) Coarse (15n), (b) Fine (15n)

4.4.2.2 Failure mechanism FELA non-associated flow rule (ψ'=0°)

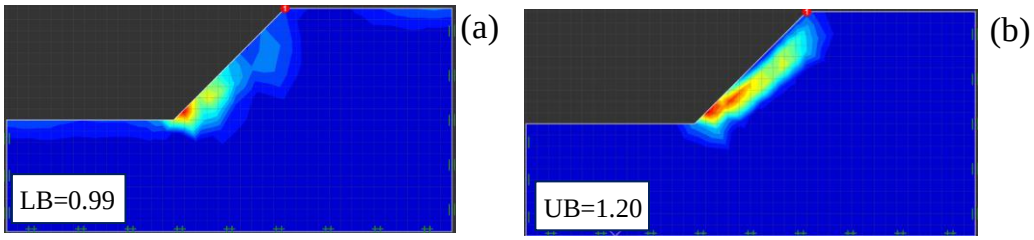

Fig. 101 Overview shear strains FELA (Davis A) for a coarse mesh (a) Lower elements, (b) Upper elements

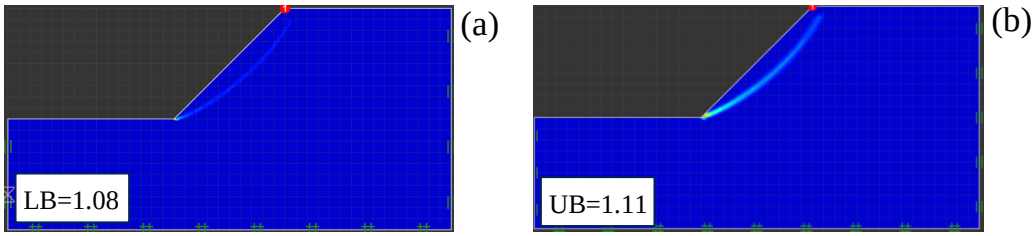

Fig. 102 Overview shear strains FELA (Davis A) for a fine mesh (a) Lower elements, (b) Upper elements

4.4.1.4 Numerical settings for non-associated flow rule (ψ'=0°)

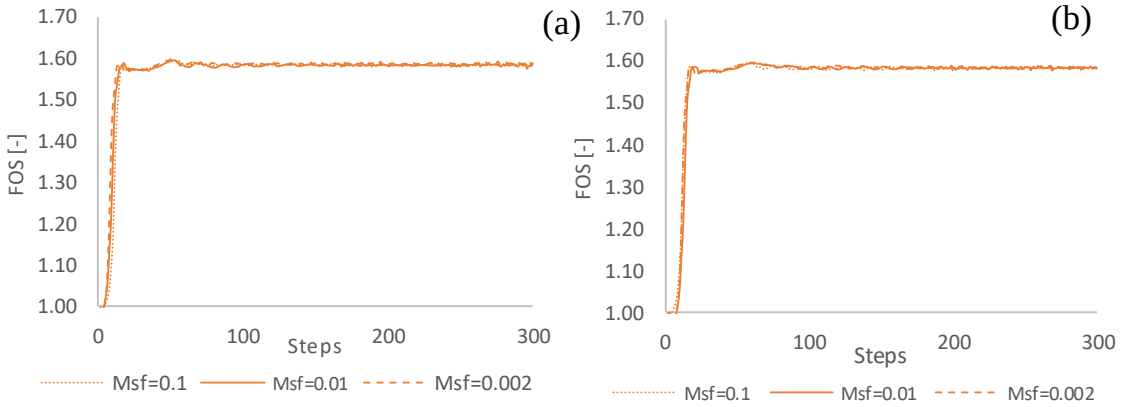

Fig. 103 Comparison influence M_{SF} for 6n-coarse mesh and ψ'=0°: (a) SRFEA implemented, (b) SRFEA modified (DLL)

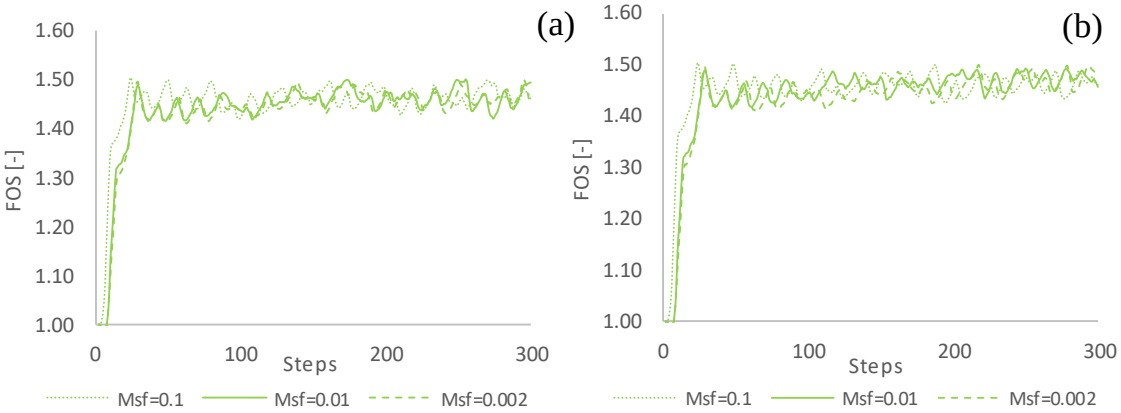

Fig. 104 Comparison influence M_{SF} for 6n-fine mesh and ψ'=0°: (a) SRFEA implemented, (b) SRFEA modified (DLL)

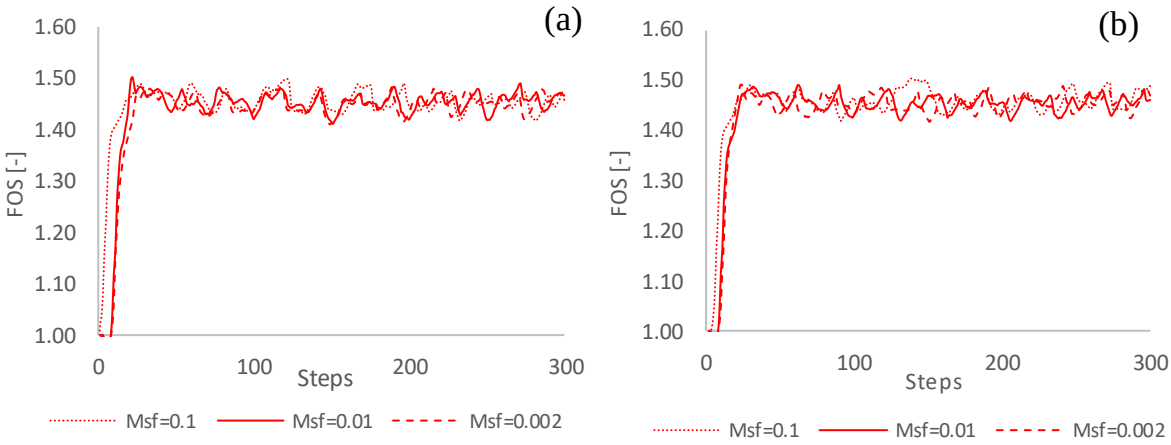

Fig. 105 Comparison influence MSF for 15n-coarse mesh and ψ'=0°: (a) SRFEA implemented, (b) SRFEA modified (DLL)

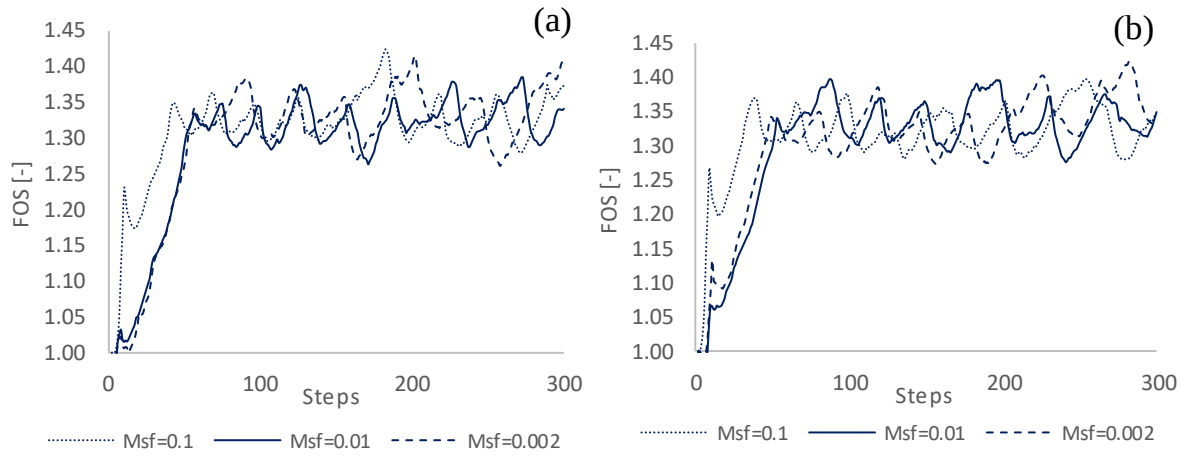

Fig. 106 Comparison influence MSF for 15n-coarse mesh and ψ'=0°: (a) SRFEA implemented, (b) SRFEA modified (DLL)

5.2.1.2 Failure mechanism 3D SRFEA associated flow rule (ψ'=φ') – standard

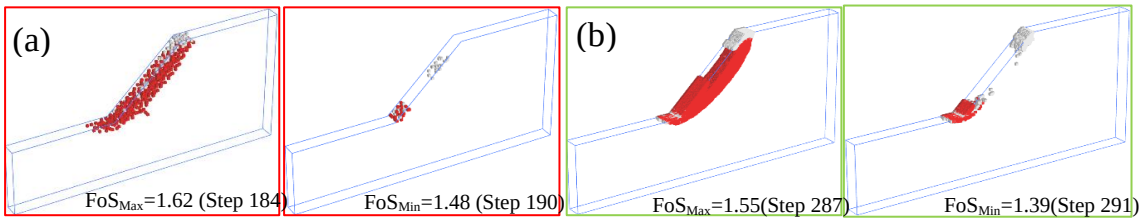

Fig. 107 Plastic points: (a) Coarse (10n), (b) Very fine (10n)

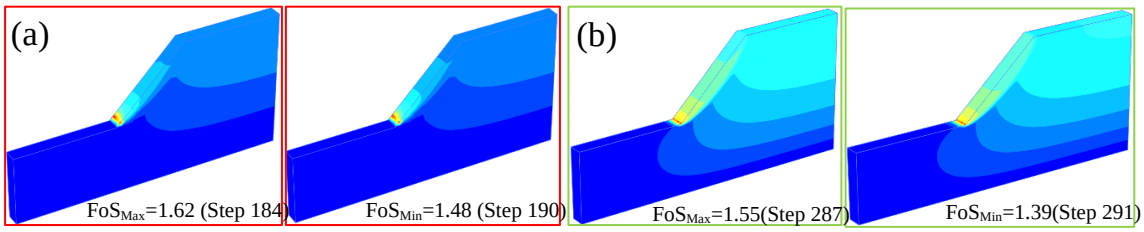

Fig. 108 Total displacements: (a) Coarse (10n), (b) Very fine (10n)

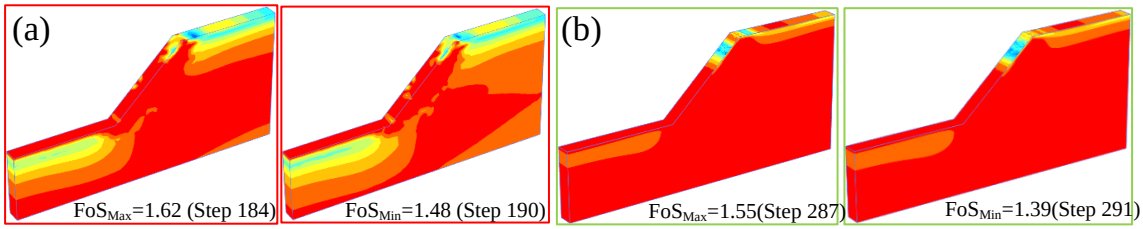

Fig. 109 Relative shear stresses: (a) Coarse (10n), (b) Very fine (10n)

5.3 3D SRFEA - Model depth 50m

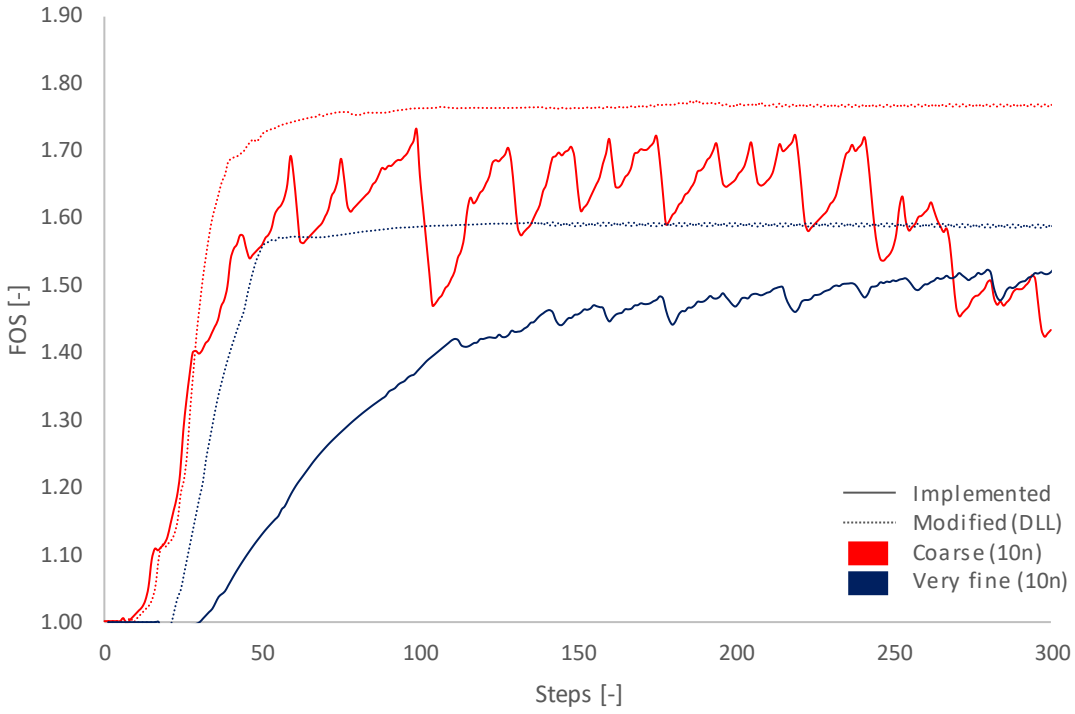

Fig. 110 Computed FoS for MC model: Comparison of SRFEA implemented and modified (DLL) for ψ'=φ'

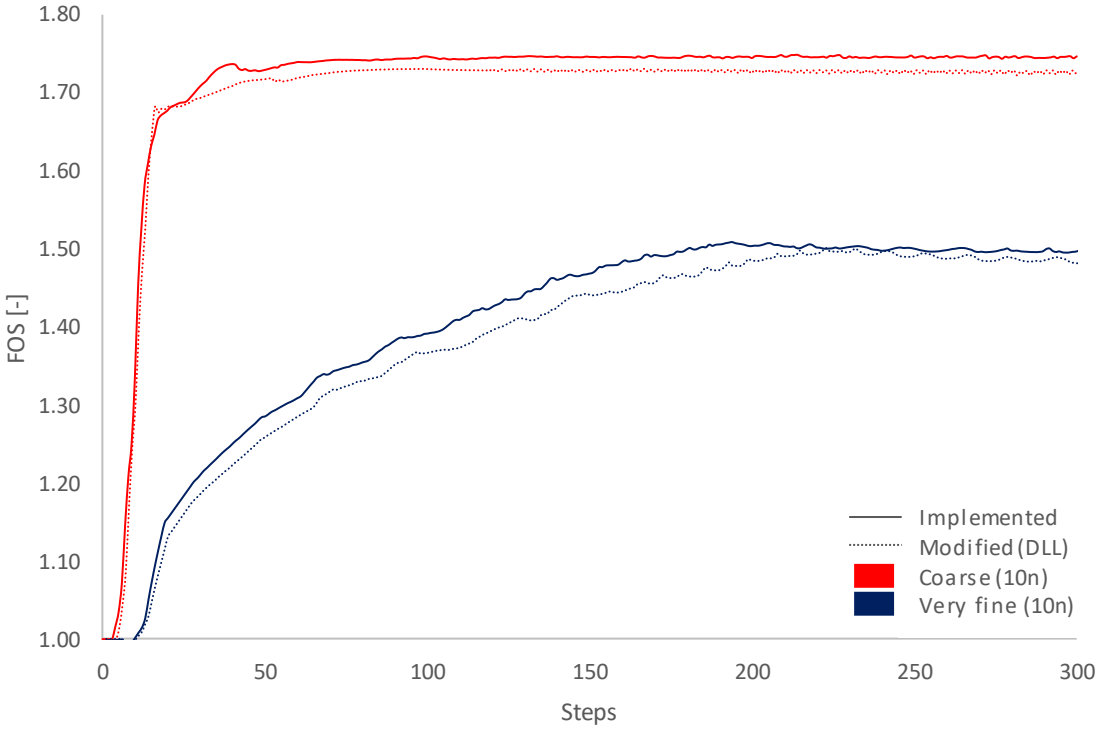

Fig. 111 Computed FoS for MC model: Comparison of SRFEA implemented and modified (DLL) for ψ'=10°

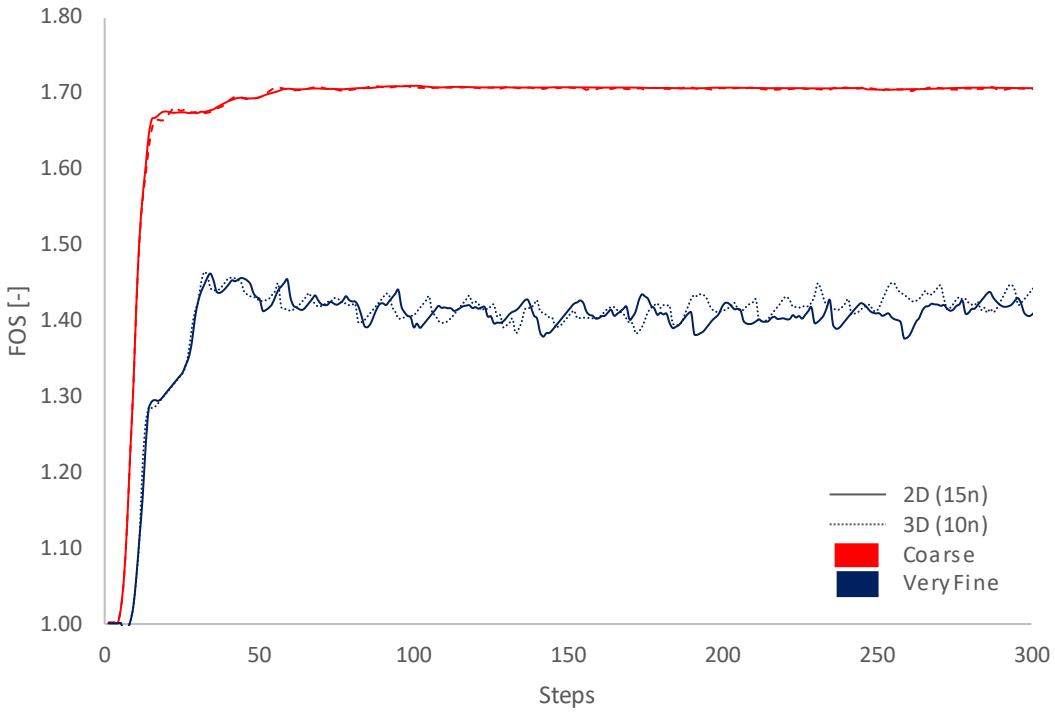

Fig. 112 Computed FoS for MC model: Comparison of SRFEA implemented and modified (DLL) for ψ'=0°

6.2.3 Development stress paths for stress point B

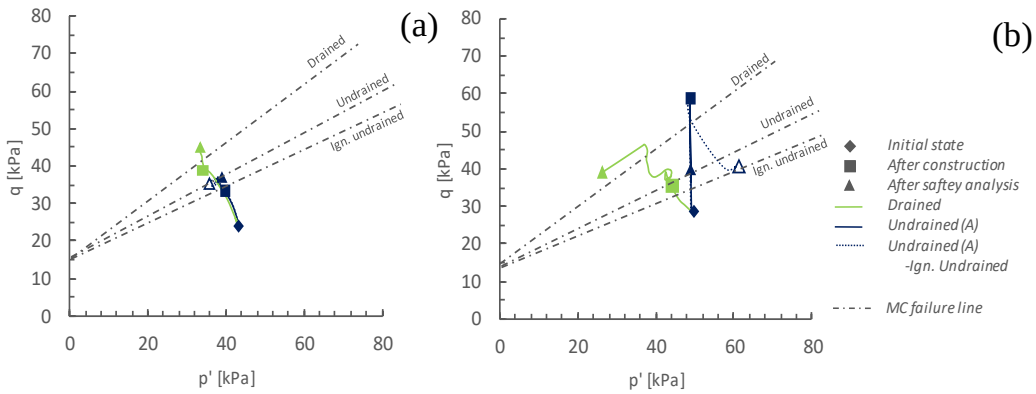

Fig. 113 Development stress paths of stress point B: (a) MC, (b) HSS

6.2.4 Development excess pore water pressures

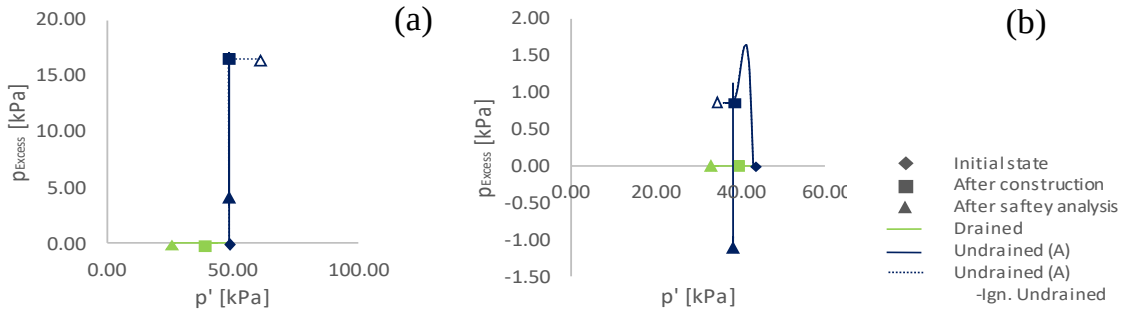

Fig. 114 Development excess pore water pressures of stress point B: (a) MC, (b) HSS

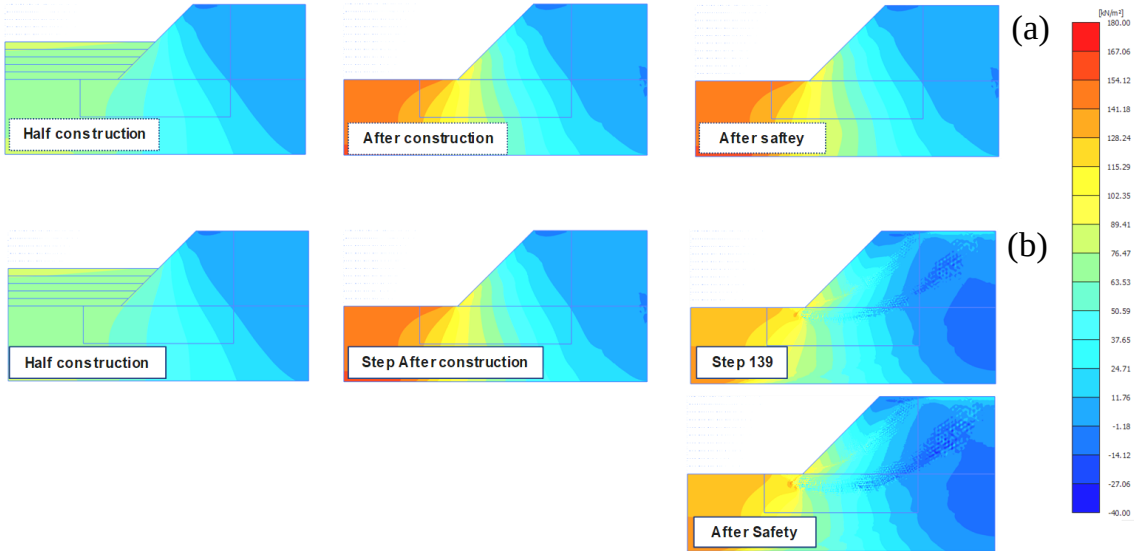

Fig. 115 Development excess pore water pressures HSS model: (a) Undrained (A) – Ign. Undrained, (b) Undrained (A)

6.2.5 Development total volumetric strains

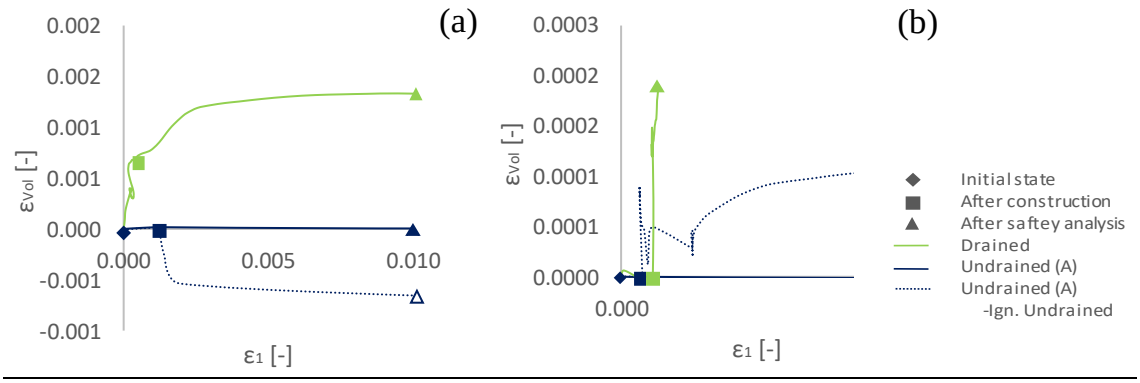

Fig. 116 Development total volumetric strains of stress point B: (a) MC, (b) HSS

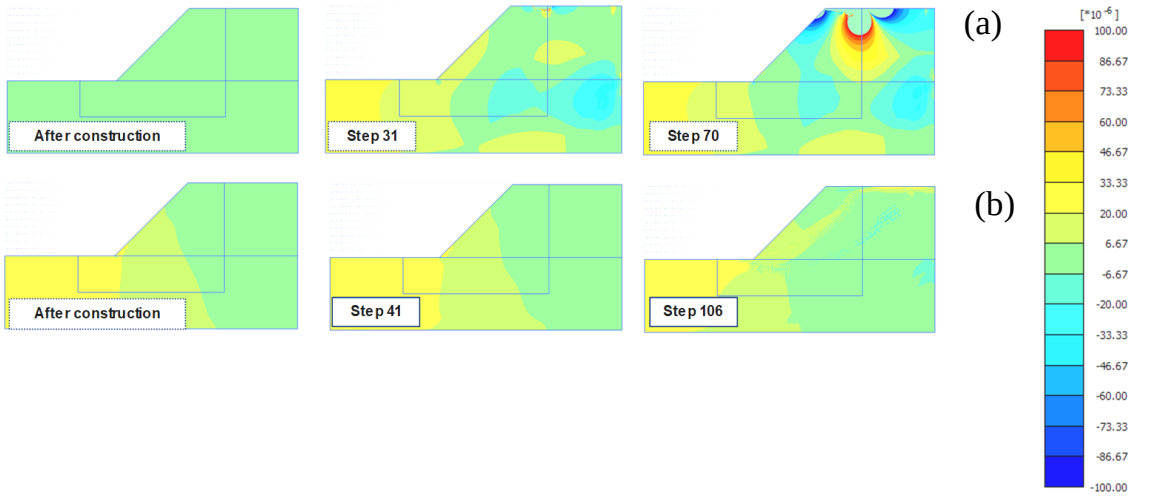

Fig. 117 Development total volumetric strains HSS model: (a) Undrained (A) – Ign. Undrained, (b) Undrained (A)